Fungal carbohydrate oxidoreductases for the production of sugar-based crosslinkers with applications in the formation of chitosan-based hydrogels

Yutong Zhang

Thesis submitted to the University of Ottawa
In conformity with the requirements for
the degree of Master of Chemistry

Department of Chemistry and Biomolecular Sciences
Faculty of Science
University of Ottawa

Abstract

Fungal carbohydrate oxidoreductases catalyze redox reactions related to the synthesis, degradation and modification of carbohydrates. Pyranose dehydrogenase from *Agaricus bisporus* (*Ab*PDH1) oxidizes xylooligosaccharides (XOS) from the hemicellulose of lignocellulosic biomass (LCB). Galactose oxidase from *Fusarium graminearum* (GalOX) can oxidize lactose. Both of these oxidoreductases can be produced at large scale by recombinant production from the low-cost *Pichia pastoris* expression system. At the same time, it is hypothesized that oxidized sugars can be used to crosslink chitosan polysaccharide, extracted from the shells of sea crustaceans, producing a chitosan-based hydrogel.

The goal of this study was to evaluate whether *Ab*PDH1 and GalOX could be used to make oxidized sugar-based crosslinkers that would contribute to hydrogel formation when mixed with chitosan.

Toward this, mid-scale production of the enzymes were completed, followed by their purification by affinity chromatography and characterization of their yields and functionalities by spectrophotometric-based assays and SDS-PAGE. The obtained enzymes were used to produce two oxidized-sugar products (oxidized-XOS and oxidized-lactose), where catalysis was confirmed by High-Performance Anion-Exchange Chromatography with Pulsed Amperometry Detector (HPAEC-PAD) and Fourier-transform Infrared (FTIR) spectroscopy. Subsequently, chitosan gels produced by the obtained crosslinkers were prepared at different pH values. The quality and stiffness of the gels was evaluated visually and by rheometric analysis. Results showed that oxidized-XOS can form gels faster than oxidized-lactose and that hydrogels formed fastest at neutral.

In conclusion, it is demonstrated that *Ab*PDH1 and GalOX can be used to make oxidized sugar-based crosslinkers that can contribute to hydrogel formation when mixed with chitosan. Due to their non-toxic characteristic for humans and the environment, such

hydrogels have the potential to be developed as new water-retaining materials for applications in agriculture and medicine. At the same time, such hydrogels enable recycling of the biomass-based waste streams, increasing the value of agricultural and marine resources.

Acknowledgements

I would like to thank everyone I met and acknowledge everything that I experienced while completing my degree. All of these, whether successful or challenging, helped me grow and build my personality and character and experience. Thank you for enabling me to work and study in such amazing environments and meet such friendly people during my Master's.

I would like to thank to my supervisor, Dr. Michele Loewen at the University of Ottawa. She helped me learn how to do research and write my thesis, during what was such a busy time for her. I am grateful to her for recruiting me into the world of science and research. I also want to thank my other supervisor at the University of Toronto, Dr. Emma Master, for her support and the opportunity to study in her excellent lab.

I also thank Owen Mototsune, who is a PhD candidate at uToronto, he guided me in my research project. He always taught me how to design logical and controlled experiments which helped me a lot. I also want to thank Dr. Olanrewaju Raji, who helped me to operate the HPLC, and Durgesh Kavishvar who helped me to operate the rheometer. Thanks to Dr. Thu Vuong who helped me troubleshoot yeast transformation and protein modelling. I also want to thank Alessandra, Khadija, Rena, William, Xuebin, Xuange and Kevin in Emma's lab, as well as Djay, Tanya, Luana, Antony, Kelly, Joanna and Fang in Michele's lab. Thank you all for making my Master's study such an excellent learning and growing experience.

Table of Contents

Lists of Figures

List of Tables

List of Abbreviations

Pyranose dehydrogenase	PDH
Pyranose dehydrogenase from *Agaricus bisporus*	*Ab*PDH1
Xylooligosaccharides	XOS
Lignocellulosic biomass	LCB
Galactose Oxidase	GalOX
Auxiliary Activities	AA
Carbon dioxide	CO_2
xylobiose	X2
xylotriose	X3
xylotetraose	X4
2^2-a-L-arabinofuranosyl-xylotriose	A^2XX
2^3-(4-O-methyl-a-D-glucuronyl)-xylotriose	$U^{4m2}XX$
2^3-(4-O-methyl-a-D-glucuronyl)-xylotetraose	$XU^{4m2}XX$
Polyallylamine	PAA
Carbohydrate-Active EnZymes	CAZy
Glucose-Methanol-Choline	GMC
Flavin Adenine Dinucleotide	FAD
Protein Data Bank	PDB
1, 4-benzoquinone	BQ
Hydroquinone	HQ
2,6-dichloroindophenolate	DCIP
Ferrocene	Fc
2,2'-azinobis(3-ethylbenzthiazolinesulfonic acid)	ABTS
Endoplasmic Reticulum	ER
Pichia pastoris	*P. pastoris*
Buffered Glycerol-complex Medium	BMGY
Buffered Methanol-complex Medium	BMMY
alcohol oxidase	AOX
Monosodium phosphate	NaH_2PO_4
Disodium phosphate	Na_2HPO_4
Sodium hydroxide	NaOH
High-Performance Anion-Exchange Chromatography	HPAEC
Pulsed Amperometry Detector	PAD
Fast Performance Liquid Chromatography	FPLC
ultraviolet-visible spectrophotometry	UV-Vis
SDS	Sodium Dodecyl Sulfate
Ctrl.	control
Std.	standard

Chapter 1

Literature Review

1.1 Biomass recycling

Biomass refers to the organic mixture of living organisms or their lifeless organic dead bodies within a specific place and ecosystem, such as forests, agricultural lands, wetlands and seas (Vassilev et al., 2010). It is quantified inside a specific area or volume, usually in the units of kilograms per square meter or kilograms per cubic meter (Bar-On., et al, 2018; McKendry, 2002). Biomass can be comprised of plants, animals, fungi, and other microorganisms, and is expected to be useable as the raw materials for making products of value, essentially recycling the organisms into something else (McKendry, 2002; Vassilev et al., 2010).

1.1.1 Ocean biomass: Crustaceans, chitosan and hydrogels

Beyond LCB, another major form of biomass is ocean biomass, including chitosan. Chitosan (Figure 1.1), a deacetylated form of chitin, is a linear-formed glucosamine polysaccharide (Rahmanian-Devin et al., 2021; Taokaew et al., 2023; Aranaz et al., 2021; Elieh-Ali-Komi & Hamblin, 2016; Li & Wu, 2020; Aguilar et al., 2019). It can be abundantly extracted from the shells of crustacean marine organisms, such as shrimps, lobsters, crabs, and so on (Islam et al., 2017; Inokuma et al., 2016; Li et al., 2024). Crustacean shells are a by-product waste of the fishing industry, such that their value-added development by technological modifications can be considered recycling of ocean biomass (Texieira-Costa & Andrade, 2021). Currently, chitosan is identified as a non-toxic, highly biocompatible and highly biodegradable natural material that has been applied in biomedicine fields as a health supplement, taking advantage of its documented antimicrobial, antioxidant and antitumoral properties (Jarmila & Vavríková, 2011; Feng et al., 2024; Xu et al., 2023).

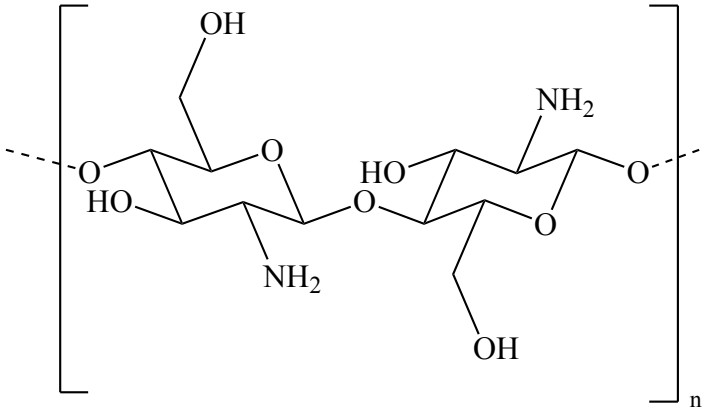

Figure 1.1: An example of the structure of chitosan.

Chitosan is the general name of a series of polymers composed of random arrangements of β-(1→ 4) linked D-glucosamine and N-acetyl-D-glucosamine residues in linear form. (Aranaz et al., 2021; Rahmanian-Devin et al., 2021; Hong et al., 2023; Xu et al., 2023; Taokaew et al., 2023). This design presents large numbers of hydrophilic groups along the polymers, including amine, NH_2. These functional groups endow chitosan with physical and chemical properties that allow it to be modified by attachment of other molecules or polymers, resulting in the synthesis of new materials; for example water-retaining hydrogels (Hong et al., 2023).

Chitosan hydrogels are a three-dimensional and porous structural network, which can retain a large amount of water within its structure (Figure 1.2) (Taokaew et al., 2023; Gawel et al., 2023). It has been proposed that other chemical molecules (such as nutrients and drugs) can also be added into the gel forming components, and subsequently incorporated in the hydrogels (Gawel et al., 2023). Therefore, it is expected that pesticides and fertilizers could be mixed within this chitosan gel for agricultural applications. For example with injection of the gel forming solutions at targeted locations (maybe the root of the plants), to maximize the potency and targeting of antifungals and nutrients, which will significantly reduce input costs and reduce excess antifungal/nutrient run-off pollution caused by those. There are also ideas

about the value of being able to potentially dissolve the gels when treatments are completed, although relevance here may be more facing human health than agriculture (Li et al., 2024).

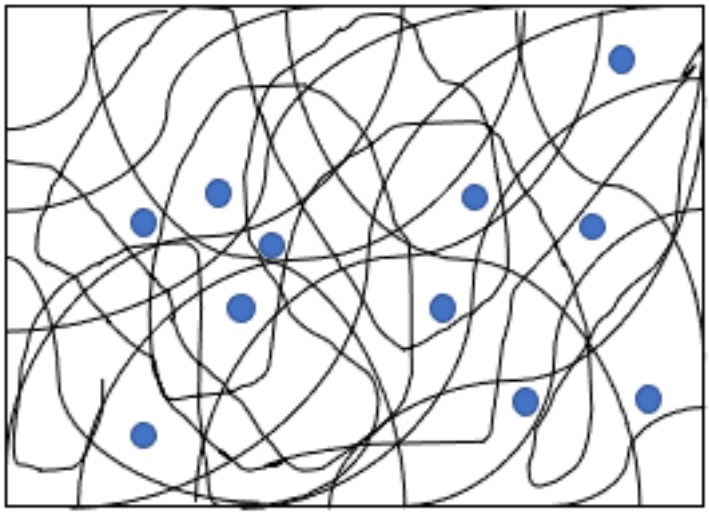

Figure 1.2: General scheme on the blockage of molecules within hydrogels. Blue circles refer to the chemical molecules, include drugs or nutrients. Black lines refer to the polysaccharides.

Currently, chitosan hydrogels can be synthesized by both physical crosslinking techniques and chemical crosslinking methods (Rahmanian-Devin et al., 2021; Xu et al., 2023; Taokaew et al., 2023; Li et al., 2024). Physical crosslinking usually uses freezing, ultrasonic wave or light to connect chitosan molecules with hydrogen bonds, ionic interactions, electrostatic interactions, or other weak non-covalent interactions, accompanied by the formation of solid gel architectures in water (Rahmanian-Devin et al., 2021; Hong et al., 2023; Xu et al., 2022; Ahmadi et al., 2015). Compared with chemical crosslinking, physical crosslinking does not require chemical agents to assist in the gel formation, such that they are low in cytotoxicity, but unstable in water. Toward trying to obtain more stable hydrogels, chemical crosslinking is now being investigated to enable the production of more structurally stable 3D covalent bond networks. For example, sugars, such as XOS obtained from hemicellulose arising from LCB, are hypothesized to be potentially suitable hydrogel crosslinkers, following their oxidation by fungal carbohydrate oxidoreductases (Xu et al.,

2023). However, the potential of XOS and other sugars to be oxidized by fungal enzymes and the cross-reactivity of any obtained oxidized-XOS with chitosan to form hydrogels remains to be investigated.

1.1.2 Lignocellulosic biomass and XOS

Lignocellulosic biomass (LCB) specifically refers to the woody biomass in a plant composed of natural fiber polymers; it is one of the most well-known and cheap renewable biomasses (Ning et al., 2021; Xu et al., 2023; Inyang et al., 2022). LCB includes forest waste (trees, grasses, leaves), agricultural waste (corn or wheat stalks, rice husk, sugarcane bagasse), and some urban waste (paper waste, construction woodworking sawdust) (Xu et al., 2016; Saidur et al., 2011; Chen et al., 2021; Inyang et al., 2022; Abolore et al., 2023). LCB is, among other things, a storage form of carbon and energy. Plants absorb energy from sunlight through a process called photosynthesis, where carbon dioxide (CO_2) is converted into sugar with the release of oxygen, essentially storing the carbon in sugar form and the energy in the form of carbon-carbon bonds (Xu et al., 2016; Bar-On et al., 2018; Saidur et al., 2011). The plant uses the sugar and the energy it contains to grow in various ways. Part of the growth process involves production of long polymers of sugars, called cellulose and hemi-cellulose that make up the plant cell wall. These polymers are naturally fibrous, imparting them with many potential applications beyond plant cell wall structure. Thus, overall, LCB is a low-emission renewable resource on earth that is likely to be vigorously exploited in the future (Parikka, 2004; Vassilev et al., 2010; Zoghlami & Paës, 2019).

Canada has large areas of undeveloped forest and agricultural lands, especially in the western provinces and northern territories (MacDonald et.al., 2023). According to the statistics of Natural Resources Canada and Agriculture and Agri-Food Canada, the area of forest is around 362 million hectares, and the area of the agricultural land is around 62.2 million hectares (Natural Resources Canada, 2023; Agriculture and Agri-Food Canada,

2023). This provides an abundant amount of cheap LCB from forest and agricultural industries as harvest waste, that has the potential to be recycled into products of value (Ning et al., 2021; Kumar et al., 2003; Abolore et al., 2023).

Traditionally, plant biomasses were used as low-value commodity products. For example, branches and trunks were burned for heating in the winter, dry grasses and stalks were used as forage for feeding domestic animals (MacDonald et.al., 2023). However, burning wood for heat releases the stored carbon back into the environment, and neither of these usages maximize the full potential of these plant wastes.

Since the 1990s, plant biomass has begun to be (bio)chemically processed into higher value-added agricultural products (Shahid et al., 2021). The most popular biomass application is the generation of biomass-based fuels, which can be used as a renewable energy source alternative to fossil fuels (Xu et al., 2016). For example, corn and soy are used to produce bioethanol and biodiesel respectively, as first-generation biofuels, while LCBs from agricultural waste are used to produce second-generation biofuels, and algae are now being used to produce third and fourth generation biofuels (Moravvej, 2019). These new biofuels can contribute to the reduction of global greenhouse gas emissions compared with direct wood combustion and fossil fuels combustion (Tursi, 2019). Until today, the first and second generation of biofuels have had only limited applications, usually mixed with traditional fuels (Shahid et al., 2021). But overall, this shows that chemical technologies allow biomass to be converted into value-added products which can benefit environmental protection.

The cell wall of terrestrial plants contains three main constituents: cellulose, hemicellulose and lignin (Figure 1.3) (Novaes et al., 2010; Mazlan et al., 2019; Zoghlami & Paes, 2019; Abolore et al., 2023). Their specific proportions are not constant, varying with the wood's type, parts, habitat temperature, humidity and so on. For example, softwoods typically contain 33-42% cellulose, 22-40% hemicellulose and 27-32% lignin, whereas

hardwoods typically contain 38-51% cellulose, 17-38% hemicellulose and 21-31% lignin (Tarasov et al., 2018; Chen et al., 2017; Zoghlami & Paës, 2019). Nonetheless, all these variants of LCB fibers can potentially be applied to manufacturing products across various fields, such as pharmaceuticals, paper, and clothing production (Tarasov et al., 2018).

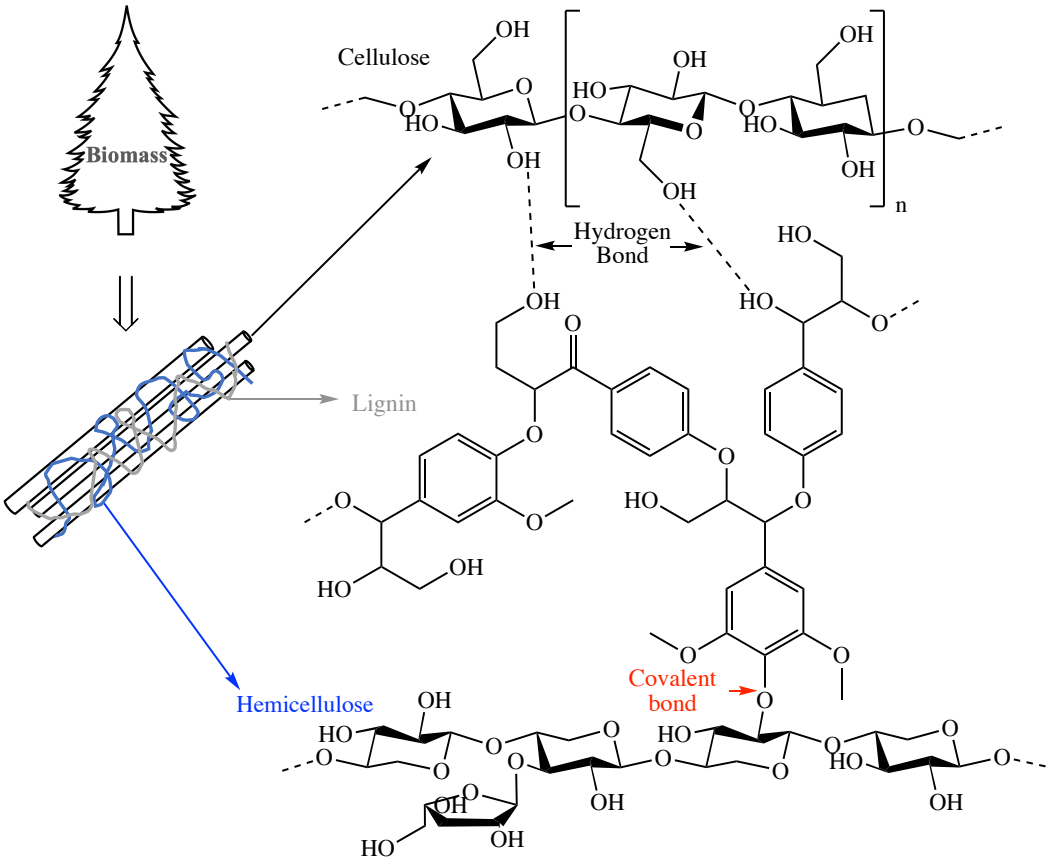

Figure 1.3 Three main compounds within the plant cell wall: cellulose, hemicellulose and lignin. Black tubes refer to the linear-formed cellulose, blue lines represent hemicellulose, grey line refers to lignin. The interactions between cellulose and lignin as well as hemicellulose are non-covalent, while the interactions between hemicellulose and lignin are covalent (Nishimura et al., 2018; Ojo, 2023; Wu et al., 2022; Brienza et al., 2024; Hasanov et al., 2020).

The values above highlight that cellulose is always present in the largest proportion within the plant cell wall compared to hemicellulose and lignin. Cellulose is an astonishingly long and unbranched homo-polysaccharide that can consist of up to 15,000 repeating individual glucose molecules connected with glycosidic linkages between C1 and C4 positions, β-1→4 linkage (Alberts et al., 2002; Morgan et al., 2016; McNamara et al., 2015;

Zoghlami & Paës, 2019). Its main function is to enhance the rigidity and strength of cell walls to support plant standing and growth (Rongpipi et al., 2019).

Hemicellulose is the second largest major component of plant cell walls after cellulose, accumulating as an amorphous cross-linked polymeric substance surrounding the linearly formed cellulose (Tarasov, 2018; Zoghlami and Paës, 2019). It is not covalently linked to the cellulose. It is a xylan matrix, which is a complex hetero-polysaccharide polymer composed primarily of multiple types of five and some six carbon sugars (Xu et al. 2023). Xylans can be pretreated by hot water hydrolysis to generate xylose or XOS, where XOS is mixtures of di, tri, tetra etc. sugar polymers as shown in Figure 1.4 (MacCormick et al., 2018). In general, xylose is the main monomeric sugar residue within the heteroxylans of hemicellulose, binding in β-1→4 linkages, playing the role of backbone. Other sugar units are attached to the xylose backbone in various glycoside linkages as branched side chains, including glucose, arabinose, pentose, mannose, galactose, glucuronic acid, etc. (Qaseem et al., 2021; Palaniappan, 2021; Santibáñez et al., 2021; Scheller et al., 2010).

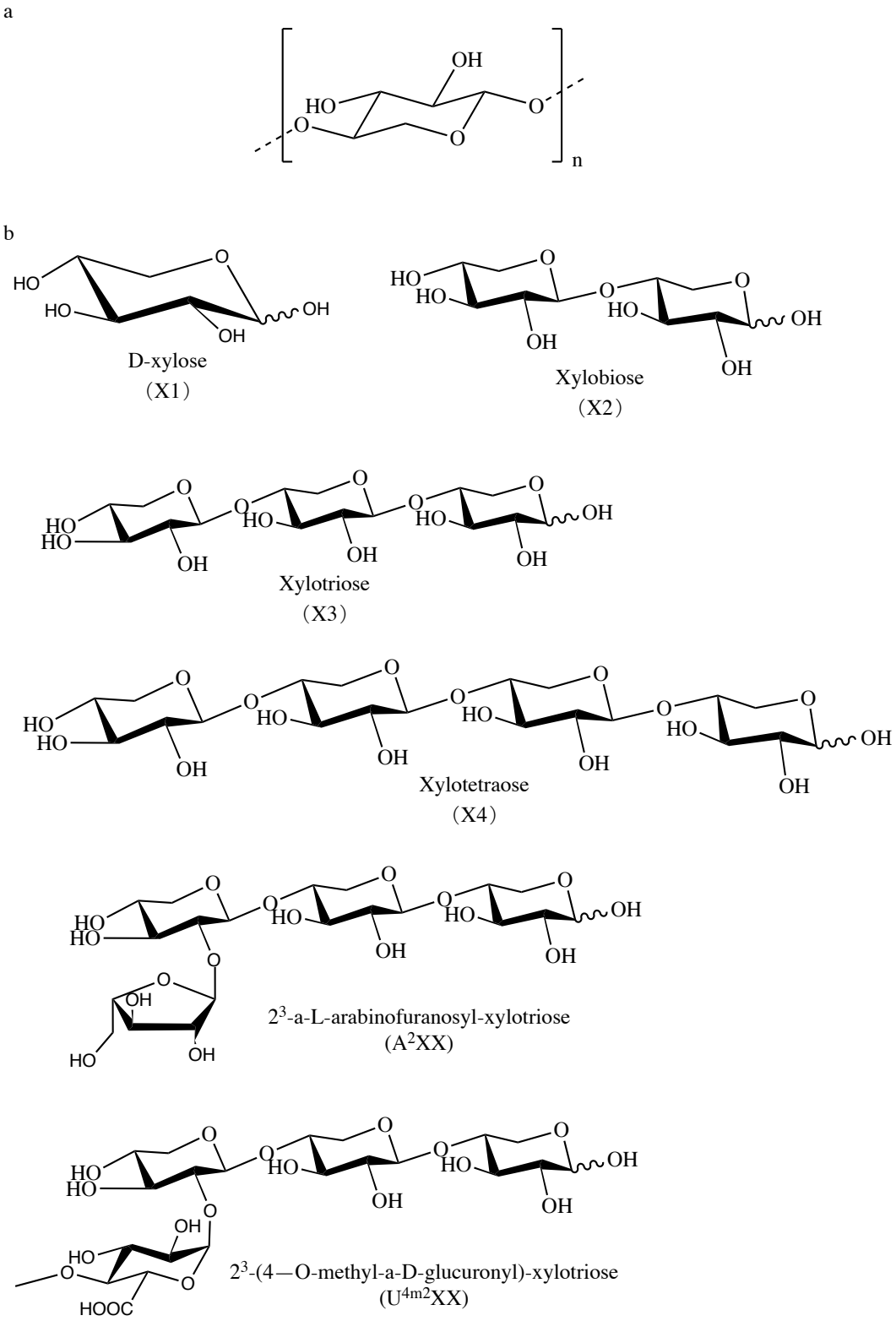

Figure 1.4 The structures of xylan and XOS. a) The general structure for xylan. b) Some examples of the structure of different XOS polymers, their names and their nomenclature (Karppi et al., 2020).

The main function of hemicellulose is to endow flexibility to the plant fiber (MacCormick et al., 2018). In this context, LCB's hemicellulose fibers from wood contribute

to modulation of the rigidity of paper in the paper industry. Its non-covalent binding to cellulose lends paper a certain degree of flexibility (Lan et al., 2024). In contract, the LCB hemicellulose fibers from cotton are much longer contributing to even higher flexibility, so it can be used to produce textiles where woody LCB cannot. However, hemicellulose utilization in industry is generally still limited because the native hemicellulose from woody LCB has poor mechanical stability due to its relative shorter fiber length, and lack of cost-effective and low-pollution methods for isolating it (Mittal et al., 2023). Nonetheless, due to the abundant amount of LCB biomass, hemicellulose still holds high potential to be developed into more value-added products in the future (Qaseem et al., 2021).

Finally, the third component of LCB is lignin, which is a non-sugar heteroaromatic polymer found in the plant cell walls, which also accumulates as an amorphous cross-linked substance surrounding the linearly formed cellulose (Sharan et al., 2024; Zoghlami and Paës, 2019). It is composed of three kinds of phenylpropanoid alcohols: 4-propenyl phenol, 4-propenyl-2-methoxyphenol and 4-propenyl-2,5-dimethoxyl phenol (Zheng et al., 2022). It is hydrophobic and helps channel water for plant growth (Vanholme et al., 2012). While it only forms non-covalent bonds to cellulose, it does make covalent bonds to hemicellulose, the latter being functional to strengthen the rigidity of the plant cell wall and support the plant standing up (Zhang et al., 2015) (Liu et al., 2018). Lignin has also been shown to provide resistance to pathogens, thereby preventing cell wall degradation and rot (Liu et al., 2018).

1.1.3 Hemicellulose-based XOS crosslinkers: a model

XOS, derived from hemicellulose, has been proposed to have potential utility as a natural crosslinker connecting other long chains of polysaccharide fibers, such as cellulose and chitosan (Xu et al., 2023). Its cross-reactivity is furthermore proposed to be improved by oxidation of its hydroxyl groups into more reactive ketones. Once the XOS is oxidized, its use for the cross-linking of fibers is proposed using the synthetic polyallylamine (PAA) fiber

as a model (Figure 1.5). Essentially, the PAA fiber initiates the cross-linking event as a condensation reaction by donating a pair of electrons from one of its primary amine functional groups. This is accepted by the ketone group on the oxidized XOS, leading to reduction of the ketone back into a hydroxyl. Subsequently, the hydroxyl obtains another hydrogen proton from acid within the solution, leading to the formation of -H_2O with positive charge, which can be released by forming a covalent double bond with the nitrogen. The final product is an imine (schiff base).

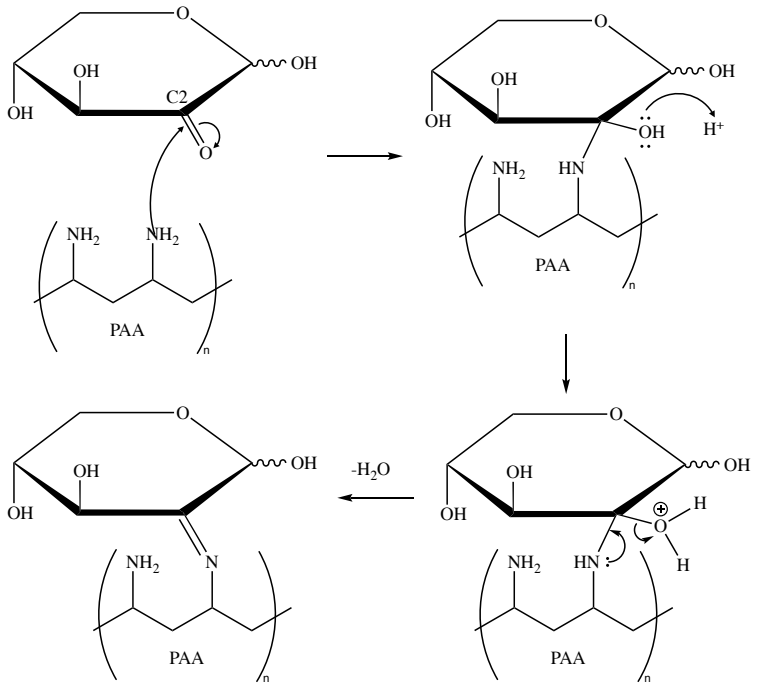

Figure 1.5 The condensation reation for the PAA-oxidized sugar (xylose) crosslinking formation (Alavarse et al., 2022). In this example, the sugar was oxidized at C2 position, so the condensation reaction also happens at this position. In this reaction, one water molecule is lost as the bond is formed with one PAA. There are mulitple PAA-oxidized sugar crosslinks generated within a resulting gel.

Notably similar cross-reactivities between oxidized XOS are proposed to be possible for other naturally occurring fibers containing amino groups, such as chitosan. As well, other abundantly available polysaccharide fibers that lack amino groups, such as cellulose, could be chemically modified by transaminase enzymes for example, resulting in addition of amine

groups along those polysaccharides, for cross-linking with oxidized XOS as well (Feng et al., 2024).

Regardless, of the fiber, according to the proposed model, the cross-reactivity of the sugar-based crosslinkers should be maximized by oxidation of the alcohols into ketones. This has been proposed to be best achieved through the activity of selected carbohydrate oxidizing enzymes (Xu et al., 2023).

1.2 Fungal carbohydrate oxidoreductases

Fungi are assimilative heterotrophs, which can symbiose with photoautotrophs, such as algae and plants (Resl et al., 2022). They acquire carbon and energy from the photoautotrophs that use sunlight as energy to convert carbon dioxide to carbohydrates (Clark et al., 2019; Umbreit, 1962). In this symbiotic relationship, carbohydrate oxidoreductases are produced and secreted by the fungus to break down the polymers in the photoautotroph's cell walls, including cellulose, hemicellulose, and lignin (Barrett et al., 2020; Benoit et al., 2015; Sun et al., 2023). In addition, the photoautotrophs themselves can produce various types of other carbohydrates, such as glucose and polyols, that are not necessarily the carbohydrates that the fungus requires. Thus, further additional carbohydrate oxidoreductases are produced by the fungus to convert those carbohydrates from the hosts into metabolites that can be used by the fungus to survive (Smith et al., 1969). Overall, carbohydrate oxidoreductases isolated from fungus have high potential to be applied in industry for the conversion of biomass fibers and sugar substrates within biomass into value-added products.

Fungal carbohydrate oxidoreductases are both specialized and generalists in substrate preferences (Resl et al., 2022). The specialization refers to the idea that different fungal species are rich in a range of different enzymes that can each catalyze specific reactions on substrates from a variety of different sources. That is to say that each enzyme has evolved

advantages in catalyzing specific reactions on specific substrates. For example, GalOX has higher enzymatic activity on the oxidation of galactose and lactose compared to other sugar substrates (Parikka et al., 2015; Paukner et al., 2015; Cleveland, 2021, Mototsune et al., 2024), because galactose and lactose sugars share similar structural features. In contrast, the generalization is reflected in the broad range of substrates that each individual oxidoreductase can work on. For instance, Pyranose Dehydrogenases (PDHs) can not only oxidize xylose but also oxidize glucose, arabinose, galactose etc. (Gonaus et al, 2015; Peterbauer, 2020; Staudigl et al., 2013). Both the specialization and the generalization arise from the adaptation of fungi to different environments, allowing fungal species to better compete for resources (Hess et al.,2020; Sun et al., 2023). The nature of evolved enzyme specificities depends on a combination of the host and growth environment, where different fungal species have evolved mechanisms to convert specific available resources into the carbohydrates it requires (Resl et al., 2022; Hess et al., 2020; Lofgren et al., 2021). The nature of the generality arises from the enzymes evolving from shared ancestors that contain similar structures and active sites, leading to the similar functions, but with the ability to accommodate a broad range of carbohydrate substrates with similar structure (C5 and C6 sugar structures generally). Fungi sharing the same environmental conditions usually contain similar enzymes that can work on a broad variety of sugars. As the sheer breadth of such enzymes was revealed, researchers developed a database to enable sorting and categorization.

1.2.1 Carbohydrate-Active EnZymes database (CAZy)

The CAZy database (http://www.cazy.org/) was created in 1991 (Yin et al., 2015). It provides a systematic protein classification system specifically focused on carbohydrate-active enzymes based on their functions, genome similarity, and structural domain similarity (Wardman et al., 2022; Cantarel et al., 2009; Ameri et al., 2022; Moriin et al., 2012). The

CAZy classification system was in particular designed to enable the development of LCB degrading enzymes across species (Ameri et al., 2022; Hage and Rosso, 2021).

At this time, five enzyme classes have been defined in the CAZy database: glycoside hydrolases (GHs), glycosyl transferases (GTs), polysacchasride lyases (PLs), carbohydrate esterases (CEs), and auxiliary activities (AAs). Of particular relevance to this thesis, the AA class of CAZy enzymes accommodates a range of redox enzymes related to plant cell wall degradation in particular (Levasseur et al., 2013; Sützl et al., 2018; Yin et al., 2015). The CAZy website shows that there are a total of 100,803 enzymes (and another 844 non-classified modules) divided into 17 AA classes, where only AA3 and AA5 will be introduced in this thesis.

1.2.1.1 Auxiliary Activities 3 Family

Or particular relevance to this thesis is the AA3 family, which belongs to the glucose-methanol-choline (GMC) structural superfamily, where each protein contains a non-protein flavin adenine dinucleotide (FAD) cofactor. The FAD covalently or non-covalently binds to the main body of the protein. FAD cofactor is able to stabilize the enzyme and allows the enzyme to catalyze the redox reaction by electron transfer. FAD first accepts two electrons and two hydrogen ions from the substrates, forming FADH2 (reduced form). Then, FADH2 releases them to the electron acceptors (such as BQ), reforming FAD. Enzymes in this family share a similar fold that enables them to oxidize and reduce substrates within their substrate-binding domain in coordination with the FAD cofactor (Levasseur et al., 2013; Sützl et al., 2019). In Figure 1.6 an overlay of some of the key structural aspects of the catalytic site of selected representative proteins in the AA3 group is shown. According to the CAZyme database, 9 types of proteins (including 2400 subtypes) have been cataloged in the AA3 family currently, including cellobiose dehydrogenase (CDH, EC 1.1.99.18, AA3_1), ecdysone oxidase (EC 1.1.3.16, AA3_2), glucose 1-oxidase (EC 1.1.3.4, AA3_2), aryl

alcohol oxidase (EC 1.1.3.7, AA3_2), oligosaccharide dehydrogenase (EC 1.1.5.-, AA3_2), glucose 1-dehydrogenase (EC 1.1.5.9, AA3_2), PDH (EC 1.1.99.29, AA3_2), alcohol oxidase (EC 1.1.3.13, AA3_3), and pyranose oxidase (EC 1.1.3.10, AA3_4). These proteins are widely distributed across multiple fungi species, and their activities on substrates contain slight differences depending on which fungal species they arise from (Sützl et al., 2019). Of particular relevance to this thesis are the PDH members of the AA3 Family described in more detail below (section 1.3).

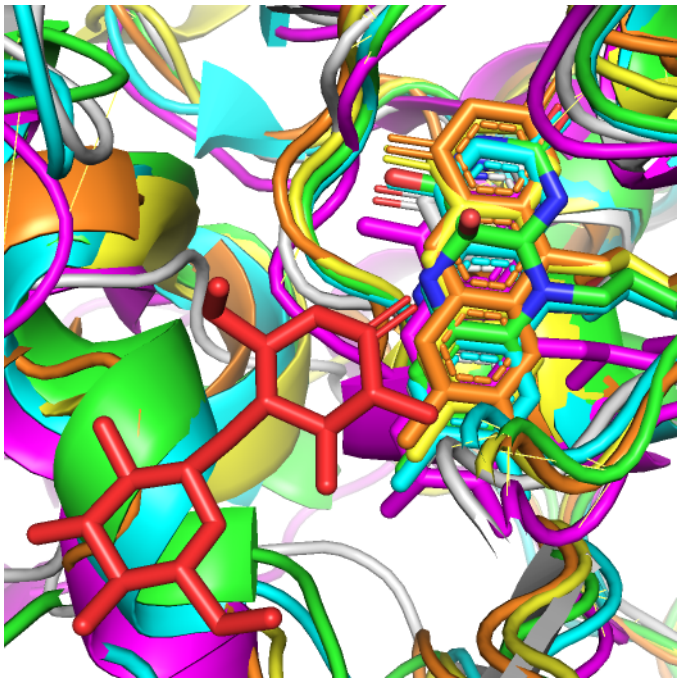

Figure 1.6 Comparison of the 3D structures of AA3 enzyme substrate-binding domains. Green refers to PDH (PDB: 4h7u), magenta refers to CDH (PDB: 4qi5), brown refers to glucose oxidase (PDB: 1cf3), light blue refers to aryl-alcohol oxidase (PDB: 5oc1), yellow refers to oligosaccharide dehydrase (PDB: 6xuu), grey refers to glucose dehydrase (PDB: 6o9n). The FAD cofactor is shown in rainbow shading matching the mainchain color, and red is the sugar substrate present in the CDH crystal structure. Small yellow lines are artefacts of the PyMOL alignment process.

1.2.1.2 Auxiliary Activities 5 Family

Another family relevant to this thesis is the AA5 family, which is the copper radical oxidases family in the CAZy database (Levasseur et al., 2013). They are produced by fungal organisms, such as white-rot fungi, and can be used in lignocellulose degradation like AA3s

(Alpdağtaş et al., 2024). The copper ion in the protein of this family can oxidize primary alcohols on the substrates to their aldehydes in the first-half reaction, where Cu (II) is converted to Cu (I); but also, oxygen (O_2) is additionally reduced to hydrogen peroxide, H_2O_2 in the second half-reaction, where Cu (I) is then converted back to Cu (II) (Yin et al., 2015). In Figure 1.7 an overlay of some of the key structural aspects of selected representative proteins in the AA5 group is shown. AA5_1 and AA5_2 are two subfamilies, where glyoxal oxidases (GlyOx, EC 1.2.3.15, AA5_1); galactose oxidases (GalOx, EC 1.1.3.9, AA5_2), raffinose oxidase (EC 1.1.3.-, AA5_2), alcohol oxidase (EC 1.1.3.13, AA5_2), 5-(hydroxymethyl)furfural oxidase (EC 1.1.3.47, AA5_2), and aryl alcohol oxidase (EC 1.1.3.7, AA5_2) (Yin et al., 2015; Andberg et al., 2017; Dijkman et al., 2015; Nguyen et al., 2018; Levasseur et al., 2013 and Whittaker, 2003; Fong et al., 2024). Of particular relevance to this thesis are the GalOX members of the AA5 Family described in more detail below (section 1.4).

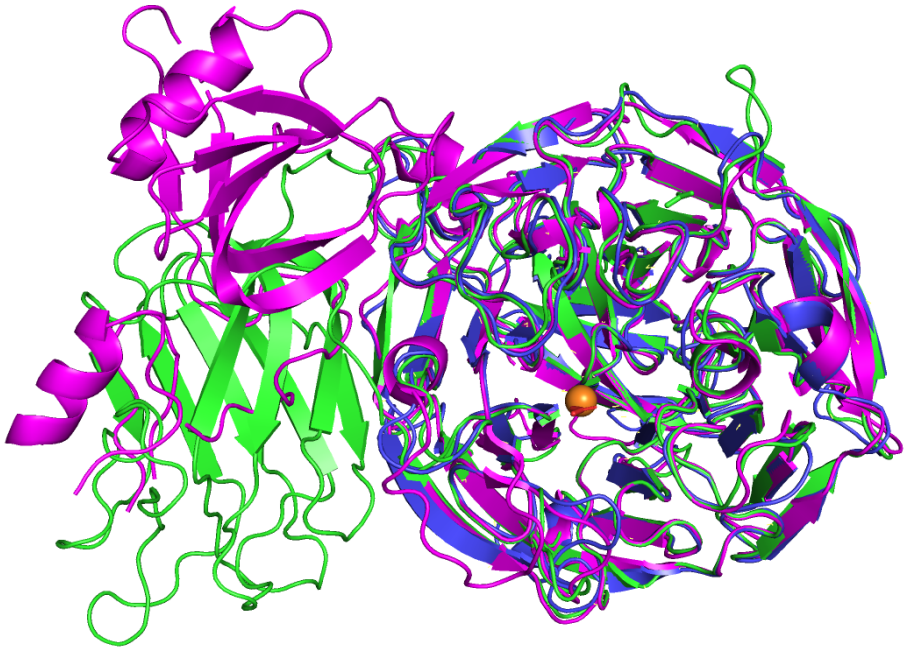

Figure 1.7 Comparison of the 3D structures of AA5s substrate-binding domains. Green refers to GalOX (PDB: 1gof), magenta refers to aryl acohol oxidase (PDB: 6ryv), blue refers to alcohol oxidase (PDB: 5c92). Red is the substrate present in the GalOX crystal structure, orange is the copper atom. Small yellow lines are an artefact arising from the PyMOL alignment process.

1.3 Pyranose dehydrogenase (PDH; AA3)

PDHs (EC 1.1.99.29, AA3_2) are structurally and functionally related to other fungal flavin-dependent carbohydrate oxidoreductases (Peterbauer, 2020; Tan et al., 2013), but are known to be the best at oxidizing C5 sugars such as xylose, as well as XOS derived from hemicellulose (Karppi et al., 2020). In particular PDHs have been shown to oxidize D-xylose at C2 to 2-keto-D-xylose (D-threo-pentos-2-ulose) and at C3 to 2,3-diketo-D-xylose (D-glycero-pentos-2,3-diulose) (Volc et al., 2000) (Figure 1.8). These oxidation reactions catalyzed by PDHs involve transfer of electrons and protons via FAD and an electron acceptor, that latter being, for the purposes of the *in vitro* experiments described in this thesis 1,4-benzoquinone (BQ). Upon oxidation of the sugar, the BQ is reduced to hydroquinine (HQ). Thus laccase (EC 1.10.3.2), a multi-functional enzyme that is also widely distributed in plant and fungi (Shraddha et al., 2011) is included as an assisting enzyme to oxidized HQ back to BQ, coupled with a two-electron loss from HQ (Lv et al., 2022) and an accompanying reduction of oxygen gas (O_2) to water. This laccase catalyzed step reduces the required BQ amount for the PDH oxidation, for decreased industrial material cost.

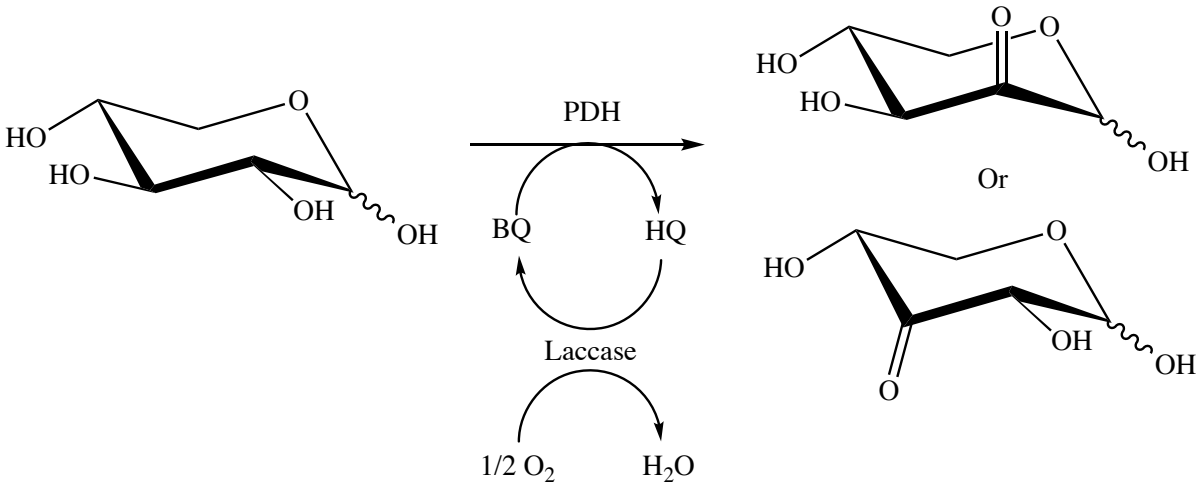

Figure 1.8 The oxidation reaction of *Ab*PDH1 on D-xylose. D-xylose was oxidized to its ketone by PDH and the electron acceptor BQ. To maximize the use of BQ, laccase was used to convert the by-product HQ in the last reaction back to BQ for cycling the reaction.

The first PDH was found in the mycelia of the white mushroom *Agaricus bisporus* in 1997 (*Ab*PDH1, UnitProt ID: K5WJK3, GenBank ID: EKM75486) (Morin et al., 2012; Volc et al., 1997). Peterbauer summarized that PDH is ecologically limited to appearing within the broader Agaricaceae family, also including Leucocoprinus, Lycoperdon, and Macrolepiota, which ecologically act as litter decomposers (Peterbauer, 2020). Five PDH variants have been identified besides *Ab*PDH1 including: *Agaricus campestris* PDH (*Ac*PDH, 68kDa, UnitProt ID: V5NDL4, GenBank ID: AHA85313.1) (Staudigl et al., 2013), *Agaricus meleagris* PDH1 (*Am*PDH1, UnitProt ID: Q3L245, GenBank ID: AAW82996.1 & AAW82997.1) (Kittl et al., 2008), *Am*PDH2 (UnitProt ID: Q3L243, GenBank ID: AAW82998.1 & AAW82999.1) (Kittl et al., 2008), *Am*PDH3 (UnitProt ID: Q0R4L2, GenBank ID: AAZ94874.1 & AAZ94875.1) (Kittl et al., 2008), and *Agaricus xanthodermus* PDH (*Ax*PDH, UnitProt ID: V5NC32, GenBank ID: AHA85314.1 & AAW92123.1) (Staudigl et al., 2013). Sequence alignments show that these share between 73 – 90 % sequence identity at the amino acid level (Table 1.1), where the total length of PDH is around 65 kDa.

Table 1.1. Percentage (%) amino acid sequence identity for the six PDH variants. The percentages were calculated using Clustal Omega.

	*Am*PDH1	*Ab*PDH1	AcPDH	*Am*PDH2	*Am*PDH3	*Ax*PDH
*Am*PDH1	100.00	75.63	73.28	75.5	76.17	75.83
*Ab*PDH1	75.63	100.00	73.91	75.29	76.46	75.13
*Ac*PDH	73.28	73.91	100.00	75.8	76.13	76.81
*Am*PDH2	75.5	75.29	75.8	100.00	84.83	88.67
*Am*PDH3	76.17	76.46	76.13	84.83	100.00	89.33
*Ax*PDH	75.83	75.13	76.81	88.67	89.33	100.00

The only available crystal structure of a PDH is that of *Am*PDH1 (PDB ID: 4h7u) recorded within the Protein Data Bank to date (Tan et al., 2013). In the 4h7u x-ray structure, the FAD cofactor was bound to the protein main body with a single covalent bond at His 103, enhancing protein stability and positioned to modulate the redox transfer of electrons and protons with the substrate (Figure 1.9) (Graf et al., 2015). In additional, molecular dynamics simulations showed that, Tyr 510, Val 511, His 512, His 556 and Gln 392 all directly bind the

glucose sugar unit within the catalytic domain (Graf et al., 2013). As explained previously, His 512 and His 556 may bind with the sugar through hydrogen bonding, but His 556 is further away and thus may contribute less to catalysis. These two main active site histidines may also contribute to different catalytic reactions, where His 512 contributes more to the D-glucose regioselectivity preference on C3 oxidation, and His 556 contributes more to the preference for C2 oxidation (Graf et al., 2013; Graf et al., 2015). Nonetheless, additional research has shown that there are several other amino acid residues (including V511, Y510, Q392 for example) in the catalytic groove of PDH that enable it to bind with the substrates by hydrogen-bonding or other stacking interactions (Graf et al., 2015).

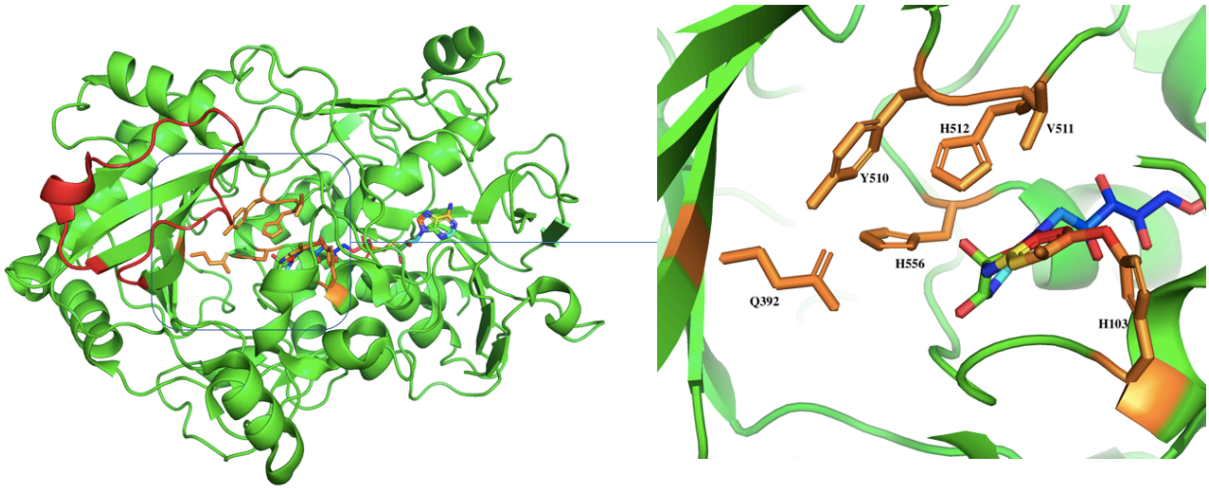

Figure 1.9 The structural of *Am*PDH (PDB: 4h7u). *Am*PDH is labelled in green. Active sites groove zoom is labeled in orange, FAD cofactor was labeled in rainbow colors.

In terms of substrates, XOS (the target for this study) refers to a polymer composed of around 2-7 xylose residues connected, or a complex of other sugar substituents attached to the main xylose chain (Yan et al., 2023; Vuong, 2022; Freitas et al., 2019) (Figure 1.3). For example, glucuronoxylose, containing glucuronic acids on the side branches, is derived from glucuronoxylan, which is one of the most abundant xylan in hardwood hemicellulose (Yuan et al., 2014). In addition, XOS can be either neutral or acidic. For instance, 2^3-(4-O-methyl-α-

D-glucuronyl)-xylotriose ($U^{4m2}XX$) and 2^3-(4-O-methyl-α-D-glucuronyl)-xylotetraose ($XU^{4m2}XX$) are acidic substrates containing the 4-O-methylated glucopyranosyluronic acid residues (Karppi et al., 2020). However, Peterbauer also mentions that PDHs generally demonstrate a broader selectivity for the oxidation of monosaccharides and polysaccharides comprised of xyloses, glucoses, galactoses, arabinoses, maltoses and lactoses (Peterbauer, 2020; Peterbauer & Volc, 2010; Staudigl et al., 2013; Tan et al., 2013; Sygmund et al., 2008; Karppi, 2020). Gonaus et al reported that *Ab*PDH1 exhibits a higher catalytic efficiency (kcat/Km) on D-glucose (22 $mM^{-1}s^{-1}$), L-arabinose (22 $mM^{-1}s^{-1}$) maltose (13 $mM^{-1}s^{-1}$), cellobise (10 $mM^{-1}s^{-1}$), and D-xylose (7.8 $mM^{-1}s^{-1}$) compared to other substrates (Gonaus et al., 2015). At the same time *Am*PDH exhibits higher catalytic efficiency towards L-arabinose (62.1 $mM^{-1}s^{-1}$), D-glucose (57.5 $mM^{-1}s^{-1}$), D-galactose (46.2 $mM^{-1}s^{-1}$), and D-xylose (22.9 $mM^{-1}s^{-1}$) (Peterbauer, 2020). In contrast *Ac*PDH only has some efficiency towards D-glucose (11.7 $mM^{-1}s^{-1}$), while *Ax*PDH has higher activity towards D-glucose (26.6 mM-1s-1) and D-xylose (20.3 $mM^{-1}s^{-1}$) (Staudigl et al., 2013). These values are compared in Table 1.2.

Table 1.2 The catalytic efficiency (kcat/Km) of ab, am, ac, ax PDHs towards substrates. The unit are in $mM^{-1}s^{-1}$. Data was taken from Gonaus et al, 2015; Peterbauer, 2020; Staudigl et al., 2013.

	Ab	*Am*	*Ac*	*Ax*
D-glucose	22	57.5	11.7	26.6
D-xylose	7.8	22.9	1.5	20.3
L-arabinose	22	62.1	0.7	5.5
D-galactose	6.9	46.2	0.7	5.0
D-mannose	0.1	0.27	-	-
Cellobiose	10	5.6	-	-
Maltose	13	5.0	-	-
Lactose	0.4	0.29	0.1	0.1
Raffinose	1.8	-	-	-
D-Fructose	-	-	-	-
Maltotriose	-	0.15	-	-
Xylobiose	-	4.7	-	-

Ultimatley, *Ab*PDH1 was selected for application in this project based on Karppi's previous studies demonstrating that wild type *Ab*PDH1, while not the most active PDH against xylose and xylobiose (Table 1.2), does yield the highest rates of oxidation on longer straight XOS, and even including some detectable activity even against longer acidic and branched hetero-xylooligosaccharides (Karppi et al., 2020), increasing the likelihood of successfully generating a crosslinker from XOS and hemicellulose more broadly.

1.4 Galactose oxidase (GalOX; AA5)

Taking into consideration the possibility of using sugars other than those derived from hemicellulose/XOS for crosslinking, an additional carbohydrate oxidizing enzyme is introduced here. GalOX (AA5_2, EC 1.1.3.9) is a free radical metalloenzyme, coordinating a copper metal atom as a cofactor that participates in substrate oxidation (Figure 1.10) (Parikka et al., 2015; Whittaker, 2003). GalOX was first isolated from *Polyporus circinatus* in 1959 (Cooper et al., 1959), and has been widely found across fungal microorganisms since then. Their molecular weights range from 65-68 kDa, and they are comprised of approximately 600 amino acids (Parikka et al., 2015). Its primary function is the oxidation on the primary alcohols to aldehydes on selected sugar substrates, accompanied by the reduction of O_2 to H_2O_2 (Parikka et al., 2015; Ito et al., 1994). Horse Radish Peroxidase (HRP, EC 1.11.1.7) and catalase (EC 1.11.1.6) can catalyze H_2O_2 decomposition, reducing it back to O_2 and H_2O. The use of these assistance enzymes in the GalOX reactions conducted in this study, helps protect the enzyme from possible oxidative damage from higher concentrations of H2O2, while also reducing any possibility of product inhibition, ensuring maximized GalOX activity (Hernandex-Rulz et al., 2001; Wu et al., 2019; Parikka et al., 2010).

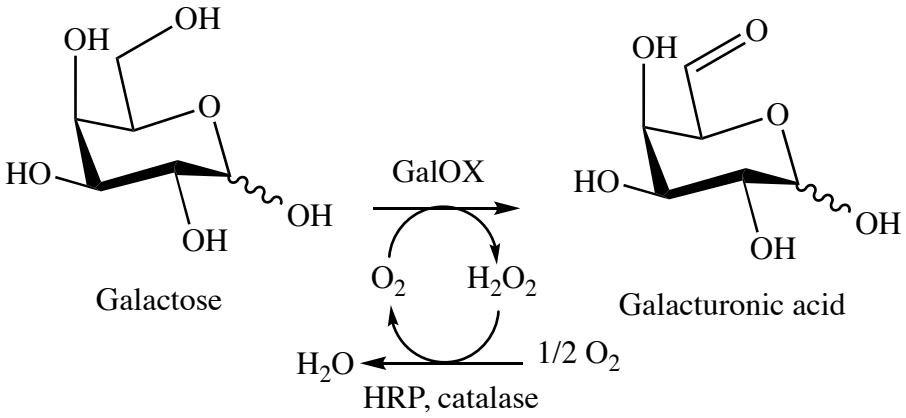

Figure 1.10 GalOX oxidation of galactose.

As per the phylogeny shown in Cleveland's article, the GalOX family includes four members arising from four different *Fusarium* species: *Fusarium graminearum Fgr*GalOX (GeneBank ID: AAO95371 & PCD36672.1), *Fusarium oxysporum* GalOX (*Fox*GalOX, UnitProt ID: V5NQ89, GenBank ID: AHA90705.1), *Fusarium subglutinans* GalOX (*Fsu*GalOX, GenBank ID: AJE27923.1) and *Fusarium sambucinum* GalOX (*Fsa*GalOX, GenBank ID: AIR07394.1) (Cleveland et al., 2021). Sequence alignments show that these share between 80 – 94.26 % sequence identity at the amino acid level (Table 1.3).

Table 1.3. Percentage (%) amino acid sequence identity for the four GalOX variants. The percentages were calculated using Clustal Omega.

	FoxGalOX	FsuGalOX	FgrGalOX	FsaGalOX
FoxGalOX	100	94.86	80.97	81.54
FsuGalOX	94.86	100	80.24	80.50
FgrGalOX	80.97	80.24	100	94.26
FsaGalOX	81.54	80.50	94.26	100

As per Parikka's description, GalOX is normally used in for quality assurance of dairy products, based on its primary substrates being galactose and the galactose disaccharide lactose. It always oxidizes the alcohol functional groups (-OH) on the terminal C6 position of both galactose and lactose (Figure 1.9) (Parikka et al., 2015). However, GalOX also has the ability to oxidize other mono- and oligo- saccharide substrates including: raffinose, melibiose, galactomannan, galactoglucomannan, galactoxylomannan, 1-methyl-β-D-

galactopyranoside and so on (Paukner et al., 2015; Cleveland, 2021, Mototsune et al., 2024), albeit it with significantly reduced effectiveness compared to galactose. Structurally, copper is in a square pyramidal geometry, containing five coordinating ligands: two tyrosine residues (Tyr 272 and Tyr 495), two histidine residues (His 496 and His 581) and one for water in the condition without catalysis or H_2O_2 during catalysis (Figure 1.11) (John et al., 2008; Figueiredo et al., 2021).

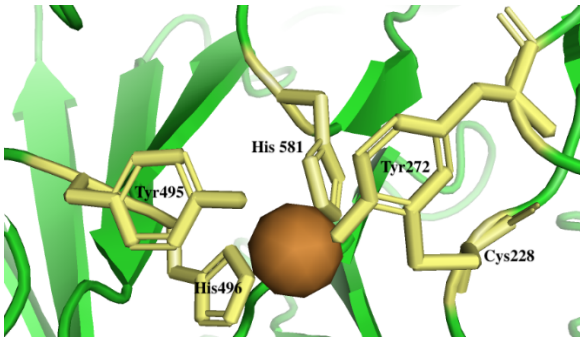

Figure 1.11 The substrate-binding domain of GalOX from *Dactylium dendroides* (PDB ID#: 1gog). Copper color refers to the copper atom.

1.5 Goals and Objectives

Chitosan, rich in amino residues (-NH_2), can undergo chemical crosslinking with its amino functional groups to produce highly stable gels with good water retention capabilites (Hong et al., 2023). In this project, the overarching goal is to produce chitosan hydrogels by crosslinking the chitosan with oxidized-XOS and separately oxidized-lactose. The following objectives were addressed. Initially, production of oxidized crosslinkers was attempted, separately, by enzymatic catalysis of XOS and lactose respectively with *Ab*PDH1 and GalOX. The derived crosslinkers were tested for their ability to crosslink chitosan to make the following hydrogels:

1.5.1 Chitosan – oxidized XOS hydrogel

XOS from hemicellulose can be oxidized by *Ab*PDH1 normally at both of the terminal sugar-unit hydroxyls, no matter the chain length (Karppi et al., 2020), which is

hypothesized, to then be useful for crosslinking chitosan fibres. In the crosslinking reaction, chitosan covalently binds with oxidized XOS through a condensation reaction, and is proposed to form a more stable hydrogel (Figure 1.12).

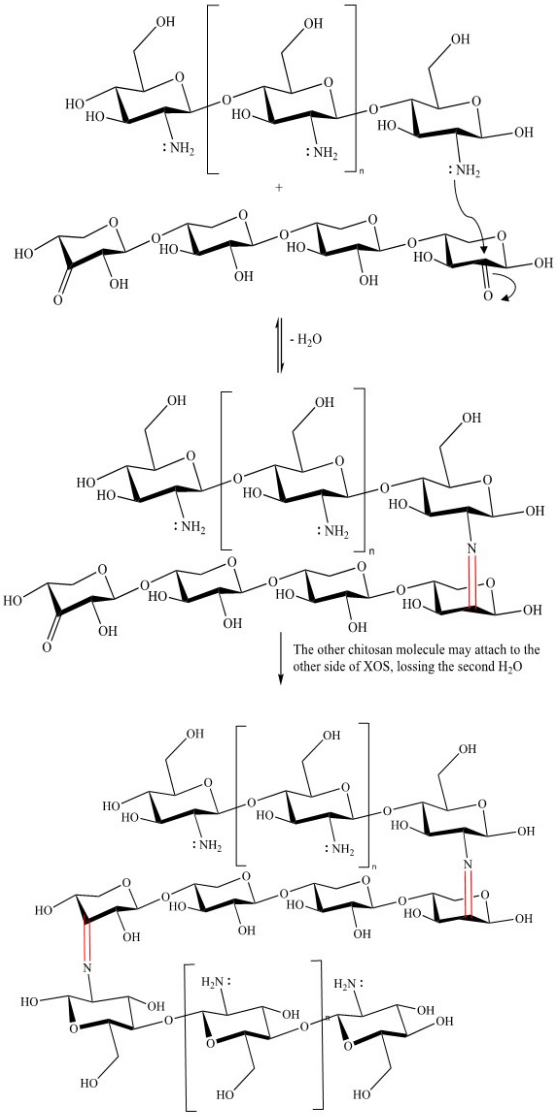

Figure 1.12 The proposed reaction of the chitosan with a hemicellulose-based crosslinker. X4 is used as an example for oxidized XOS that has been oxidized by *Ab*PDH1.

1.5.2 Chitosan – oxidized lactose hydrogel

Lactose can be oxidized by GalOX at the C6 position (Mototsune et al., 2024). The mechanism of chitosan attaching with the ketone on C6 is also proposed to be a condensation reaction as shown in Figure 1.13**.** Thus, the oxidized lactose may serve as an alternative crosslinker as well. But in this case, it is having to rely on GalOX to weakly oxidize the

glucose moiety (which is can do, albeit not favorably). Thus while it may also be possible to form a few crosslinking connections with the glucose unit to make the second crosslink to a second chitosan polymer, gel formation is expected to be slower/poorer than with oxidized-XOS.

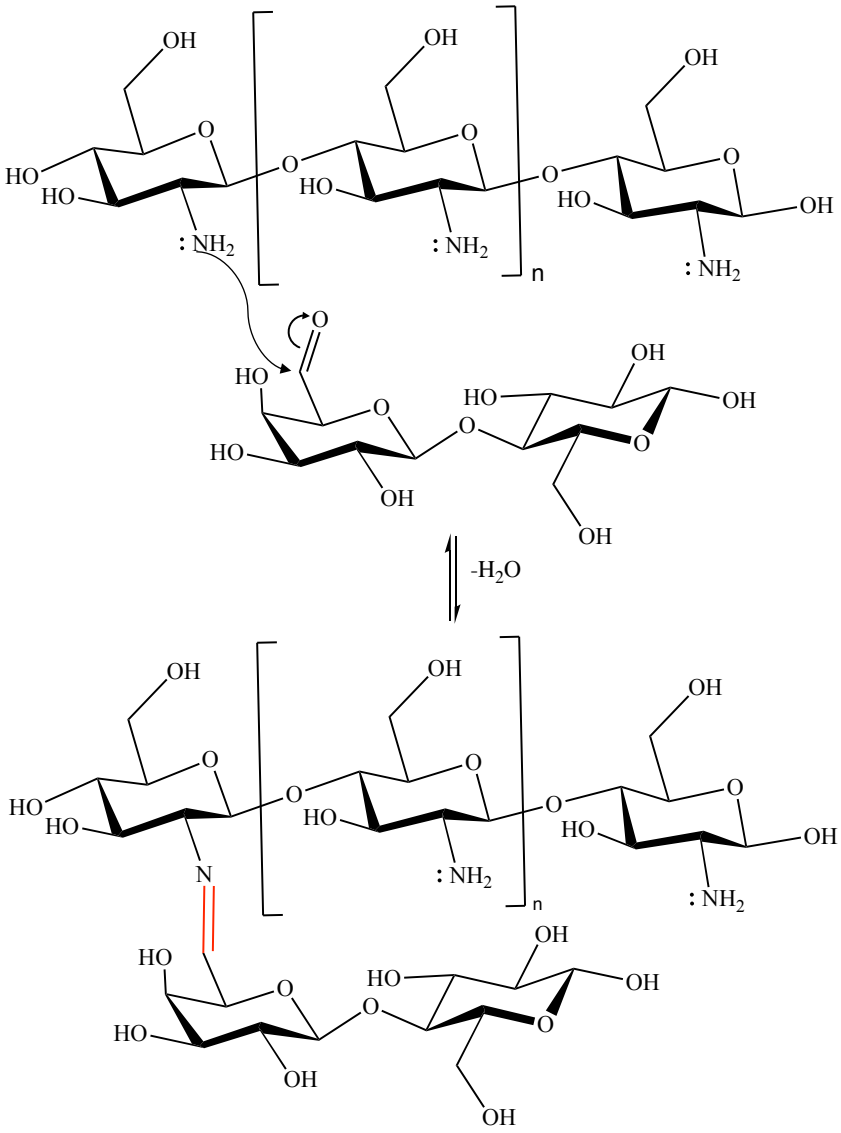

Figure 1.13 The proposed reaction of chitosan with a lactose-based crosslinker. Chitosan plays as the role of PAA, connecting with the galactose unit of oxidized lactose. GalOX can weakly oxidize glucose as well in a low efficiency, so it is also possible to form a few crosslinking connections on the glucose unit.

Chapter 2

Methods and Materials

2.0 Materials

The growth medium chemicals: yeast extract, peptone, yeast nitrogen base, D-glucose, D-xylose, D-galactose, agar and salts were purchased from Bioshop (Canada). Hydroquinone (HQ), Copper (II) sulfate, catalase from bovine live, Horse Radish Peroxidase (HRP) and electron acceptors: ferrocenium tetrafluoroborate, 1, 4-benzoquinone (BQ) and sodium 2,6-dichloroindophenolate (DCIP) were purchased from Sigma Aldrich, as were any other chemicals mentioned in this thesis, unless indicated otherwise. Zeocin was purchased by InvivoGene (USA). Laccase from *Aspergillus* was purchased from Novozyme. UV Transparent Plate (96 well) was purchased from Thermofisher (Canada). ABTS diammonium salt, the DNA extraction kit and the PCR Purification Kit were purchased from Bio basic (Canada) and QIAGEN. PDHs-KM71H, GalOX-KM71H, empty KM71H cells and empty DH5 alpha cells were provided by our collaborator, Dr. Emma Master at the University of Toronto. Xylooligosaccharide (XOS) was purchased from Changsheng (China).

2.1 Recombinant production of *Ab*PDH1 and GalOX

2.1.1 The *Pichia Pastoris* expression system

The *Ab*PDH1 and GalOX enzymes were produced recombinantly in *Pichia pastoris*. cDNAs encoding the wild type *Ab*PDH1 and GalOX were previously transformed following the procedure defined in the EasySelect™ *Pichia* Expression Kit USER GUIDE, 2010; Mengwasser et al., 2011), into the methylotrophic yeast *Pichia pastoris* strain KM71H, which has been widely used in industry to produce recombinant proteins, largely based its post-translation modifications (Chang et al., 2018). Fungal carbohydrate oxidoreductases require glycosylation to occur in the endoplasmic reticulum (ER) and Golgi apparatus to ensure

proper folding, such that bacterial expression systems cannot be applied and the yeast system was used instead (Reily et al., 2019). The KM71H *P. pastoris* strain enables the secretion of recombinantly produced enzymes that include a secretion signal, into low-cost media. KM71H cells transformed to include cDNA encoding the enzyme targets, were incubated in BMGY (Buffered Glycerol-complex Medium) [BMGY: 1 % (w/v) yeast extract, 2 % (w/v) peptone, 1.34 % (w/v) yeast nitrogen base, 1 % glycerol, 100 mM potassium phosphate buffer pH 6.0, $4x10^{-5}$ % (w/v) biotin] to produce more cells by consuming glycerol as the carbon source. Upon transfer of the obtained cells into BMMY (Buffered Methanol-complex Medium) [BMMY: 1 % (w/v) yeast extract, 2 % (w/v) peptone, 1.34 % (w/v) yeast nitrogen base, 1 % methanol, 100 mM potassium phosphate buffer pH 6.0, $4x10^{-5}$% (w/v) biotin], they metabolize methanol as sole carbon source, which co-incidentally stimulates the expression of the heterologous target enzymes.

The protein expression induction system is mainly controlled at the transcription step of the AOX (alcohol oxidase) genes in *Pichia pastoris,* AOX1 and AOX2. When the cells are grown in glycerol or glucose, even in the presence of methanol, the transcription of AOX genes by the P_{AOX} promoter is repressed. When methanol becomes the sole carbon source, the P_{AOX} promoters (naturally regulating expression of the AOX genes) are derepressed, activating the expression of any heterologous proteins under their regulation. The AOX1 gene itself plays a main role on the transcription regulation, where cells containing it grow very fast using methanol as a carbon source, resulting in consumption of a large amount of methanol and generally lower yields of target enzyme. To reduce the growth rate in the presence of methanol, the Mut^S, Arg^+ *P.pastoris* (phenotype) strain KM71H can be used, replacing the native AOX1 gene with arg4aox1::ARG4 genotype (Schotte et al., 2016). This means that that ARG4 gene (argininosuccinate lyase gene) is inserted to disrupt the AOX1 gene. While it may lead to the yeast cell requiring arginine, this phenotype is methanol

utilization slow due to the loss of AOX1 (EasySelect™ *Pichia* Expression Kit, 2010; Mengwasser et al., 2011), potentially decreasing input costs at industrial scale preparation.

2.1.2 Large scale recombinant production of wild-type *Ab*PDH1 enzyme

*Ab*PDH1 (NCBI assession number: Q3L1D1) was expressed in *Pichia pastoris* strain KM71H. pPICZB expression constructs encoding this protein were produced in the laboratory of Dr. Emma Master at University of Toronto, included a 6X His tag at the C-terminus and were transformed into KM71H cells. These were stored at -80 ℃ in 50% glycerol. For protein production, the *Ab*PDH1-KM71H cells were inoculated onto a YPD agar plate with 100 µg/ml zeocin, and incubated at 30 ℃ for 3 days. A single colony from this agar plate was used to inoculate 100 mL of YPD liquid media and the culture incubated at 30 ℃ overnight with shaking at 180 rpm. A total of 10 mL each of this overnight culture was added in 6 x 4 L shake-flasks each containing 1L of BMGY medium, and the cultures were incubated at 30 ℃ with 180 rpm shaking (New Brunswick Scientific, USA) overnight. The cells from the 6 L of culture were collected by centrifugation (Beckman Coulter, USA) at 3980 x g for 5 mins at room temperature, and then re-suspended in a total 1.2 L of BMMY containing 1 % methanol in one 4 L shake-flask for induction of *Ab*PDH1 expression. This culture was incubated at 15 ℃ with 160 rpm for 4 days, where 12 mL methanol was added to the culture every 24 h to keep the methanol at 1 %. After 4 days, the culture supernatant was collected by centrifugation at 8983 x g for 15 mins at 4 ℃, and filtered with a 0.45 um sterile Whatman® aqueous solution filter (Global Life Sciences Solutions Operations, UK). The *Ab*PDH1 in the 1.2 L filtered supernatant was subsequently concentrated to about 600 mL using a 10 kDa Pellicon XL Cassette with Biomax Membrane (EMD Millipore Corporation), and stored at 4 ℃ overnight (shorter is better) ahead of purification.

2.1.3 Large scale recombinant production of GalOX

GalOX (NCBI assession number: NP0CS93) was also expressed in *Pichia pastoris* strain KM71H. Its expression method was the same as *Ab*PDH1 production described above, but 0.2 mM of copper sulfate pentahydrate, $CuSO4 \bullet 5H_2O$ was separately added into the cultures at both of the BMGY and BMMY culturing stages.

2.2 Affinity purification of recombinantly produced *Ab*PDH and GalOX

Concentrated culture supernatants containing recombinantly produced *Ab*PDH and GalOX were initially adjusted to pH 7.5 with sodium hydroxide (NaOH). The supernatants (600 mL) were then loaded using a superloop, through a 5 ml Ni-NTA (nickel-nitroloacetic acid) resin column (Cytiva, USA) attached to a Fast Performance Liquid Chromatography (FPLC) Instrument (BioRad, USA), such that the His-tagged recombinant protein targets would stick to the resin, while the rest of the contaminating proteins would flow through. The FPLC was run at a flow rate of 2-4 mL/min for all steps. The loaded column was washed with washing buffer (50 mM NaH_2PO_4, 300mM NaCl, 10 mM imidazole, pH 7.5), and the recombinant His-tagged proteins eluted with elution buffer (50 mM NaH_2PO_4, 300mM NaCl, 500 mM imidazole, pH 7.5) into 2.5 mL fractions, monitoring protein elution at A280 nm. Following the initial round of purification, the original flowthrough was re-loaded onto the column for an additional round of purification to extract any residual target protein that did not bind in the initial round due to the large loading volume.

The eluted fractions containing protein were combined and buffer exchanged into sodium phosphate buffer at pH 6.0 by centrifugal filtration with a 10 kDa membrane cut-off (Amicon) with centrifugation 5000 x g at 4 ℃ for 30 mins, four times. Finally, the obtained sample was diluted 1000-fold, concentrated to 2 mL and aliquoted into 50 μL fractions, and the concentrated enzymes fast frozen by liquid nitrogen and stored at -80 ℃.

2.3 Initial enzyme activity measurements and enzyme quantification

To quantify the amount of enzyme obtained and its enzymatic activity before application to crosslinker generation at a large-scale, smaller scale 250 µL reactions were performed at 30 ℃ with 432 rpm shaking in a 96-Well UV plate (Thermofisher, Canada) with monitoring by UV-Vis measurement with the Infinite® M Plex plate reader (Tecan, USA).

2.3.1 *Ab*PDH1 activity measurement

In the case of the *Ab*PDH1 oxidation reaction, a metal containing compound is required to serve as an electron acceptor, which can also be used as a dye to track enzymatic activity. The absorption of light by the metal containing compound changes depending on its redox state. Thus, as the enzyme reaction proceeds and the metal is reduced as it accepts electrons, its UV-Vis absorbance profile can be monitored to directly measure the amount of reduced metal compound, indirectly representing *Ab*PDH1 activity. Therefore, the enzymatic activity of *Ab*PDH1 on xylose and XOS can be detected by UV-VIS measurement with three different redox electron acceptors/indicators Fc/Fc+ (ferrocene), BQ/HQ (1,4-benzoquinone/hydroquinone) and DCIP/DCPIPH_3 (2,6-dichlorophenolindophenol) (Peterbauer et al., 2020).

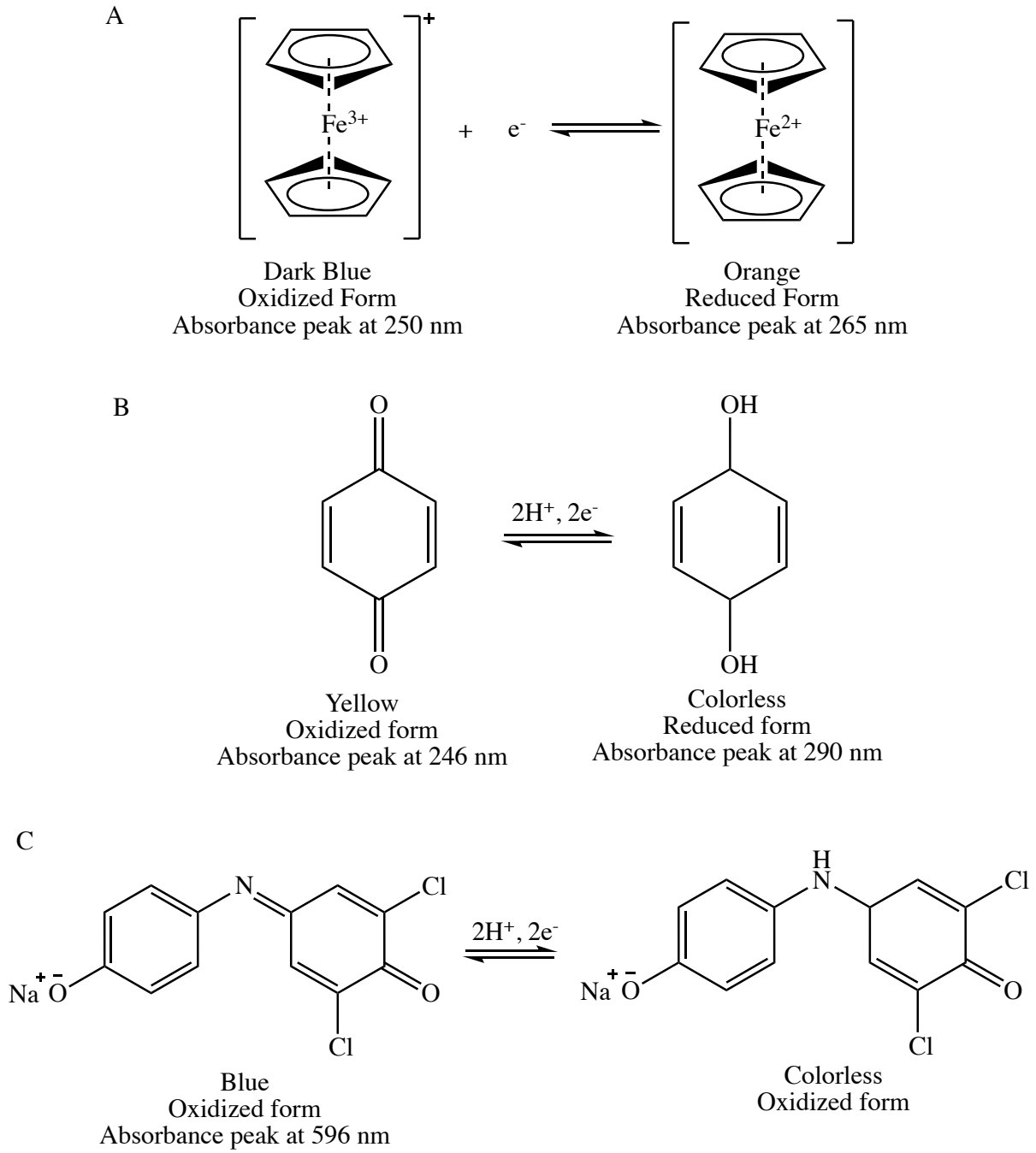

Figure 2.1: The redox cycles for the *Ab*PDH1 colorimetric assays. Fc+, BQ and DCIP receive 2 hydrogen ions and 2 electrons from the oxidation reaction catalyzed by *Ab*PDH1. The obviously color change indirectly instruct the *Ab*PDH1 reaction process. A) Fc+/Fc redox cycle: monitoring absorbance at 250 nm, measuring the decrease of Fc+ concentration (Fabbrizzi, L. 2020). B) BQ/HQ redox cycle: monitoring absorbance at 290 nm, measuring the formation of HQ concentration. The absorbance can also be monitored at 246 nm, measuring the formation of BQ. C) DCIP/DCPIPH3 redox cycle: monitoring absorbance is at 520 nm, measuring the decrease of DCIP concentration. The absorbance at the peak (596 nm) is too high to measure.

The BQ/HQ redox cycle was selected to test the *Ab*PDH1 activity. It was measured by reacting *Ab*PDH1 (15 µl) with the substrate (100 mM D-xylose or 30 mM D-galactose) and the electron acceptor 3 mM BQ (Sigma-Aldrich, Germany) ($\varepsilon_{abs290nm}$ = 2.24 $mM^{-1}cm^{-1}$), separately in 50 mM sodium phosphate buffer at pH 6.5 for xylose and 50 mM sodium acetate at pH 5.0 for galactose. The concentrated *Ab*PDH1 was diluted to 1000X, 10,000X, 100,000X and 1000,000X, and each dilution was measured in triplicate. The reactions with BQ were measured at 290 nm. Laccase expressed from Aspergilus sp. (Novozyme, # 51003) was also exchanged into sodium phosphate buffer at pH 6.0 as described above. The activity of the laccase was measured by reaction with 3 mM HQ (Sigma Aldrich, Germany) ($\varepsilon_{abs249nm}$ = 17.25 $mM^{-1}cm^{-1}$) in 50 mM sodium acetate at pH 5.5. A total of 15 µL of the obtained laccase at 1000X, 10,000X, 100,000X and 1000,000X were reacted in triplicate and monitored at 249 nm to measure its activity.

2.3.2 GalOX activity measurement

ABTS [2,2'-azinobis(3-ethylbenzthiazolinesulfonic acid)] can be used as the colorimetric chemical to measure how much H_2O_2 is produced by the GalOX catalysis reaction. It can be visually seen by eye and also can be monitored spectrophotometrically (Parikka et al, 2015). With the reaction with H_2O_2, ABTS molecule can be converted to a $ABTS^{+\bullet}$ cation that causes the aqueous buffer to turn to green, a color that can be measured at 418 nm (Figure 2.2) ($\varepsilon 418nm = 36$ $mM^{-1}cm^{-1}$).

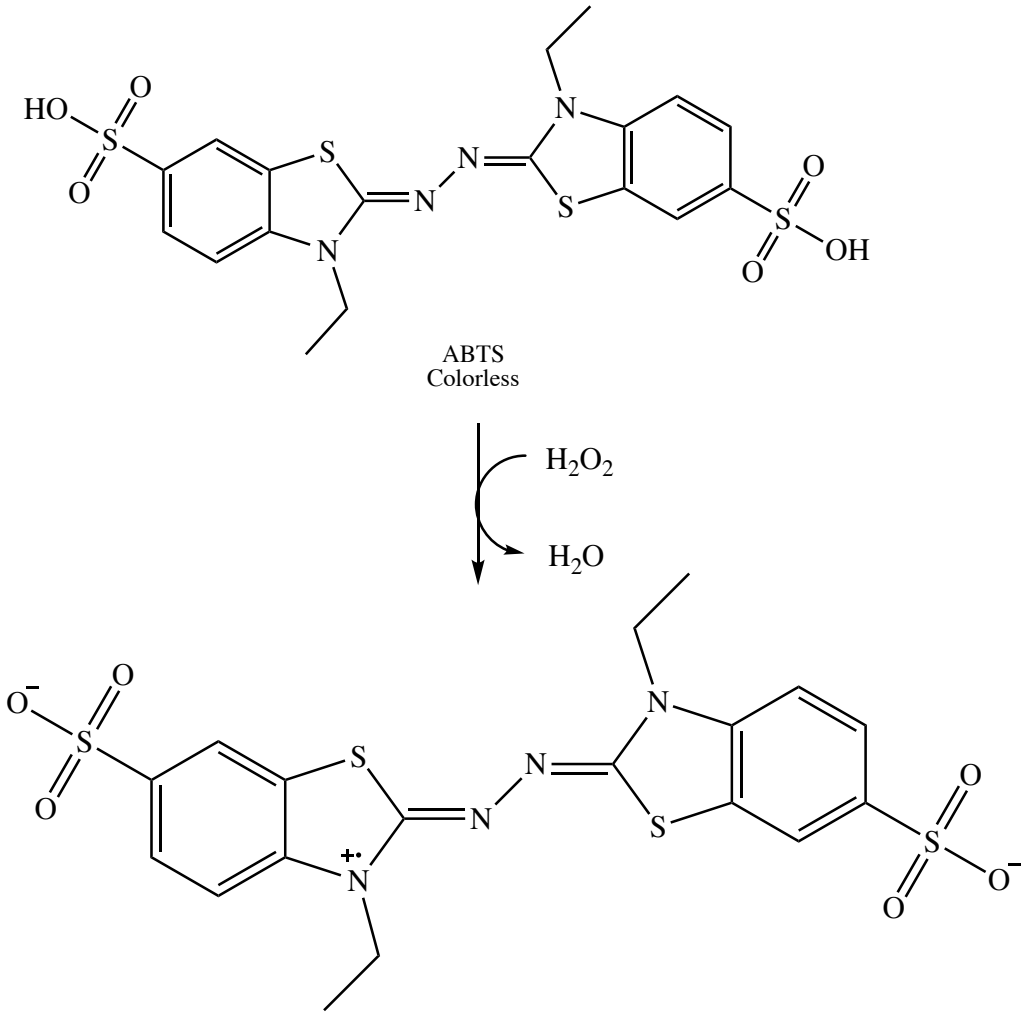

***Figure 2.2*: The reaction ABTS to $ABTS^{+\bullet}$ cation (Dolz et al., 2023).**

The concentrated GalOX was also diluted to 1000X, 10,000X, 100,000X, 1000,000X and 10,000,000X. Each dilution (15 µL) was measured by reacting with 30 mM D-galactose (25 µL) in 210 µl of ABTS buffer (6.5 U/ml horseradish peroxidase (HRP), 2.4 mM ABTS, 62.5 mM sodium phosphate pH 7.25). HRP was used to promote the GalOX activity as described previously (Wu et al., 2019; Tressel & Kosman, 1980). A total of 2 nmol, 4 nmol, 6 nmol, 8 nmol and 10 nmol of H_2O_2 in 40 µL ddH2O were added into the 210 µL of ABTS buffer to produce a standard curve to quantify the H_2O_2 production in the GalOX oxidation

on substrates. The reactions were measured at 420 nm (Woo et al., 2003; Ilyasov et al., 2020), each reaction was performed in triplicate as well.

2.3.3 SDS-PAGE analysis for enzyme quantification

Enzymes were loaded on 10% stacking gel to assess and quatify the produced enzymes, where the gels were run in the running buffers [0.25 M Tris HCl, 1.92 M glycine and 1% (w/v) Sodium Dodecyl Sulfate (SDS), pH ~8.3] at the voltage 120V for around 1.5 h until the sample dye reached the bottom of the gel. After running, the gel was stained with Coomassie Brilliant Blue G-250 (BioRad, United Kingdom) and imaged by Bio-RAD ChemiDocTM XRS+ Molecular Imager®.

2.4 Crosslinker production

2.4.1 Large scale enzymatic oxidation of XOS by *Ab*PDH1

The XOS oxidation reactions (300 ml total) were prepared by mixing 50 mL of 60 mg/mL XOS solution, 12 mL of 25 mM BQ, 2.7 mL of 334 U/mL laccase and 1.2 mL of 300 U/mL *Ab*PDH1 in 234 mL of ddH_2O. The reaction solution was initially adjusted to pH 6.3 by adding 250 μL of 0.17 M acetic acid, and then was divided into six 250 mL flasks with 50 mL of the reaction solution in each. A control (ctrl.) reaction without *Ab*PDH1 and a standard (std.) reaction were prepared as well at 50 ml volume (See Table 2.1 for details). The flasks were incubated at 30 ℃ with shaking at 200 Lpm for 24 h. The pH value reduced during the reaction process, so the reaction solutions in the six flasks were combined and the pH adjusted to 6.3 by adding NaOH, at 2 h, 4.5 h, 20 h and 26 h and then divided back into 50 mL reactions. A total of 50 μL of solution at each of these time points was kept for product analysis. After 26 h, the reaction solution was centrifuged at 5000 x g for 10 mins at 4 ℃, and filtered with 0.45 μm filter. Finally, enzymes were removed from the solution by centrifugal filtration with a 10 kDa concentrator at 5000 x g for 20 mins at 4 ℃, where the flowthrough

containing the oxidized sugar was collected and frozen at -20 ℃. The frozen samples were transferred to -80 ℃ and then lyophilized to dryness.

Table 2.1: The concentration of each reagent in the XOS oxidation reaction by *Ab*PDH1.

Sample	XOS (mg/ml)	BQ (mM)	Laccase (U/ml)	PDH (U/ml)	Total Volume
PDH-XOS	10	1	3	1.25	300
XOS-ctrl	10	1	3	0	50
XOS-std	10	0	0	0	50

2.4.2 Large scale enzymatic oxidation of lactose by GalOX

A 1965 U/ml HRP solution was prepared by dissolving 5 mg of HRP in 5 ml ddH_2O**;** a 22204 U/ml catalase solution was prepared by dissolving 70 mg of catalase from bovine liver (Sigma-Aldrich, Germany) in 10 ml ddH_2O. Both HRP and catalase were added to promote the GalOX oxidation activity as described previously (Wu et al., 2019; Tressel & Kosman, 1980). Enzyme mixtures were additionally prepared for lactose oxidation reaction by GalOX, containing 54252 U of GalOX (1.2 mL of GalOX stock in the concentration of 45210 U/mL), 8056 U of HRP (4.1 mL of 1965 U/mL HRP) and 162089 U of catalase (7.3 mL of 22204 U/mL catalase), for a total volume of 30 mL (17.4 mL of ddH_2O). GalOX oxidation of lactose reaction (100 mL total) was prepared by reacting 30 mL of the GalOX enzyme mixture with 50 mL of 300 mM lactose solution in 20 ml of ddH2O. And then, the 100 mL of lactose oxidation reaction by GalOX was separated into five flasks with 20 mL of the above mixture for each. A no-GalOX enzyme mixture was prepared for the control reaction for lactose oxidation by GalOX, containing 0.82 mL of 1965 U/mL and 1.46 mL of 22204 U/mL catalase in 3.72 mL of ddH_2O. The control reaction (20 mL total) was prepared by mixing 6 mL of non-GalOX enzyme mix, 10 mL of 300 mM lactose and 4 mL ddH_2O. The standard reaction was prepared by adding 10 mL of 300 mM lactose and 10 mL of water

as well. See Table 2.2 for a summary of reactions. The reactions were incubated at 30 ℃ with saking at 180 rpm for 6 h. During this time, 50 μL samples were taken from the reaction at 1 h, 3 h, 4.5 h and 6 h for product analysis in the next step. The final reactions were subsequently centrifuged at 3500 x g for 10 mins at 4 ℃ and filtered with 0.45 µm filter. Enzymes were also removed from the solution by centrifugal filtration with 10 kDa Mw limit membrane concentrator, centrifuged at 5000 x g for 20 mins at 4 ℃, where the flowthrough containing the oxidized sugars was collected and frozen at -20 ℃. The frozen solution was transferred to -80 ℃ and then lyophilized.

Table 2.2: The concentration of each reagent in the lactose oxidation reaction by *GalOX*.

Sample	Lactose (mM)	GalOX (U/ml)	HRP (U/ml)	Catalase(U/ml)	Total Volume
GalOX-lac	150	581	81	1622	100
GalOX-lac-ctrl	150	0	81	1622	20
Lac-std	150	0	0	0	20

2.4.3 Quantification of the production of oxidized-XOS and oxidized-lactose

A total of 25 µL of each obtained oxidized sugar sample were separately mixed with 225 µL of 2 mM NaOH solution in Nunc^{TM} 96-well polypropylene microplate (Thermo Fisher Scientific, USA), covering with Nunc^{TM} 96-well silicone cap mats (Thermo Fisher Scientific, USA). Quantification of the oxidized carbohydrates was performed by high-performance anion-exchange chromatography with pulsed amperometry detector (HPAEC-PAD). There were two elution solutions for HPAEC-PAD. Solution A was 100 mM NaOH and Solution B was 100 mM NaOH + 1 M NaOAc. The elution flow rate was 0.25 mL/min. At 0-35 mins, Solution A was 90% and Solution B was 10%. Solution A was decreased to 80

% from 35 min to 45 min. Then Solution A was increased back to 90% from 45 min to 55 min, and then increased to 100 % from 55 min to 60 min.

2.5 Crosslinked chitosan hydrogel production and characterization

Crosslinked chitosan hydrogels were produced by mixing the oxidized-XOS or the oxidized-lactose with chitosan all at the indicated concentrations. To form the gel, the high molecular weight chitosan extracted from shrimp shells, practical grade (Sigma-Aldrich) was dissolved in acetic acid solution, where 2 % chitosan solution was prepared in 1 % acetic acid, and 3 % chitosan solution was prepared in 1.5 % acetic acid.

The reactions were tested at different pH by adjusting the content of sodium phosphate dibasic (Na_2HPO_4). Small scale (100 µL) and large-scale reactions (1 mL and 5 mL) reactions were attempted. Chitosan in acetic acid solution is too viscous to transfer by pipettes, so it was difficult to measure it by volume. Assuming the density of the chitosan solution is the same as water (i.e. $\rho_{\text{aqueous solution}}$ =1 g/mL), the viscous chitosan solution was measured on the basis of weight. E.g. 1 g of chitosan solution is 1 mL. To prepare the 100 µL gel, the chitosan-Na_2HPO_4 solution (8 mg/mL for a final 7.4 mg/mL chitosan gel, 15 mg/mL for a final 13.8 mg/ml chitosan gel) was initially prepared by weighing (2 % or 3 %) chitosan solution in a 50 mL tube, and then the Na_2HPO_4 in different amount was added, followed by vortexing. The chitosan-Na_2HPO_4 solution was mixed with the oxidized-sugar crosslinkers by pipetting given amounts, to achieve the desired test conditions, into PCR tubes. The gel formation was assessed visually by inverting and shaking the PCR tubes, where gel was identified as having formed if the tube contents would not flow down. To prepare the 5 mL gel (Table 2.3), 3 % chitosan solution in 1.5 % acetic acid was weighed in vials (1.23 g for preparing 7.4 mg/ml gel and 2.3 g for preparing 13.8 mg/ml gel). ddH_2O (2.19 mL) was added into the vials for 7.4 mg/ml gel, and then vortexed to mix with chitosan. ddH_2O was not required for the 13.8 mg/ml gel formation. Na_2HPO_4 (0.5 M) was added into each vial,

followed by more vortexing immediately to prevent the chitosan solubility decreasing due to exposure to localized high pH. At last, crosslinkers were added into the solution and vortexed immediately. After gel formation, no violently shaking was permitted. See Table 2.3 for details

Table 2.3: The reaction preparation for 5 ml chitosan gel formation.

Reagent	7.36 mg/ml chitosan sample	13.8 mg/ml chitosan sample
3 % chitosan in 1.5 % acetic acid (g)	1.23	2.3
1 M Crosslinkers (ml)	0.2	0.2
0.5 M Na_2HPO_4 (ml)	1.38	2.5
ddH_2O (ml)	2.19	0

2.6 Rheological methods

Chitosan gels solutions (5 mL) were prepared in a vial and mixed well by vortexing as per Table 2.3, where the oxidized-XOS crosslinker was the last reagent added into the solution. The vials were immediately vortexed, and then transferred to the fixed plate (bottom plate) of the Discovery Hydrid Rheometer (TA Instruments, USA) before the gel formation. By clicking start on the computer, the rotating plate (top plate) was lowered to press the gel sample. The extra gel solution outside the dynamic plate was removed by Kimwipes. The distance between two plates was set to 500 μm. The rotating plate was rotated at 10 rad per second to apply an extensional pressure to the gel. Two stress results were measured: the storage modulus G' (Pa) and the loss modulus G'' (Pa). The ratio of G''/G' is called tan (δ), which is an indicator for identifying gel formation (determine liquid form or solid form), showing the conflict between the stress given by the top plate and the deformation of the gel. G' is also called elastic modulus, and the gel should be in elastic (gel) behaviour when G'>G''; G'' is also called viscous modulus, and the gel should be in viscous (liquid) behaviour when G'' >G'.

Chapter 3

Results

3.1 Production and purification of oxidizing enzymes

3.1.1 *Ab*PDH1 production and purification

Following large scale growth of KM71H cells transformed with pPICZB-*Ab*PDH1 in BMGY and induction of *Ab*PDH1 expression in BMMY, the obtained BMMY supernatants were adjusted to pH 7.5 with the addition of NaOH and subjected to Ni-NTA affinity chromatography using an FPLC instrument (Figure 3.1a). However, after the first round of purification, there was still *Ab*PDH1 remaining in the flowthrough (0-4 min). Thus, a second round of Ni-NTA purification was completed, reloading the flowthrough fraction through the column (Figure 3.1b). A unique peak was eluted at 14-24 min for round 1 and 15-24 min for round 2. The tubes containing the eluted protein were combined, buffer exchanged into 50 mM of sodium phosphate pH 6.0, and concentrated to a total of 2.2 mL. This was considered the *Ab*PDH1 stock solution.

A

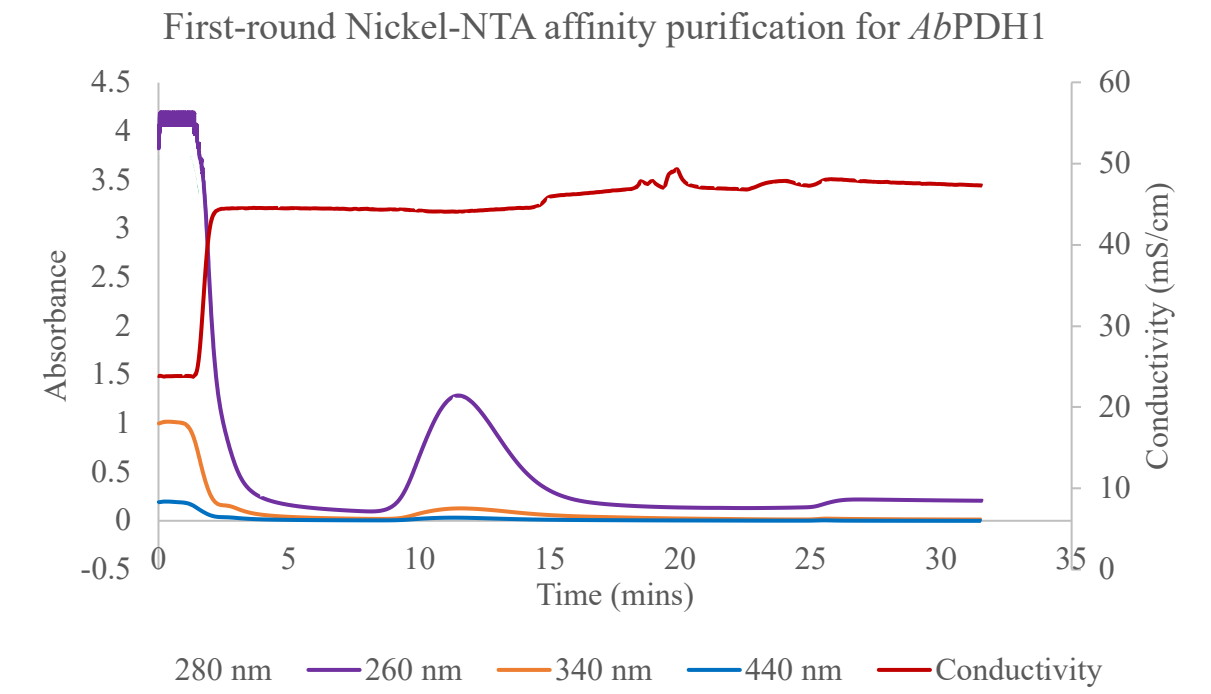

B

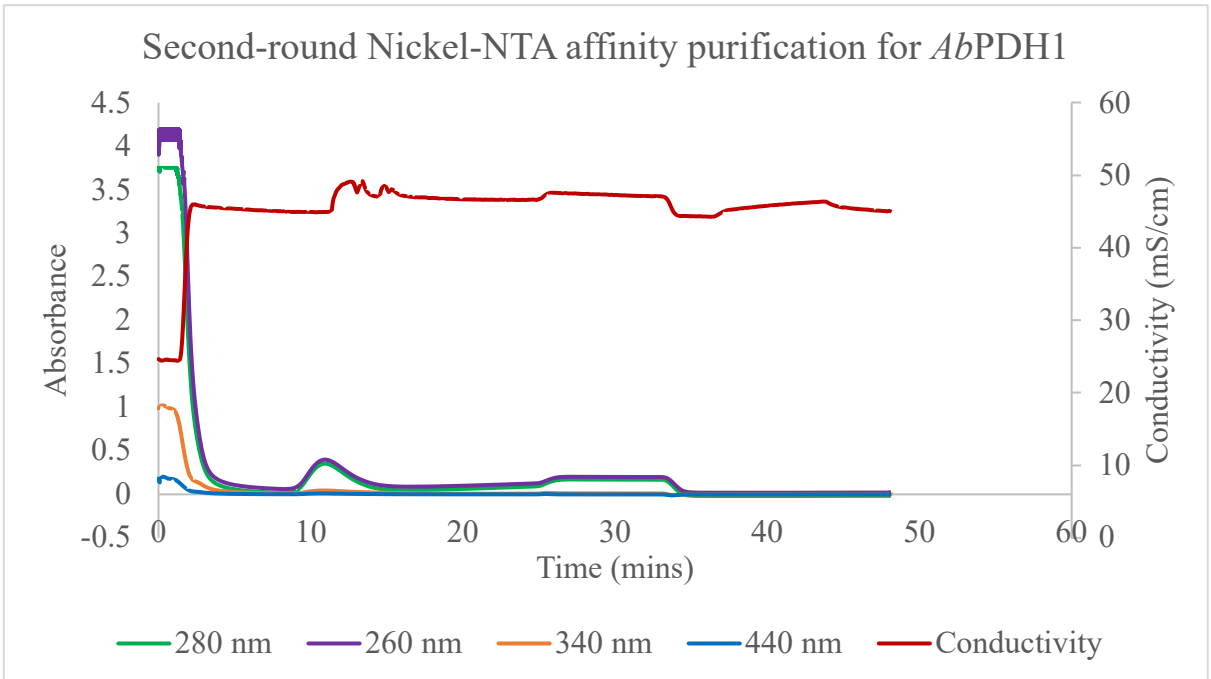

Figure 3.1: Nickel-NTA affinity purification elution profiles for wild-type *Ab*PDH1 using FPLC. a) First-round purification. b) Second-round purification of the flow through arising from the first-round purification. For both panels, the axis x is time (min) and the y axis (left) is absorbance and y axis (right) is conductivity (mS/cm). For the lines, green is the absorbance at 280 nm, purple is the absorbance at 260 nm, orange is the absorbance at 340 nm, blue is the absorbance at 440 nm, red is the conductivity. Flow through is 0-4 minutes in both cases.

The concentrated enzyme stock was diluted 5 x and 10 x for SDS-PAGE analysis. Karppi et al., mentioned that the expected MW of *Ab*PDH is 65 kDa, but its corresponding SDS-PAGE band is always shown at around 92 kDa due to glycosylation (Karppi et al., 2020). The SDS-PAGE results here are consistent with this, where a broad band ranging from 75-100 kDa was observed (Figure 3.2). The total amount of expressed *Ab*PDH1 from 6 L of BMGY was estimated based on comparison to a bovine serum albumin (BSA) standard curve on the gel, showing a yield of 16.5 mg *Ab*PDH1 expressed from 6 L of culture, and producing an *Ab*PDH1 stock concentration of 7.5 mg/mL for the 2.2 mL stock. This was calculated by averaging the loaded protein amount results of 5 µL of 5x dilution, 5 µL of 10x dilution and 10 µL of 10x dilution of the *Ab*PDH1 stock. The substantial band observed at around 15 kDa MW may be a breakdown fragment of the protein.

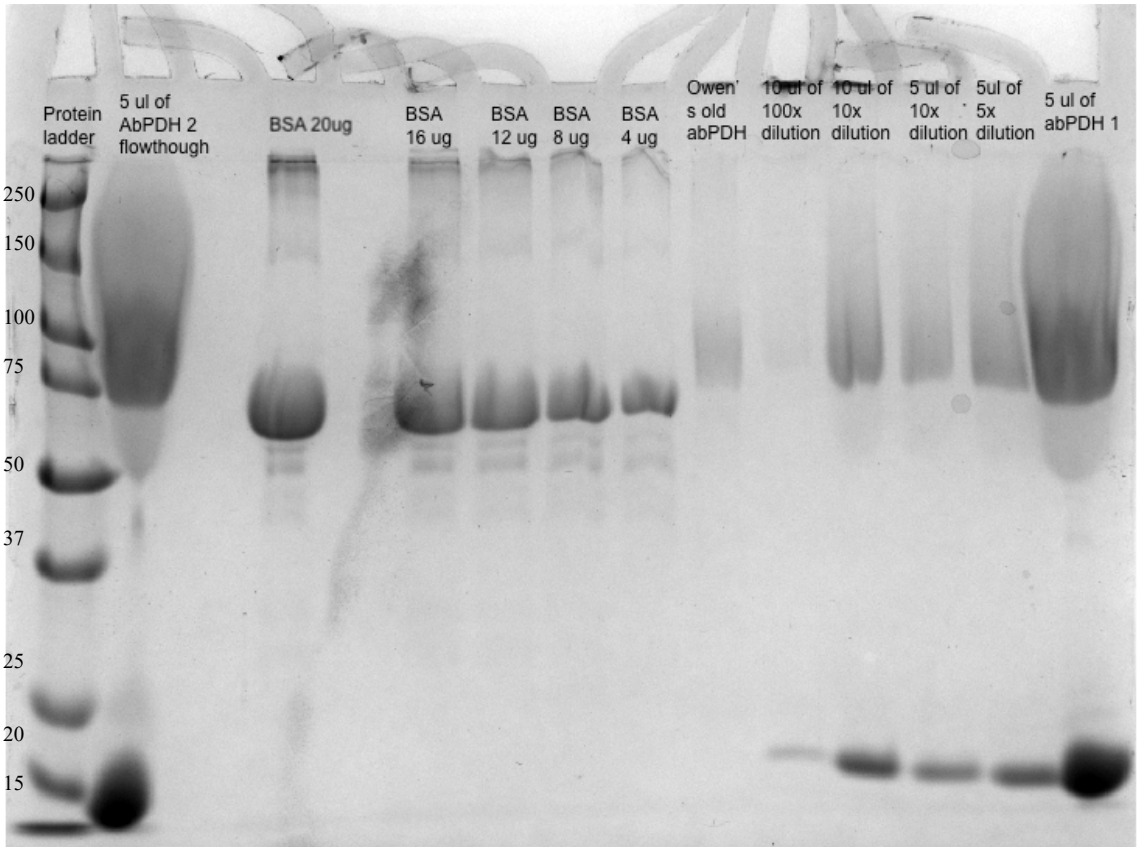

Figure 3.2: SDS-PAGE gel quantifying the concentration of purified *Ab*PDH1 in the obtained stock (2.2 mL sample). *Ab*PDH1 was purified by Ni-NTA affinity chromatography in two rounds, an initial round and then reapplication of the flowthrough from round one, as a second round. The obtained fractions were pooled and concentrated to 2.2 ml in sodium

phosphate pH 6.0. The concentrated *Ab*PDH1 was diluted and loaded onto the gel as indicated. Band intensities were compared to those arising from bovine serine albumin (BSA). The protein ladder is Precision Plus Protein Dual Color Standards (Bio-RAD, USA) with kDa molecular weights indicated.

The *Ab*PDH1 stock was additionally diluted 100x, 1000x, 10000x for quantifying enzymatic activity. Activity measurements are reported in Figure 3.3 and Table 3.1 and indicate 270.7 U of activity per mL in the 2.2 mL *Ab*PDH1 stock (i.e. 36.1 U/mg ± 3.7), where 1 U of *Ab*PDH1 refers to 2 µmol of BQ reduced to 1 µmol of HQ per minute. Previously Karppi mentions their *Ab*PDH1 activity on D-xylose is 43-45 U/mg (Karppi et al., 2020), consistent with results herein.

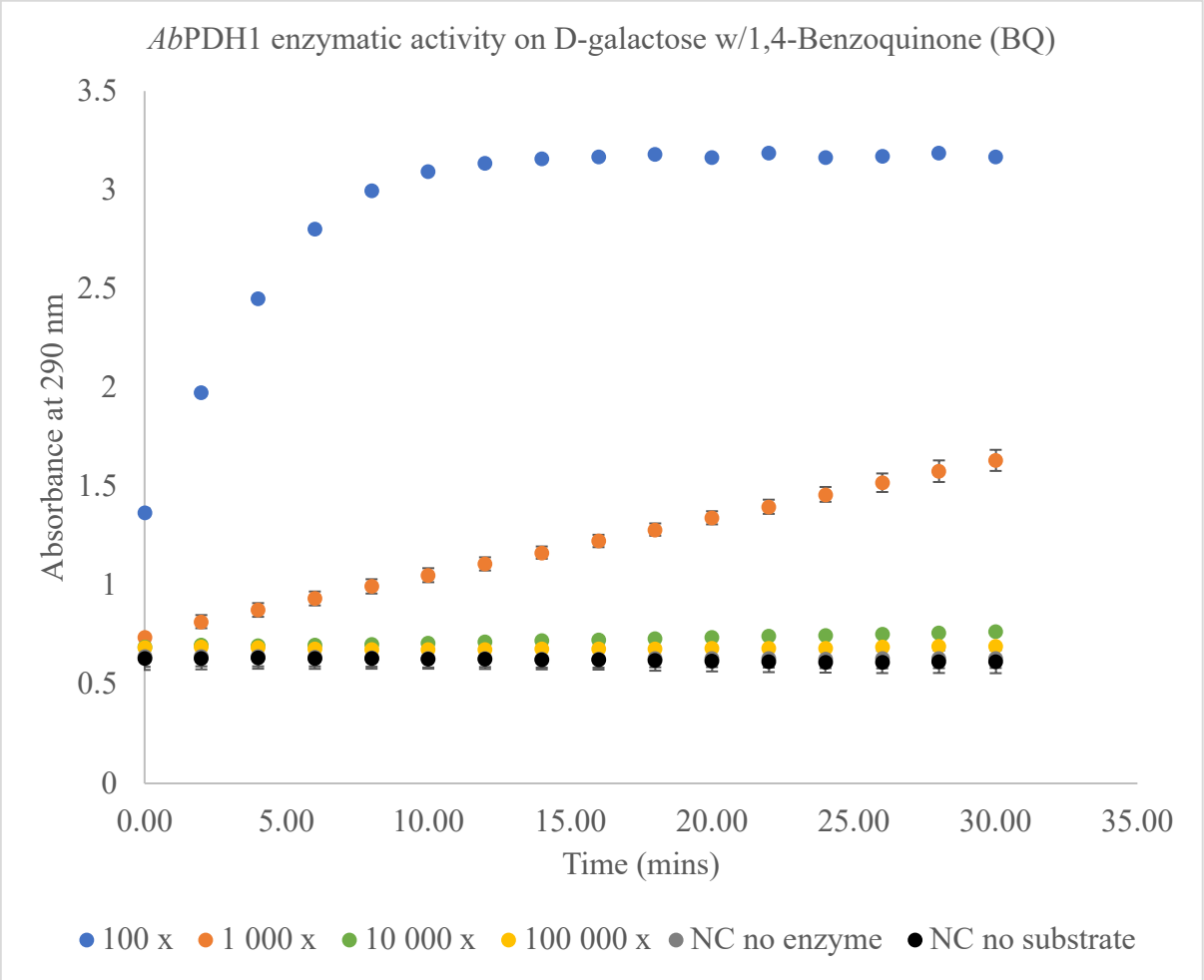

Figure 3.3: Enzymatic activity of the *Ab*PDH1 stock (2.2 ml sample). UV-Vis spectroscopic measurement of *Ab*PDH1 ability to oxidize D-galactose. The conversion of BQ to HQ is measured at 290 nm. Error bars show the standard deviation of n=3 experiments at each time point.

Table 3.1: Enzymatic activity of the *Ab*PDH1 stock (2.2 ml sample). Obtained from the slope (first 6 minutes for 100x; Figure 3.3) obtained upon conversion of BQ to HQ measured at 290 nm, after subtraction of any detected activity in the negative control, no enzyme sample. The stock *Ab*PDH1 was diluted as indicated. Error is the standard deviation of n=3 repetitions.

	100x dilution	*1000x dilution*	*10 000x dilution*
Slope (mAbs/min)	239.2 ± 4.6	29.7 ± 0.8	2.9 ± 0.1
Total Enzyme Activity (U)	515.18 ± 9.9	640.2 ± 17.9	630.9 ± 11.1
Activity Concentration (U/ml)	234.2 ± 4.5	291.0 ± 8.1	286.8 ± 5.1
Specific Activity (U/mg)	31.2 ± 0.6	38.8 ± 1.1	38.2 ± 0.7

3.1.2 GalOX production and purification

The method of production of GalOX was the same as for *Ab*PDH, except that $CuSO_4$ was added to both the BMGY and BMMY media during *P. pastoris* growth and induction. Purification was also based on Ni-NTA chromatography. In this case no significant GalOX was detected in the flow through fraction, such that a second round of purification was not necessary. Only a single peak at 12 minutes was detected upon elution , representing the GalOX (Figure 3.4).

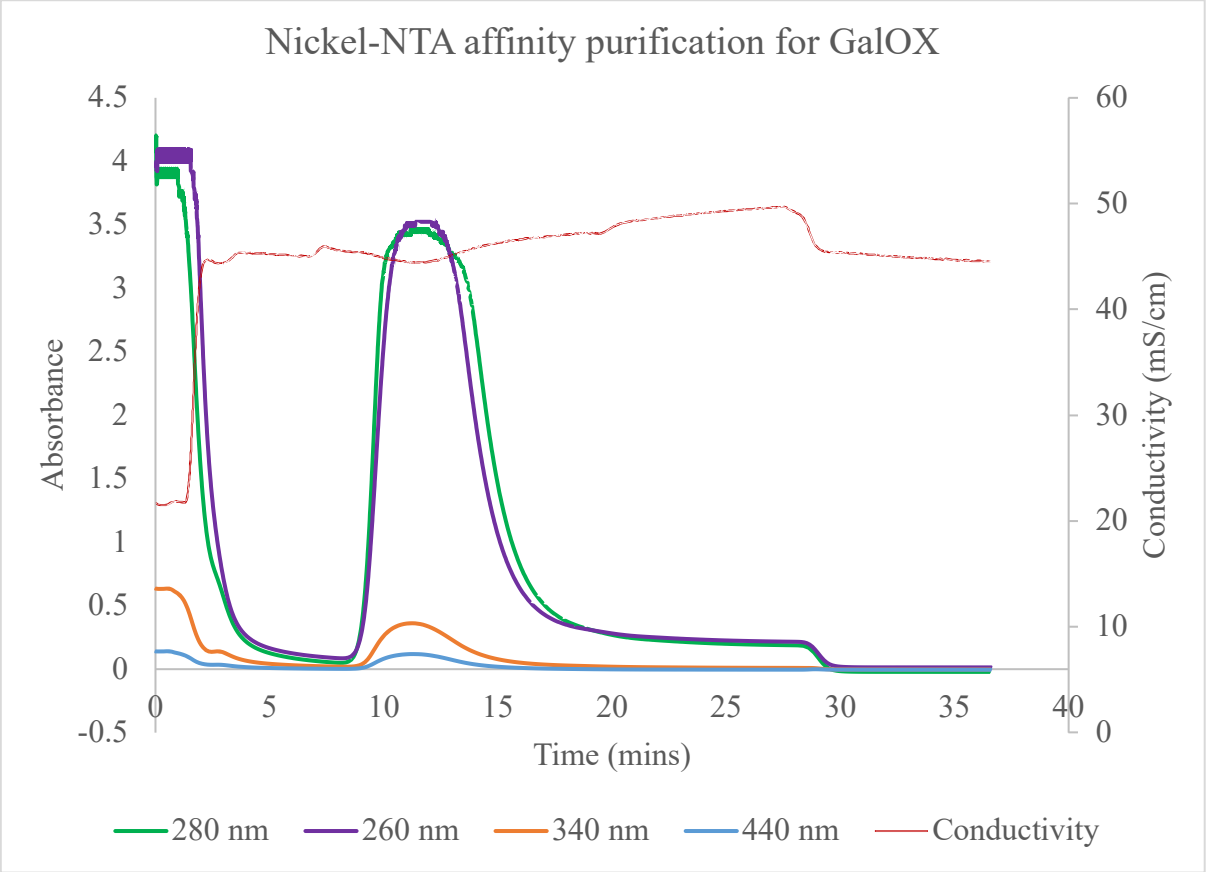

Figure 3.4: Nickel-NTA affinity chromatography for purification of wild-type GalOX, using an FPLC. The axis x is time (min), the left y axis is absorbance and the right y axis is conductivity (mS/cm). For the lines, green is the absorbance at 280 nm, purple is the absorbance at 260 nm, orange is the absorbance at 340 nm, blue is the absorbance at 440 nm, red is the conductivity.

SDS-PAGE was used to track accumulation of GalOX in the media during the growth phase (Figure 3.5), where the expected MW of GalOX is approximately 65 kDa (Mototsune et al., 2024), consistent with observations here. Fractions were pooled and the sample concentrated and buffer exchanged into a final stock of 2.0 mL.

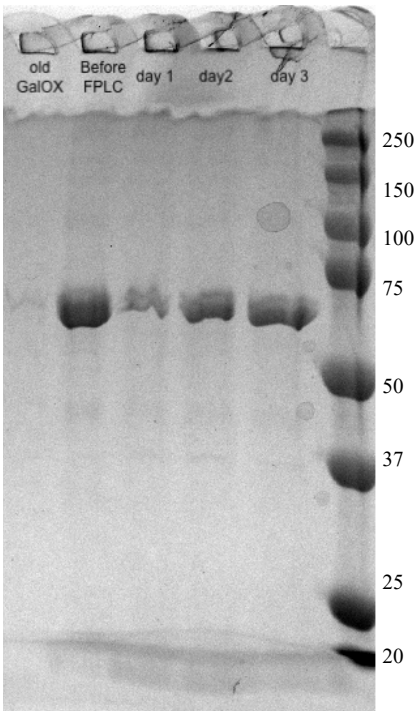

Figure 3.5: SDS-PAGE showing accumulation of GalOX over time during induction. A total of 10 μL of the BMMY supernatant at day 1-3 during cell induction was loaded on the gel. The right most unlabelled lane is Precision Plus Protein Dual Color Standards (Bio-RAD, USA) with kDa molecular weights indicated. The 'old GalOX' was a gift from the lab of Emma Master.

Quantification of the concentration of GalOX stock solution by SDS-PAGE comparison to BSA standards (Figure 3.5) revealed 95.7 mg/mL GalOX. This value was obtained by averaging results of loading 2 µL of 10 x dilution, 1 µL of 10 x dilution, 8 µL of 10 x dilution, 10 µL of 10 x dilution and 5 µL of 10 x dilution.

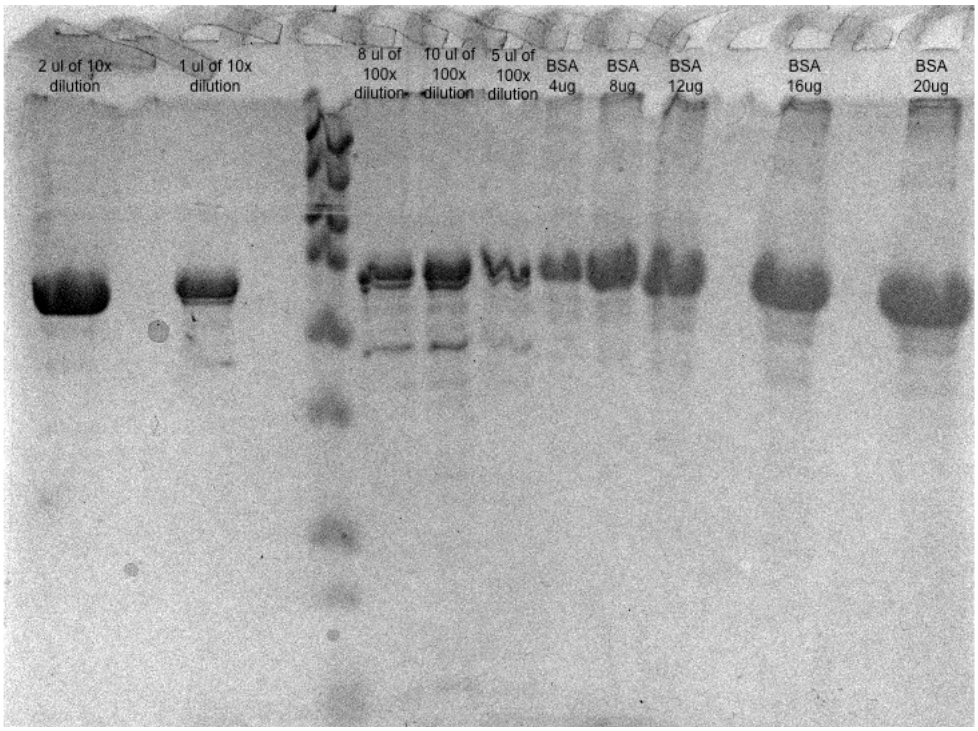

Figure 3.5: SDS-PAGE gel quantifying the concentration of the purified GalOX stock solution (2.0 mL). GalOX was purified by Ni-NTA affinity chromatography. The obtained fractions were pooled and concentrated to 2.2 mL in sodium phosphate pH 6.0. The concentrated GalOX was diluted and loaded onto the gel as indicated. Band intensities were compared to those arising from bovine serine albumin (BSA). The protein ladder is Precision Plus Protein Dual Color Standards (Bio-RAD, USA) with kDa molecular weights indicated.

The GalOX stock solution was additionally diluted to 100 000 x, 1 000 000 x, 10 000 000 x to quantify enzymatic activity. Activity measurements are reported in Figure 3.6 and Table 3.2 and indicate 51996 U/mL in the 2.0 mL GalOX stock (543 U/mg) (only considering the average of 1 000 000 x and 10 000 000 x), where 1 U of GalOX refers to 1 µmol of H_2O_2 produced per minute, and also refers to the conversion of 2 µmol of ABTS to ABTS cation as well. The previous test on GalOX activity on galactose is 980 U/mg (un published data Emma Master's Lab), suggesting that the GalOX activity may have been slightly underestimated here.

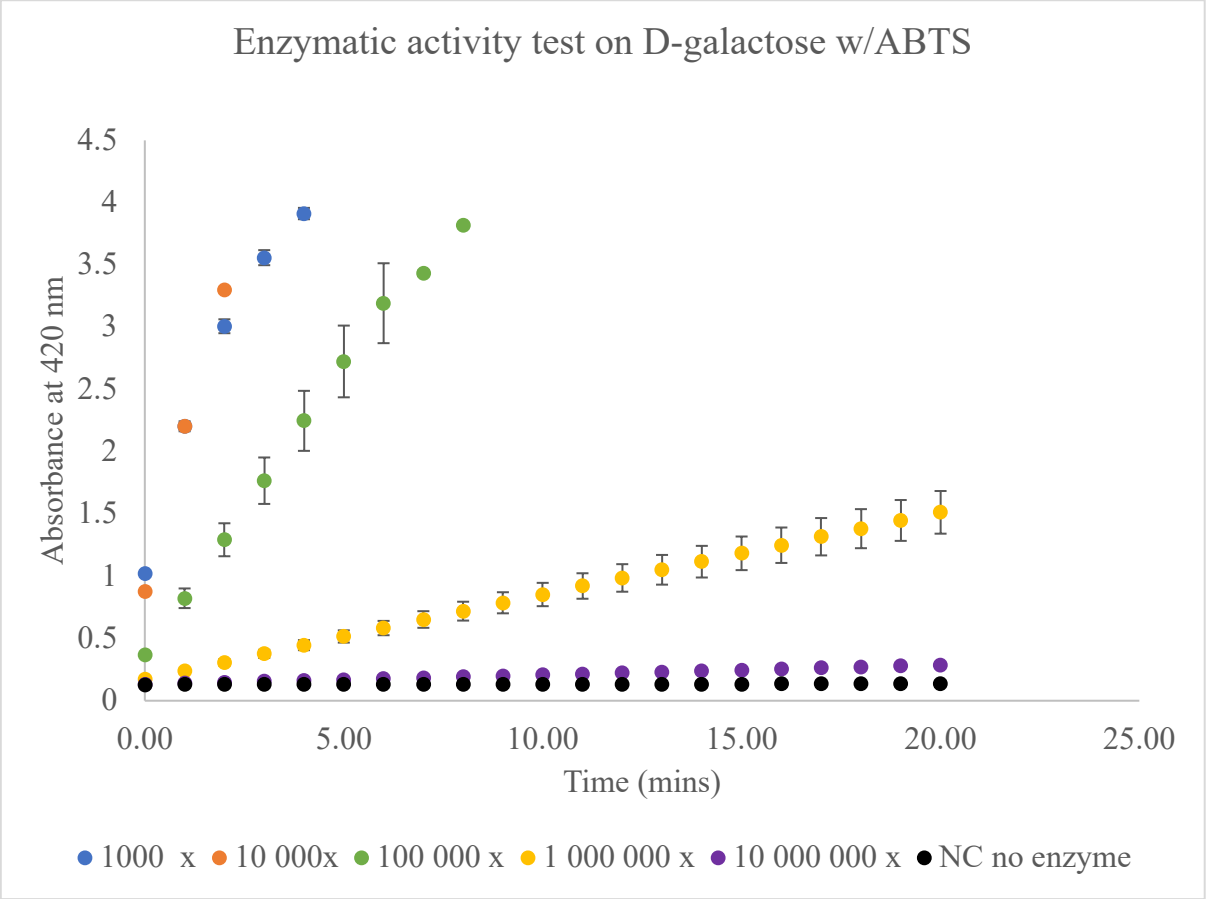

Figure 3.6: Enzymatic activity of the GalOX stock (2.0 ml sample). UV-Vis spectroscopic measurement of GalOX ability to oxidize D-galactose. The conversion of ABTS to ABTS•+ measured at 420nm. Error bars show the standard deviation of n=3 experiments at each time point.

Table 3.2: Enzymatic activity of the GalOX stock (2.0 ml sample). Based on the detected the slope arising from the conversion of ABTS measured at 420 nm as shown in Figure 3.6 and using the slopes for the times plotted. The GalOX stock was diluted as indicated. Error bars show the standard deviation of n=3 repetitions.

	100 000x dilution	*1 000 000x dilution*	*10 000 000x dilution*
Slope (mAbs/min)	471 ± 50	67 ± 8	7 ± 1
Total Enzyme Activity (U)	69767 ± 7139	98867 ± 12339	109367 ± 10368
Activity Concentration (U/ml)	34941 ± 3730	49438 ± 6126	54555 ± 5077
Specific Activity (U/mg)	365 ± 39	517 ± 64	570 ± 53

3.2 Production of crosslinkers

The obtained *Ab*PDH1 and GalOX stock samples were used separately to oxidize XOS and lactose respectively. The oxidized sugar products are intended to be used as crosslinkers to form crosslinking networks with chitosan, yielding novel hydrogels. The oxidization reactions were sampled over time and analyzed/quantified by High Performance Anion Exchange Chromatography-Pulsed Amperometric Detecter (HPAEC-PAD) to confirm the oxidation reactions occurred.

The HPAEC-PAD method can detect the original xylose and its polymers that comprised the un-oxidized XOS substrate. The decrease in the amount of the un-oxidized XOS substrate is monitored over reaction time, rather than accumulation of the oxidized product, being that the specific nature of the oxidized-product is unknown at this time. Substrate levels are compared to known amounts of the unreacted XOS substrate for quantification. As shown in Figures 3.7A and Table 3.3, all of the x2, x3, x4 and x5 peaks decrease over time. Base on the first measurement, the x2 peak area decreased by 96% after 26 h. The x3 peak area decreases by 92 % after 26 h. While the x4 peak area decreases by 88 % after 26 h and the x5 peak area also decreases after 26 h as well. Figure 3.7B shows a tabulation of changes over time, highlighting that shorter substrates (excluding x1) can be oxidized faster by *Ab*PDH1 than longer substrates, but also that AbPDH1 does show activity against the longer substrates, consistent with previous observations (Karppi et al., 2020). For instance, after a 2-hour reaction, 73% of x2 were oxidized, 31% of x3 were oxidized, and 17% of x4 were oxidized. Notably, the significance of these values remains to be established in the future when additional repetitions of the experiment can be completed. No attempt was made to actually quantify loss of substrate or assume any specific amount of oxidized product was formed. However, we conclude more generally, that an *Ab*PDH1 oxidized-XOS sample was produced for testing as a crosslinker.

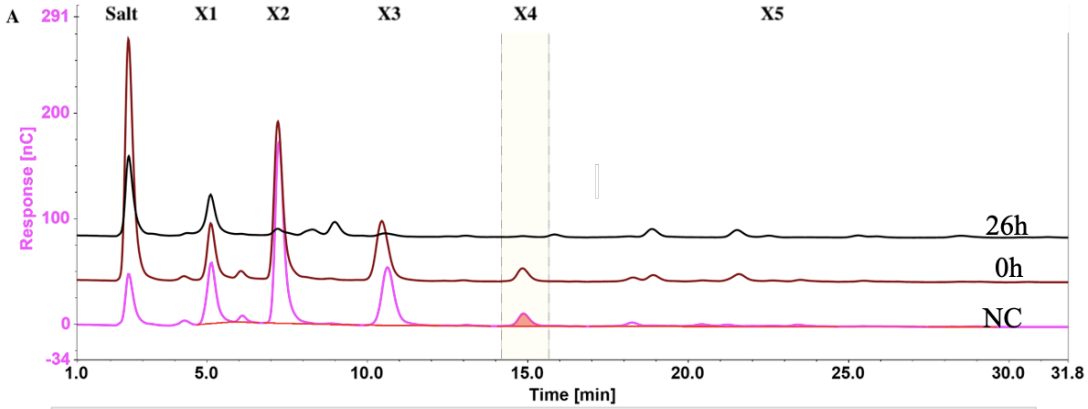
A
Salt
X1
X2
X3
X4
X5
291
200
100
0
-34
Response [nC]
26h
0h
NC
1.0
5.0
10.0
15.0
20.0
25.0
30.0
31.8
Time [min]

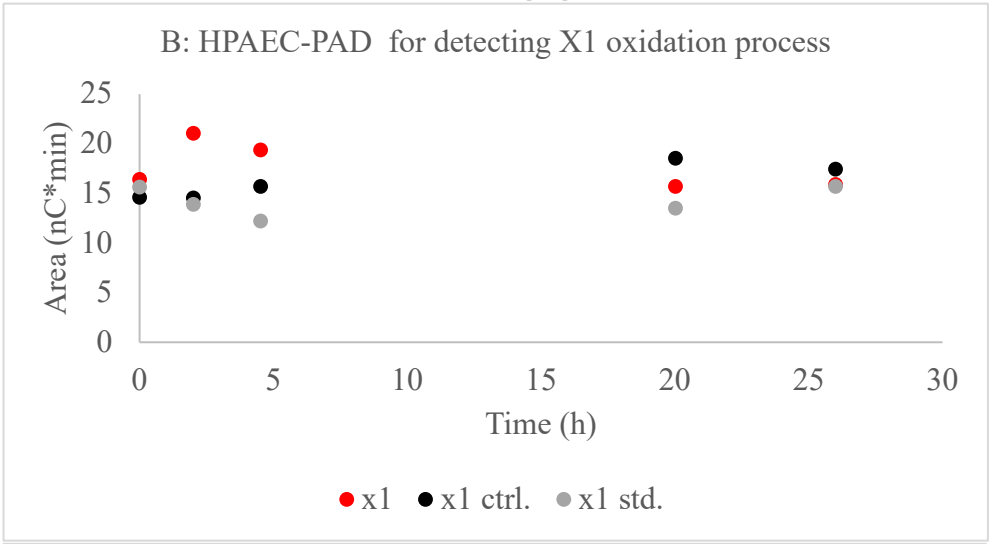
B: HPAEC-PAD for detecting X1 oxidation process
Area (nC*min)
25
20
15
10
5
0
0
5
10
15
20
25
30
Time (h)
x1
x1 ctrl.
x1 std.

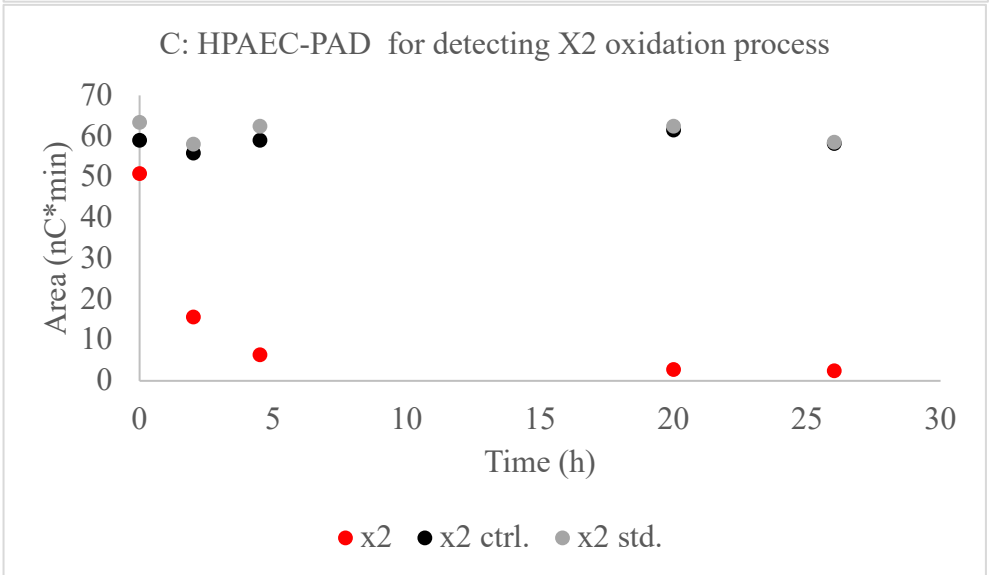
C: HPAEC-PAD for detecting X2 oxidation process
Area (nC*min)
70
60
50
40
30
20
10
0
0
5
10
15
20
25
30
Time (h)
x2
x2 ctrl.
x2 std.

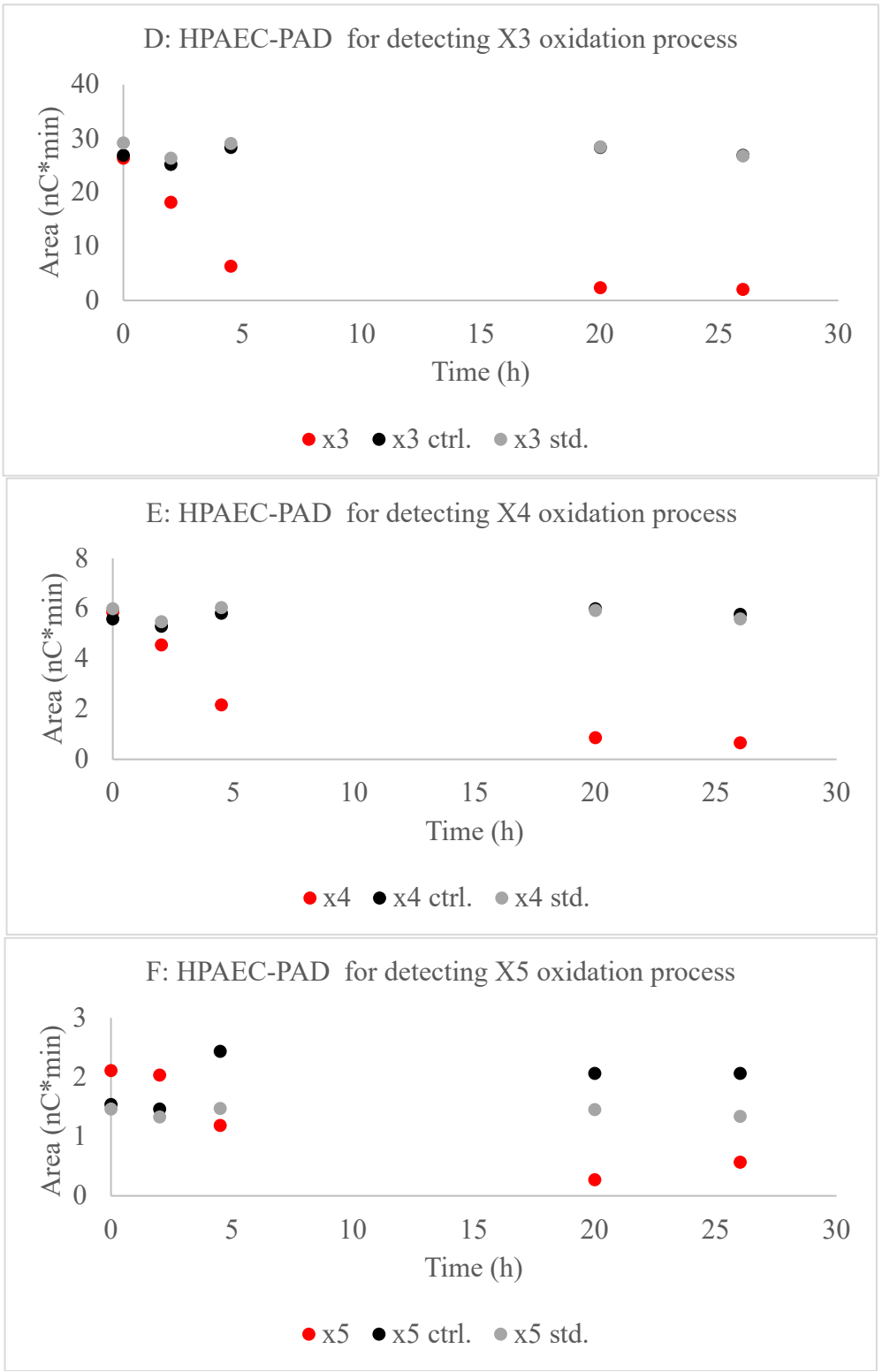

Figure 3.7: The HPAEC-PAD result for *Ab*PDH1-XOS oxidation reaction. a) HPAEC-PAD analysis comparing 0 h (brown) and 26 h (black) reactions, with the unreacted control (XOS substrate only (pink)). B-F) Plot of peak areas for each substrate X1 to X5 component upon reaction with *Ab*PDH1 over time vs their control and std, where red refers to the substrates, black refers to the control and grey refers to the standard. n=1 for all time points.

Table 3.3: Tabulation of HPAEC-PAD peak areas for XOS substrates upon incubation with *Ab*PDH1 (nC*min) (n=1)

Sample name	Xylose (X_1)	Xylobiose (X_2)	Xylotriose (X_3)	Xylotetraose (X_4)	Xylopentaose (X_5)
XOS PDH 0h	16.4459	50.8461	26.3543	5.8587	2.1085
XOS PDH 2h	21.0575	15.6734	18.1838	4.5507	2.0368
XOS PDH 4.5h	19.401	6.3488	6.389	2.1556	1.1866
XOS PDH 20h	15.7472	2.7995	2.3633	0.862	0.2682
XOS PDH 26h	15.8867	2.5381	2.0752	0.6509	0.5686

In the case of GalOX oxidation of lactose, the HPAEC-PAD detected both substrate depletion and some new peaks likely representing oxidized sugar products. These have been labelled products 1 and 2. Figure 3.8 and Table 3.4 show that the GalOX reaction on lactose was completed by 3 h. The peak representing the substrate (lactose) (which shifts between 8-9 minutes depending on the run (see two different control runs in blue/pink), for unknown reasons) deceased to undetectable levels at 3h, consistent with previous characterization of this enzyme (Paukner et al., 2015; Cleveland, 2021, Mototsune et al., 2024). In contrast, the area size of product 1 increased from 49.25 to 123.57 nC*min after 1 h. The area size of product 2 increased from 0.25 at 0 h to 9.35 nC*min at 4.5 h. Again, no attempt was made to actually quantify loss of substrate or product or assume any specific amount of oxidized product was formed. However, we conclude more generally, that a GalOX oxidized-lactose sample was produced for testing as a crosslinker.

a

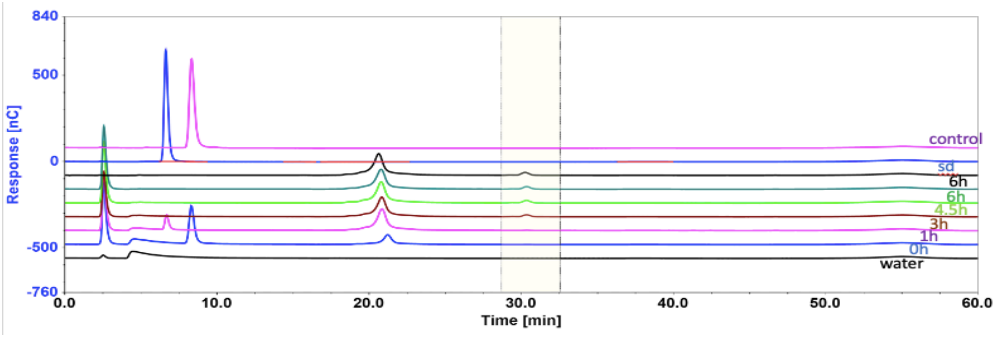

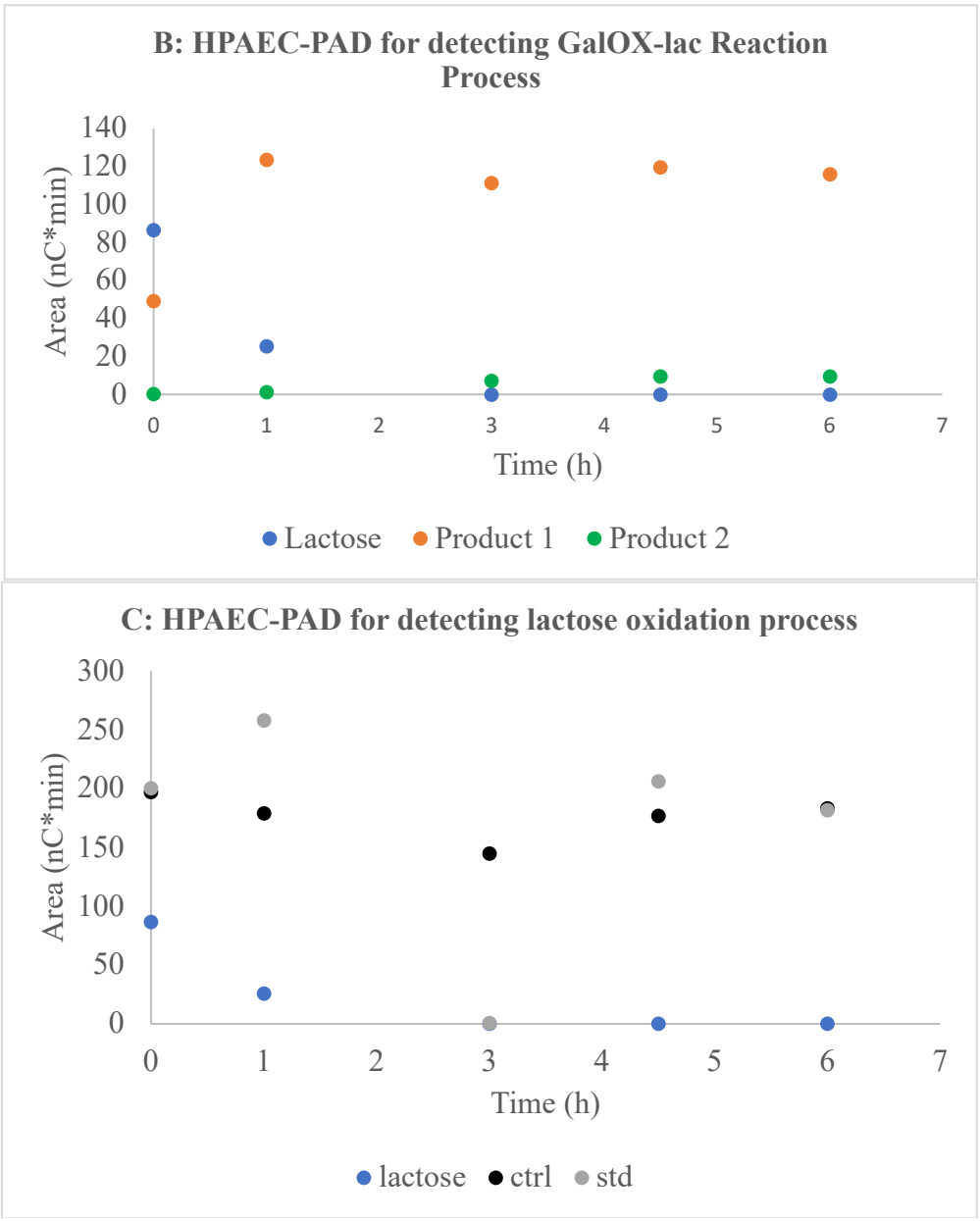

Figure 3.8: The HPAEC-PAD result for GalOX oxidation of lactose. a) HPAEC-PAD analysis comparing reaction profiles timepoints from 0h and 6h and controls. b) Plot of peak areas for each substrate component over time, where blue refers to lactose, orange refers to product 1 and green refers to product 2. c) Plot of peak area of lactose (blue) vs its ctrl (black) and std (grey).

Table 3.4: Tabulation of HPAEC-PAD peak areas for lactose substrate and unknown products (nC*min)

	Lactose	Product 1	Product 2
GalOX-Lac 0h	86.48	49.25	0.25
GalOX-Lac 1h	25.37	123.57	1.02
GalOX-Lac 3h	n.a.	111.39	7.22
GalOX-Lac 4.5h	n.a.	119.59	9.35
GalOX-Lac 6h	n.a.	115.82	9.59

3.3 Chitosan gel formation

Oxidized sugar products obtained from the catalysis of *Ab*PDH1 and GalOX as described above were used as 'crosslinkers' to 'make connections between high Mw chitosan fibers from shrimp, and ultimately a 3D network that has gel like properties (hydrogel). Chitosan must be dissolved at low pH (in acetic acid) because it cannot be dissolved at neutral pH. Previous experience in the lab of Dr. Emma Master showed that only high MW chitosan enables hydrogel formation, where medium and low MW chitosan cannot form a gel. Now high Mw weight chitosan gel formation was optimized by testing different chitosan concentrations, different 'crosslinker' concentrations and different pH values at small scale. Large-scale gel formation (5 mL) was prepared as well to allow characterization of its stiffness by rheological measurement.

3.3.1 Optimization of pH and chitosan concentrations

The pH range for chitosan gel formation was initially assessed by forming hydrogels with 7.4 mg/mL (Figure 3.9 & Table 3.5) and 13.8 mg/mL (Figure 3.10 & Table 3.6) chitosan solutions at different concentrations of Na_2HPO_4. The pH of the 7.4 mg/mL chitosan solution with Na_2HPO_4 was measured initially and values are reported in Figure 3.8. The crosslinker solutions of oxidized XOS or oxidized lactose (characterized above) were then added separately and mixed by pipette. Gel formation was subsequently monitored by visually evaluating whether the solution stuck in the bottom of the PCR tube or not when inverted and shaken, where sticking in the bottom of the tube represents successful gel formation. The 7.4 mg/mL chitosan, gel formed in the pH range of 6.98 – 7.32 (Table 3.5). A negative control was also run that was the same condition, but lacking the oxidized crosslinker.

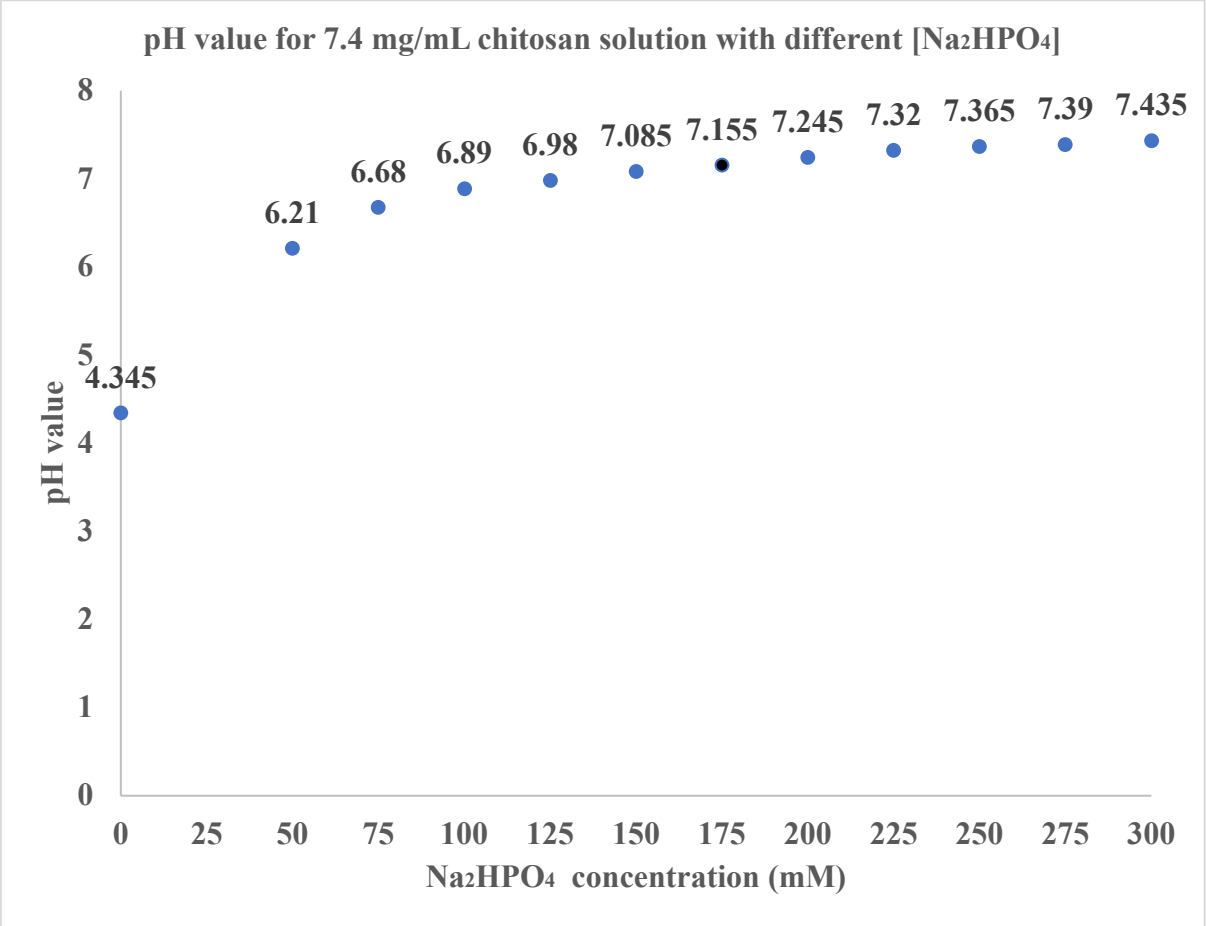

Figure 3.9: pH of 7.4 mg/mL chitosan solutions containing different Na_2HPO_4 concentrations (n=2).

Table 3.5: Result of oxidized-XOS and oxidized-lactose induced gel formation with 7.4 mg/mL chitosan sat various pH values. NC – negative control set up as the test samples but lacking either of the oxidized sugar crosslinkers.

pH value	Oxidized-XOS	Oxidized-lactose	NC
4.345	No gel	Gel after 7 days	No gel
6.21	No gel	No gel	No gel
6.68	No gel	No gel	No gel
6.89	No gel	No gel	No gel
6.98	Gel form after 110 mins Gel degradation after 6 days	Gel form overnight	No gel
7.085	Gel form after 40 mins	Gel form overnight	No gel
7.155	Gel form after 20 mins	Gel form after 5h	No gel
7.245	Gel form after 40 mins	Gel form overnight	No gel
7.32	Gel form after 110 mins	Gel form overnight	No gel
7.365	No gel	No gel	No gel
7.39	No gel	No gel	No gel
7.435	No gel	No gel	No gel

Similarly, for the 13.8 mg/mL chitosan, gel formed in the pH range of 6.23 – 6.925 (Figure 3.10 and Table 3.6). Based on these optimizations, the mid-value of pH 7.155 was selected to move ahead with, using the lower concentration of chitosan. It is nonetheless interesting to note the overall narrow pH range available for hydrogel formation and that it is essentially a requirement for neutral pH, consistent with biological systems. This is most likely due to the nature of the chemical formation of an imine bond (Figure 1.5). Essentially this reaction is known to slow down at both low and high pH. At low pH, the amine reactant becomes non-nucleophilic because it's tied up as its ammonium conjugate acid and thus would not be expected to form a bond. Similarly, at high pH there isn't enough acid to protonate the OH in the intermediate.

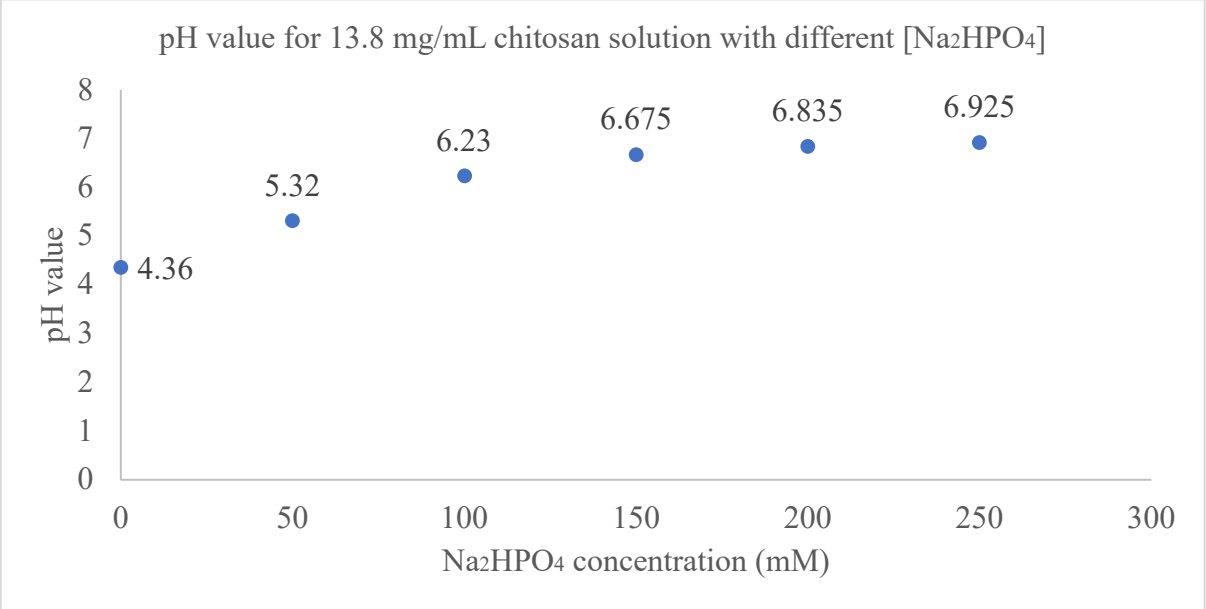

Figure 3.10: pH measurement for 13.8 mg/mL chitosan solutions with different Na_2HPO_4 concentrations (n=2).

Table 3.6: Result of oxidized-XOS and oxidized-lactose -induced gel formation with 13.8 mg/mL chitosan solution at various pH value.

pH value	Oxidized XOS	Oxidized lactose
4.36	No gel	No gel
5.32	No gel	No gel
6.23	1h	Overnight
6.675	30 mins	Overnight
6.835	1h	Overnight
6.925	1h	Overnight

3.3.2 Optimization of crosslinker concentration

The chitosan gel at 7.4 mg/mL was also prepared with different concentrations of crosslinkers (Table 3.7). The results show that higher concentrations of crosslinkers always result in faster gel formation, regardless of whether oxidized-XOS or oxidized-lactose was used. Thus, the final selected crosslinker concentration for large scale gel formation was the highest concentration tested, 40 mM. Lactobionic acid has a similar structure to the non-oxidized sugars, so it was used as the negative control and no gel was expected to form with it. Glutaraldehyde molecule contains two aldehyde functional groups similar to the oxidized sugars structures, and as such was used as the positive control. The gel with glutaraldehyde formed immediately. The differences in rates of gelation between the different crosslinkers (lactobionic acid < oxidized-lactose < oxidize-XOS < glutaraldehyde) is most likely due to their overall size and the number of reactive ketones per crosslinker molecule, impacting their ability to diffuse through the system and form imine bonds. The glutaraldehyde is a small C5 straight chain molecule with an aldehyde group on each end. The oxidized-lactose, in addition to being a dimer (and thus a larger metabolite) is only expected to be oxidized on one C6 (Figure 1.10; Paukner et al., 2015; Cleveland, 2021, Mototsune et al., 2024), with only inefficient oxidation of any of the glucose hydroxyls, reducing the likelihood of obtaining molecules with two reactive reactive ketones. The slower more limited gelation using oxidized-lactose is consistent with this. The nature of the oxidized-XOS is less defined, but previous characterization (Karppi et al 2020), emphasize the possibility of oxidations at either the C2 and C3 positions and on both terminal sugar moieties in a given chain. As such there is a higher probability of the oxidized XOS presenting molecules with multiple reactive ketones, more similar to the glutaraldehyde, and thus consistent with the observed higher levels of gelation compared to oxidized-lactose.

Table 3.7: The gel formation at different crosslinker concentration. 7.36 mg/ml chitosan at pH 7 was reacted with various amounts of the two oxidized sugar crosslinkers as indicated. Lactobionic acid and glutaraldehyde were used in place of the crosslinkers as negative and positive controls respectively.

Type of Crosslinker	40 mM	12.5 mM	4 mM	1.25 mM
Oxidized XOS	Gel at 23 mins	Gel at 1 h 35 mins	No gel	No gel
Oxidized XOS ctrl.	Gel overnight	No gel	No gel	No gel
Oxidized XOS std.	No gel	No gel	No gel	No gel
Oxidized lactose	Gel overnight	Gel after 2 days	No gel	No gel
Oxidized lactose ctrl.	No gel	No gel	No gel	No gel
Oxidized lactose std.	No gel	No gel	No gel	No gel
Lactobionic acid (NC)	No gel	No gel	No gel	No gel
Glutaraldehyde (PC)	Gel immediately	Gel immediately	Gel immediately	Gel immediately

3.3.3 Optimization of large-scale gel formation

Subsequently, gels were prepared again, at both 7.4 and 13.8 mg/mL chitosan concentrations separately with oxidized-XOS (Table 3.8) and oxidized-lactose (Table 3.9) at larger scale (5 mL). In both cases the higher concentrations of chitosan led to faster gel formation than the lower concentration gel. As well, oxidized-XOS induced formation of gels faster than oxidized-lactose at either chitosan concentration consistent with smaller scale observations. Images of the gels obtained are included in Appendix A.

Table 3.8: Large-scale chitosan gel formation (5 mL) with oxidized XOS crosslinker.

7.36 mg/ml chitosan		13.8 mg/ml chitosan	
oxidized-XOS	Almost gel after 3h Fully gel overnight	oxidized-XOS	Fully gel within 30 mins
oxidized-XOS ctrl.	Very viscous overnight, but never fully gel	oxidized-XOS ctrl.	Very viscous overnight, but never fully gel
oxidized-XOS std.	No gel	oxidized-XOS std.	No gel
Chitosan + ddH_2O	No gel	Chitosan + ddH_2O	No gel

Table 3.9: large-scale chitosan gel formation (5 mL) with oxidized-lactose crosslinker.

7.36 mg/ml chitosan		13.8 mg/ml chitosan	
Oxidized lactose	Gel overnight	Oxidized lactose	Viscous after 3 h Fully gel overnight
Oxidized lactose ctrl.	No gel	Oxidized lactose ctrl.	No gel
Oxidized lactose std.	No gel	Oxidized lactose std.	No gel
Chitosan + ddH_2O	No gel	Chitosan + ddH_2O	No gel

3.4 Characterization of optimized gels by rheological evaluation

Visual observation provides largely qualitative data. Thus, for a more quantitative analysis, rheological measurements were conducted to identify the formation (gelling point) and stiffness (viscoelastic properties) of the hydrogels formed at the two different chitosan concentrations induced by 40 mM oxidized-XOS crosslinker (Stojkov et al., 2021). These measurements were completed using a dynamic rheometer (Figure 3.11). Outcomes were that the 13.8 mg/mL chitosan gel response was higher pressure than the 7.4 mg/ml chitosan gel. This shows that the gel at higher chitosan concentration has higher stiffness than the lower concentration gel. Loss modulus (G'') refers to the losing energy (in the form of heat) due to the friction between internal molecules within a material during deformation. A material with higher loss modulus means it is more viscous. Storage modulus (G') refers to the ability (stored energy) of a material to resist deformation caused by external forces given by the rheometer. A material with higher storage modulus means it has stronger elastic response for recovering its original state. When G" > G', the material is in liquid-like behavior; when G' > G", the material is in solid gel-like behavior. The crossing point between G'' and G' shown in Figure 3.11 meaning the time for gel formation. The data also show that the G' value becomes higher than the G'' value at 5 mins for 13.8 mg/mL chitosan gel and at 13 mins for 7.4 mg/mL gel. Thus, the required time for 13.8 mg/mL chitosan gel formation is 5 mins, and 13 mins for 7.4 mg/mL. This shows that gel formation occurs faster

at the higher concentration of chitosan than the lower chitosan concentration, consistent with visual observations.

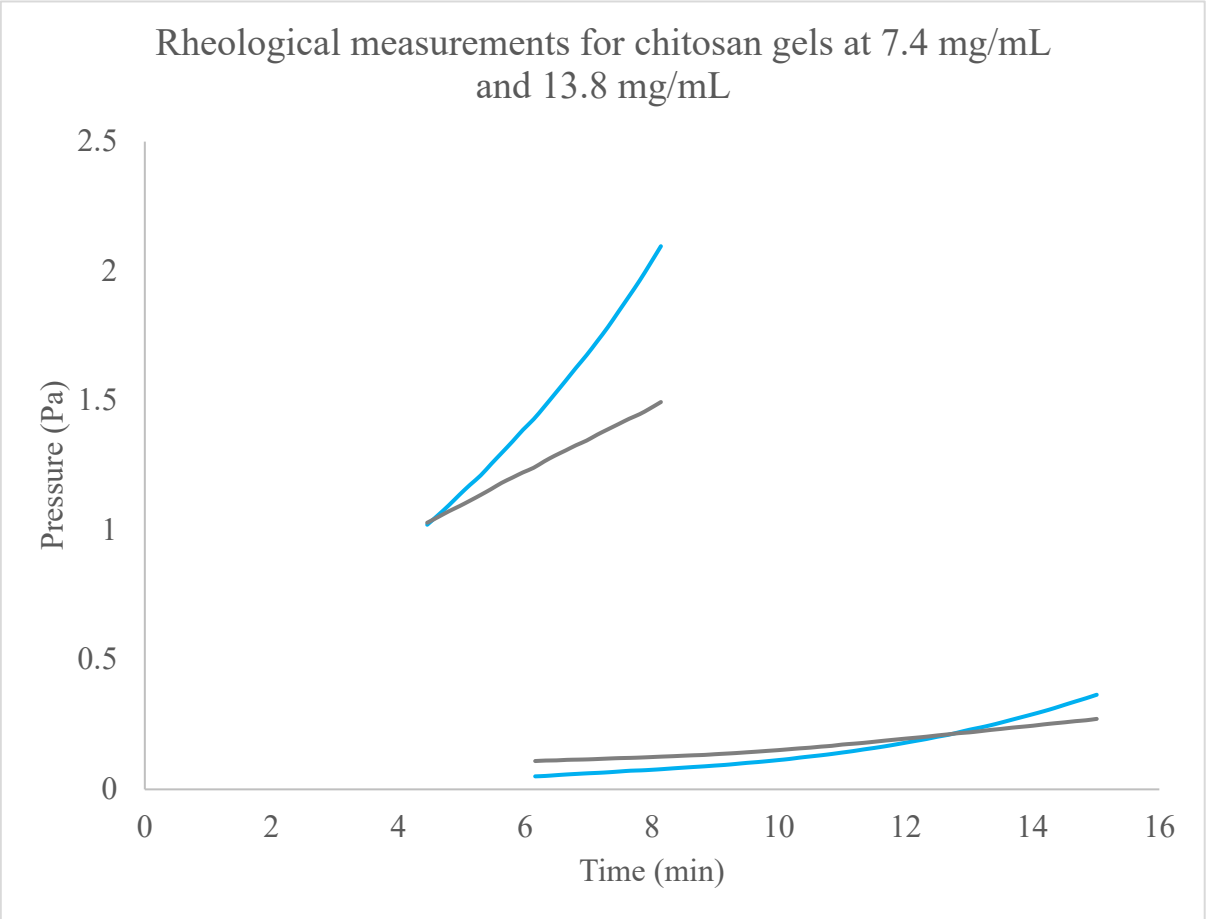

Figure 3.11: Rheological measurements for chitosan gels. X axis refers to time (s), y axis refers to the pressure (Pa). The green line refers to the loss modulus (G'') and the blue line refers to the storage modulus (G'). The lines located at upper position are for 13.8 mg/mL chitosan oxidized-XOS gel, and the lines located at lower position are for 7.4 mg/mL chitosan oxidized-XOS gel. In both cases 40 mM oxidized-XOS was used to induce gell formation.

3.5 Degradation of pre-formed hydrogels

Finally, that the chitosan gels can be formed in a specific pH range has been shown herein (Tables 3.5 and 3.6). Therefore, it is hypothesized that the gel can be degraded by either lowering or raising the pH by addition of HCl (hydrochloric acid) or NaOH (sodium oxide). Recall again that gel formation is based on imine bond formation between chitosan polymers and the crosslinkers (Figure 1.5). It is expected that the imine bond formation is reversible, allowing the gel to degrade.

To test this hypothesis, ten tubes of oxidized-XOS gel were prepared at the 7.4 mg/mL chitosan concentration using 40 mM oxidized XOS crosslinker at pH 7 and at room temperature. An additional tube was set up as a negative control (lactobionic acid; tube 11). Gel formation was observed after being allowed to solidify overnight (Figure 3.12: top panel). The next morning (at 17 hours), the tubes were up-ended and flicked gently with a finger to judge whether the gel had been formed, and then treated with acid or base, with or without vortexing, with visual images of the results immediately after additions included in Figure 3.12 (bottom panel). There was no immediate change in either of the untreated control tubes (1 and 2). In the case of the addition of acid, an observable degradation of the surface was immediately notable for both concentrations (tubes 3 & 5 & 7), with the depth of the degraded layer becoming larger upon vortexing (tube 4 & 6 & 8). The addition of base led to a similar outcome, with the vortexed sample (tube 10) becoming a liquid that flowed down the tube wall when inverted. The lactobinoic negative control remained liquid. Thus overall, it was concluded that the gels are degraded by adding acid or base, and vortexing increases the gel degradation, likely by increasing penetration and diffusion of the acid and base into the gel.

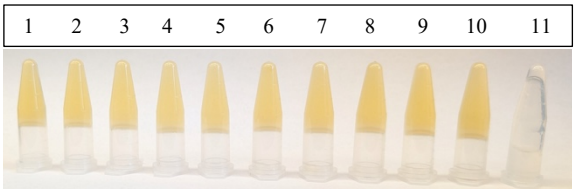

17 h: Overnight gel formation

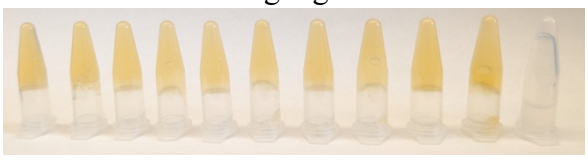

17 h: Gel degradation after addition of acid

Figure 3.12 Dissolution of gels at 17 h. top panel: showing formed gels at 17 hours. Bottom panel: showing gels immediately after addition of HCl and NaOH with or without vortexing. Two tubes were left untreated without (tube 1) or with (tube 2) vortexing. Four additional tubes had 127.2 mM of HCl layered on the surface of the gel with no vortexing (tubes 3 & 5) or with vortexing (tubes 4 & 6). Two additional tubes were treated with a higher

concentration of HCl (254.2 mM), without (tube 7) or with (tube 8) vortexing. Finally two tubes were treated with 127.2 mM NaOH, either without (tube 9) or with (tube 10) vortexing.

The tubes were subsequently put upright and left for 90 minutes, and then inverted again at 18 h 30 mins, showing that the NaOH liquified gel had re-formed (Figure 3.13, top panel). Interestingly, when the vortexed tubes were vortexed and inverted again at this time (Figure 3.13, second panel), for both the NaOH and untreated samples (tubes 2 and 10) the gel dropped down to the lid, suggesting some similar transformation in gel quality of the reformed gel and the untreated gel. The tubes were set up right and left to incubated until 42 h, and observed again before and after vortexing of the vortexed tubes (Figure 3.13 bottom two panels). The vortexed untreated and vortexed NaOH returned to a liquid state (tubes 2 and 10).

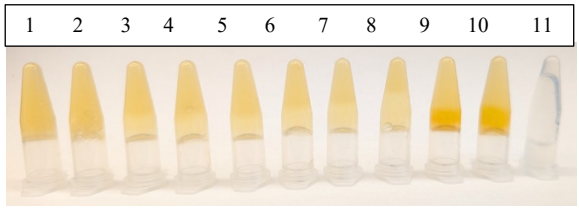

18 h 30 min

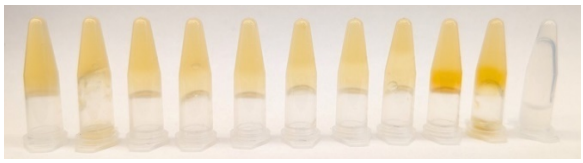

18 h 30 mins, after vertexing 2,4,6,8,10 again

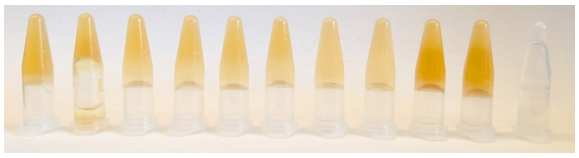

42h

42 h after vortexing 2,4,6,8,10 again

Figure 3.13 Dissolution of gels at 18.5 and 42 h. top two panel: showing formed gels at 18.5 hours. Bottom two panel: showing gels after 42 hours of incubation. Two tubes were left untreated without (tube 1) or with (tube 2) vortexing. Four additional tubes had 127.2 mM of HCl layered on the surface of the gel with no vortexing (tubes 3 & 5) or with vortexing (tubes 4 & 6). Two additional tubes were treated with a higher concentration of HCl (254.2 mM), without (tube 7) or with (tube 8) vortexing. Finally two tubes were treated with 127.2 mM NaOH, either without (tube 9) or with (tube 10) vortexing.

Subsequently, to fully mix the gel with acid or base, the vortexed gels (#2,4,6,8,10) were physically mixed by spatula at 42 h., causing them to largely lose all gel behavior (flowing to the lid of the inverted tubes; Figure 3.14, top panel). At this time 127.2 mM of NaOH was added to attempt neutralization of tubes # 5 and #6, with the expectation that the gel might re-form. Three hours later at 45 h, while this was not found to be the case, it was interesting to note that the original HCl and NaOH treated vortexed gels (tubes 4 and 10), which had liquified upon spatula mixing, had re-formed. That, the neutralized gel did not re-gel suggests that adjusting to the original pH value may not be effective for reasons that remain unclear.

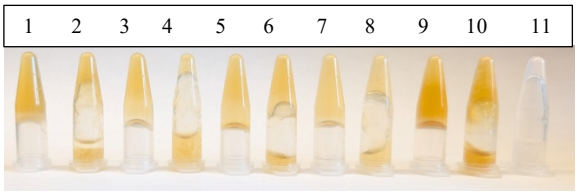

42h: After mixing 4,6,8,10 with spatula

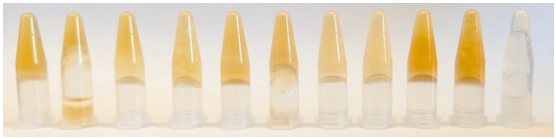

45 h: (including addition of NaOH to samples 5 and 6 after spatula mixing)

Figure 3.14 Dissolution of gels at 42h and 45 h. top panel: showing formed gels mixed with spatula at 42 hours. Bottom panel: showing gels after 45 hours of incubation. Two tubes were left untreated without (tube 1) or with (tube 2) vortexing. Two tubes had 127.2 mM of HCl layered on the surface of the gel with no vortexing (tubes 3) or with vortexing (tubes 4). Two tubes were treated the same as tubes 3 and 4, but then have 127.2 mM NaOH added at 42 h without (tube 5) and with (tube 6) vortexing. Two additional tubes were treated with a higher concentration of HCl (254.2 mM), without (tube 7) or with (tube 8) vortexing. Finally two tubes were treated with 127.2 mM NaOH, either without (tube 9) or with (tube 10) vortexing.

In conclusion, adjusting pH up or down contributed to gel degradation, consistent with the hypothesis that the imine bonds are not stable at low and high pH. The degradation effect was more prominent when the pH adjustment was combined with physical mixing either by vortexing or spatula. Interestingly, in the absence of physical mixing, gel reformation behavior was automatic within several hours (tubes 3, 5, 7 & 9), highlighting the importance of the physical mixing for diffusion of the acid or base throughout the gel to elicit degradation. That, the gel that was degraded by adding HCl with vortexing, could no re-form a gel by adding the same amount of NaOH to bring the pH back to neutral (tube 6) was unexpected, with no clear explanation available at this time. Therefore, additional investigations into regulation of gel formation by modulation of pH remains for the future, perhaps most notably, starting by testing the actual obtained pH of the gels under the different treatment conditions and quantifying gel states by rheometric analysis.

By way of an addendum, in most cases the gel naturally degraded on its own after around 8 days (Figure 3.15). This may be caused by the breaking down of the bonds within the chitosan polymer (long polymer breaks down to shorter polymers), rather than the reversal of the imine bonds, or possibly other factors such as bacterial or fungal contamination of the samples due to secretion of degrading enzymes. In future experiments it is recommended that a small quantity of an antibacterial salt be added to the hydrogels to account for this last possibility.

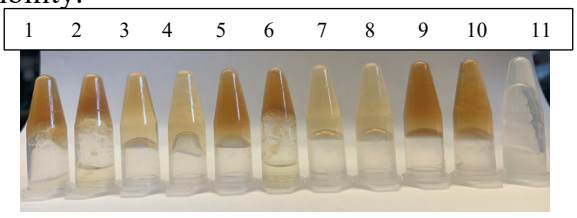

Day 8

Figure 3.15 Dissolution of gels at day 8. It shows the gel begin to degrade since day 8. Two tubes had 127.2 mM of HCl layered on the surface of the gel with no vortexing (tubes 3) or with vortexing (tubes 4). Two tubes were treated the same as tubes 3 and 4, but then have 127.2 mM NaOH added at 42 h without (tube 5) and with (tube 6) vortexing. Two additional tubes were treated with a higher concentration of HCl (254.2 mM), without (tube 7) or with (tube 8) vortexing. Finally two tubes were treated with 127.2 mM NaOH, either without (tube 9) or with (tube 10) vortexing.

3.6 FTIR characterization of the crosslinkers during gel formation

Quantities of the obtained oxidized-XOS, oxidized-lactose crosslinker stock solutions (see Section 3.2) as well as ctrl. without *Ab*PDH1 or GalOX and std.with only XOS samples were lyophilized and then analyzed by Fourier-transform infrared spectroscopy (FTIR). At the same time, gels (7.4 mg/mL chitosan with 40 mM crosslinker) formed using these crosslinkers as well as ctrl. and std. samples were also analyzed by FTIR.

In the case of the oxidized-XOS stock, an extra peak at 1735 cm^{-1} (Figure 3.16; black square) compared to std and ctrl samples, is likely representative of the newly formed ketone group on the oxidized-XOS. At the same time, the peak at 1735 cm^{-1} was lost upon gel formation, consistent with the idea of the ketone contributing to imine bond formation. The resulting ester is however, not obvious in the spectrum. Finally, there is a peak observed at 1648 cm^{-1} in the oxidized-XOS gel sample, that is not observed in either of the gel ctrl or gel std conditions, although the significance of this peak remains enigmatic. Possibly this peak is masked by overlap with a peak at 1558 cm^{-1} in the ctrl and std conditions.

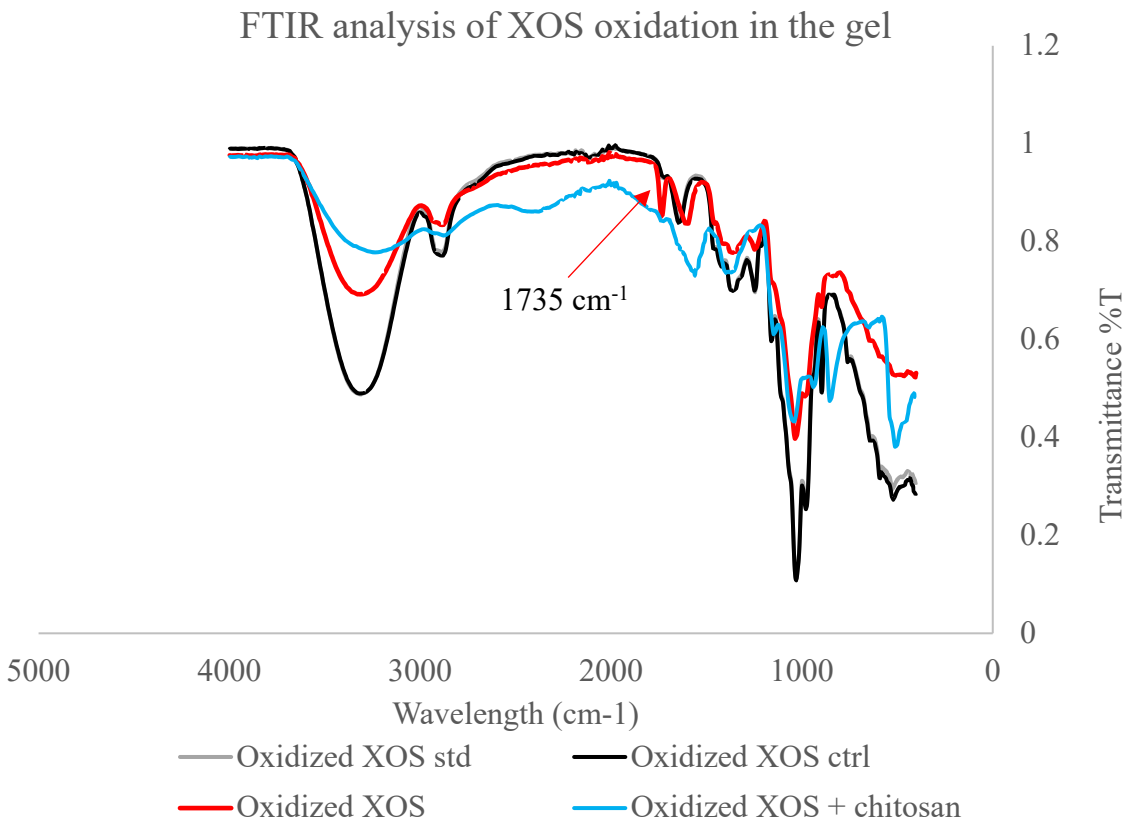

Figure 3.16: FTIR analysis of oxidized-XOS before and after chitosan gel formation. Red refers to oxidized XOS std.; purple refers to oxidized XOS ctrl.; light blue refers to oxidized XOS; green and dark yellow refers to the gel already formed with the oxidized XOS crosslinker; dark blue refers to the mixture with oxidized XOS std. crosslinker and the chitosan; black refers to the mixture with oxidized XOS ctrl. and chitosan.

A similar analysis was conducted in the case of oxidized-lactose gel. For the oxidized-lactose stock solution an extra peak is observed at 1731 cm^{-1}, likely representative of the newly formed ketone on the lactose, compared to ctr without *Ab*PDH1 and std with only XOS samples (Figure 3.17; black box). At the same time, the peak at 1731 cm^{-1} was lost upon gel formation, consistent with the idea of the ketone contributing to imine bond formation. The resulting ester is again, not obvious in the spectrum.

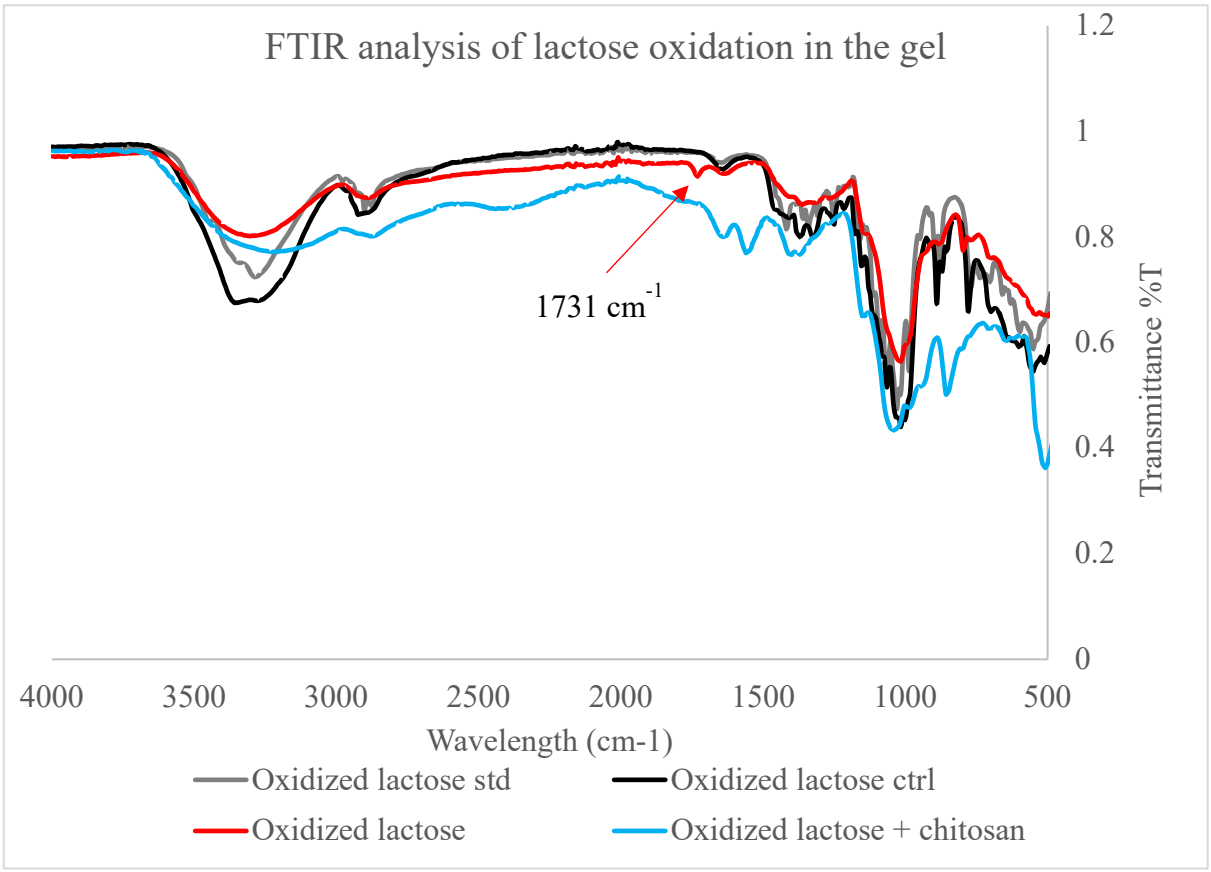

Figure 3.17: FTIR result for the formation of GalOX-lactose chitosan gel. Black refers to oxidized lactose std; orange refers to oxidized lactose; green refers to oxidized lactose ctrl.; purple refers to the mixture containing oxidized lactose ctrl. and chitosan; blue refers to the gel already formed with the oxidized lactose crosslinker; dark yellow refers to the mixture containing the oxidized lactose std. crosslinker and the chitosan.

Chapter 4

Discussion

4.1 *Ab*PDH1 production and analysis

From the results, it is obvious that the final yield of *Ab*PDH1 is relatively low (16.5 mg from 1.2 L of BMMY media), compared to GalOX (191.4 mg from 1.2 L of BMMY media). The amount of protein production can be affected by multiple factors. For example, the numbers of *Ab*PDH1 encoding plasmids within the *Ab*PDH-KM71H transform strain may be lower (fewer plasmids transformed into KM71H in the transformation step), resulting in lower protein expression during induction. However, this is not the only reason. Based on the SDS-PAGE (Figure 3.2) and activity measurements, there was a lot of *Ab*PDH1 lost in the flowthrough from both the Ni-NTA column as well as the 10 kDa centrifugal concentrator. The reason for these loses remains enigmatic. However, the most obvious factor may be the partial degradation of *Ab*PDH1, possibly combined with losses through pore irregularity and micro-tears in the membranes. Consistent with this, the SDS-PAGE shows there is a large band at around 15 kDa, which maybe degraded *Ab*PDH1. If such truncated versions maintain the active site of *Ab*PDH1 as well, this could be the reason why the *Ab*PDH1 in the microfiltration flowthrough is still active.

The SDS-PAGE for *Ab*PDH1 (Figure 3.2) shows a large, smeared band centered at approximately 100 kDa. This is significantly higher than the protein's expected MW of 65 kDa and is reflective of the high degree of glycosylation observed for *Ab*PDH1 (Karppi et al., 2020) that is a kind of post-translation modification. *Ab*PDH1 requires glycosylation to be functional, insinuating that it is required for proper folding. However, the absolute amount of carbohydrate and glycerol attach to *Ab*PDH1 is likely variable, leading to the smeared appearance of the band on the SDS-PAGE and its overall higher MW than expected.

Glycosylation occurs within the endoplasmic reticulum (ER) and Golgi apparatus (Reily et al., 2019). However, glycosylation is not available in prokaryotes (bacteria for example), such that *Ab*PDH1 must be expressed in eukaryotic cells, such as yeast.

4.2 GalOX production and analysis

GalOX was also produced using KM71H as the host in this study. However, as previously described by Paukner's group, GalOX, which is not notably glycosylated, can also be expressed using bacteria, *E.coli* BL21 for example (Paukner et al., 2015; Gomes et al., 2018). Nonetheless, that *P. pastoris* expression system can still be useful to produce high yields is based largely on the idea that it is just as convenience as *E.coli* to work with, but can also be notably more cost-effective at the industrial scale industry (Gomes et al., 2018).

GalOX is a radical copper oxidase that requires a copper atom to support the proteins in its proper structure and activity (shown in Figure 1.11). In the process of its' production, copper (II) sulfate should be added into the BMMY buffer during protein induction. In the absence of the additive, the obtained expressed GalOX yields only very low levels of oxidation against sugar substrates. These observations herein are consistent with the idea that the Cu atom is an essential component of the active site, and is directly involved in substrate oxidation. As Figueiredo (Figueiredo et al., 2022) and Whittaker (Whittaker, 1999) in their articles have highlighted, GalOX oxidization of substrates relies on the transfer of electrons and protons between the three oxidation states of Cu as well as Tyr 222 and Cys228 as described in the Introduction.

4.3 Chitosan gel degradation

Formed chitosan hydrogels are also sensitive to the pH, limited to a very narrow pH range of 6.98-7.32 as per findings reported in this thesis. This pH range may be determined

by the optimum pH for the condensation reaction between chitosan and the ketones on the oxidized-sugar crosslinkers. The optimum condition for a chitosan condensation reaction should be close to the neutral pH value (around 7), where acid can provide protons in the reaction, but the overall reaction condition should still be mildly basic (slightly above 7) by adjusting with Na_2HPO_4 to keep the imine (Schiff base) stable. The gel formed by induction with oxidized-XOS degraded after the addition of highly concentrated HCl or NaOH. In theory, the condensation reaction of the imine bond formation should be reversible. Thus, it is most likely that the hydrogels degraded after addition of HCl (shown in Figure 3.13 & 3.14) due to the reversible hydrolysis reaction for the condensation reaction under acidic conditions. On the other hand, that the hydrogels degrade after addition of NaOH, may be because of the reduced solubility of the chitosan polymer at a high pH, resulting in precipitation. However, it was unexpected that the degraded gels were re-formed after several hours at really high and low pH values, as was the inability to re-form a gel upon neutralization. The detailed reasons for these observations remain enigmatic, but could be related to the idea that the 3D crosslinking in the gel is elastic such that it can maintain structure integrity even when some connections within the crosslinking network are broken due to a sudden change in pH, or that a derived degradation state is irreversible due to breakdown of the chitosan fibers. This latter hypothesis would be consistent with the observation that although the gel cannot be immediately and totally degraded by adjusting pH, it can still auto-disintegrate overtime. During auto-disintegrate of the hydrogel, the chitosan polymers are proposed to break down into small polymers over time without adding anything, which typically takes around one week, although the imine bonds may still remain intact.

Overall, the industrial application of gels remains limited by our ongoing lack of understanding of the relationship between the gel and pH, emphasizing the need to validate

the actual pH values achieved in the degradation experiments and further investigate the possibility of microbial contamination and analyze degraded for fiber structure.

The role of physical mixing (vortexing) is another factor that must be considered in the degradation of gels. On the one hand vortexing likely enables additional penetration of the degrading acidic solution, the shaking itself may also lead to hydrogel degradation directly by breaking down aspects of physical crosslinking (such as hydrophobic interactions and electrostatic interactions etc.), which also supports the gel's 3D structure along with the oxidized-sugar covalent crosslinking. Overall, it is concluded that upon gel application, shaking should be avoided to maintain the integrity of a formed gel. But at the same time, mild sonication could also be utilized as a method to degrade gels *in situ* when their application is no longer required.

4.4 Comparison of oxidized-XOS and oxidized-lactose

Oxidized-XOS forms gels at a faster rate than oxidized-lactose. It may be because XOS contains more oxidation points than lactose. First, XOS consitutents include two or more sugar units, making them longer than lactose, and contains more alcohol functional groups available for oxidation, where lactose only includes one. XOS is typically oxidized at both of the terminal units, whereas each lactose molecule can only be oxidized at one end unit (Karppi et al., 2020). At the same time, XOS can be oxidized at both C2 and C3 positions by *Ab*PDHs, lactose can only be oxidized at C6 by GalOX (Karppi et al., 2020; Kirsti et al., 2015; Mototsune et al., 2024). x2 is an example of XOS (Figure 4.1), which contains four possible hydroxyls for oxidation by *Ab*PDH1 to ketone, and thus four additional connections with chitosan to form the crosslinks. Even if only one of each of the C2 or C3 may be selected to be oxidized on each of the two sugar moieties in a single x2 molecule, , the product should still end up with two oxidized positions for forming crosslinks. By

contract, each lactose molecule only contains one possible hydroxyl at C6 for oxidation by GalOX, such that any crosslinking arising from oxidized lactose will have to rely on the less reactive hydroxyls on the ring carbons.

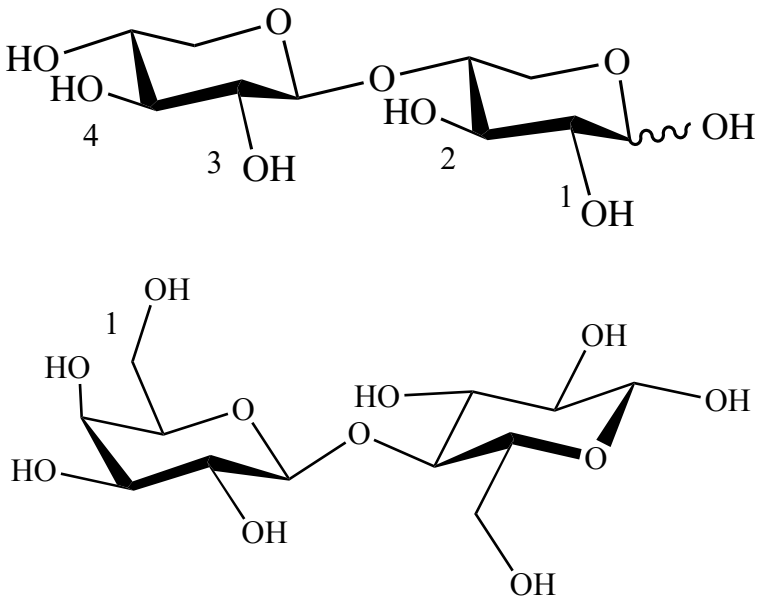

Figure 4.1: The crosslinking points comparison between XOS (X2) and lactose.

From this perspective it is important to consider that if a gel forms too fast, the gel may have already formed before the solutions from which it is comprised are injected into the targeted location (Ou et al., 2021). For example, the higher concentration chitosan gel (13.8 mg/mL) with 40 mM oxidized-XOS crosslinker is predicted to form in only 5 mins after vortexing, which may cause the gel to form during the transferring process. On the other hand, if the gel forms too slowly, gel solutions may spread out from the required area before gel formation, causing gel loss, and loss of any associated drug that was to imbedded in the gel. This could lead to untreated infection if for example the drug was an antibiotic being applied to an internal wound (Ou et al., 2021). The gels formed with 40 mM oxidized-lactose as crosslinker required overnight incubation to form a gel, so this is likely not relevant for medicine or agriculture at this time. In comparing the two kinds of crosslinkers, oxidized-XOS can form gels faster than oxidized-lactose, whereas gel made of oxidized-lactose seem

to be more stable over time than oxidized-XOS. Thus, considering a gel's potential application to agricultural technologies, oxidized-XOS would likely be preferred, because it can form gels faster. There is also a satisfaction associated with returning XOS to the plant world from where it was derived.

Finally, it is worth mentioning the observation that the oxidized-XOS ctrl. (ie untreated XOS, shown in Table 2.1) sample formed gels as well, although required significantly longer times to form gels compared to samples that included oxidized-XOS. And this is also in contrast to the oxidized-XOS std sample which did not form a gel at all. One first possible contributing factor may be the BQ used in the *Ab*PDH1 reaction. The structure of BQ includes two ketones, which could be reactive with the chitosan. However, the total amount of BQ in the gel formation reaction should be too low to contribute to any significant crosslinking. Another possible reason may be the presence of laccase, which was added to the *Ab*PDH1 reaction to recycle the HQ back to BQ. Laccase has been previously shown to have the potential to crosslink polymers directly (Osma et al., 2010). And laccase is also potential to catalyze redox reaction so it may also be able to partially oxidize the substrates. To further determine the factors causing to the crosslinking in the oxidized-XOS control reaction, more control reactions without BQ and without laccase should be performed.

4.5 Future directions

4.5.1 Project next steps

The first step from here is to conduct more controlled experiments to investigate why the oxidized-XOS ctrl. can form a gel as well. Larger-scale production of oxidized-sugar crosslinkers should be performed and larger-scale gels should be made. Gel degradation should also be additionally researched, and the rheometer should also be used to better understand the stiffness changes associated with modifying pH values. Finally, the next step

would be to look more closely and start testing potential applications in agriculture. To research its application, pesticide and nutrients for promoting plant growth should be added into gels during production and tested on plants. It will allow assessment of whether the gel can play the expected function to benefit agricultural production.

4.5.2 Potential applications of chitosan hydrogels

Chitosan hydrogels are a biosafe material that has the potential to be used in medicine and agriculture. In the medical field, the gel can form an anti-inflammatory protection cover for skin wound healing and bone regeneration (Guillén-Carvajal et al., 2023; Li et al., 2024; Gawel et al., 2023). The gel is also degradable with the catalysis of lysozymes secreted in vitro after a period, which may eliminate additional surgical removal as is required for other orthopedic stents (Rahmanian-Devin et al., 2021; Li et al., 2024). Thus, the chitosan crosslinking polymer may be used as an injectable material in surgery that assists in wound and bone repair (Li et al., 2024, Ou et al., 2021).

The hydrogel can not only provide a protective layer, but the 3D network gel can also be used as a carrier for drugs, that can enable more accurate delivery the drug to a targeted wound or other area (Aguilar et al., 2019). The gel can be used to enable a slow within a target area to achieve the lowest dose of drugs accurately delivered to the required location on or in the animal or plant. This could allow the use of reduced amounts of medication, reducing toxic side effects caused by the medication utilization and reducing drug costs (Li et al., 2024). At the same time delivery of the drug directly to the targeted area, could significantly reduce exposure of major organs and tissues to the drug further reducing side effects. For instance, the research of Bektas and their group demonstrated that the phenolic compound, vitexin, which is clinically used for the wound healing, can be added into a hydrogel, and leads to enhance drug absorbance both in vivo and in vitro upon application of the gel (Bektas et al., 2020; Li et al, 2024).

Although the chitosan hydrogels made using oxidized-XOS as the crosslinker is currently planned to be applied in agriculture rather than in medicine, it may be developed in the medical field after more clinical tests. In compared to other chitosan hydrogels made of other chemical or physical crosslinkers, oxidized-XOS and oxidized-lactose are natural non-toxic sugars, so they will not reduce biocompatibility like other chemical agents. This characteristic makes it more likely to be able to be adapted to human applications in medicine (Xu et al., 2023). Some possible examples are described below.

4.5.2.1 Chitosan hydrogel applications on skin burn treatment

Chitosan hydrogel can be used as an anti-inflammatory protection layer for incubating skin self-healing (Che et al., 2024, Elangwe et al., 2022). It may be applied to the treatment of extensive skin burn usually accompany by a large amount of skin or muscle tissues loss, which is always difficult to be surgical sutured (Borhani et al., 2023; Dai et al., 2012). Aguilar mentions that the chitosan naturally contains an abundance of positive charges, which enables it to form electrostatically interactions with the negative charged proteins and glycolipids on the surface of red blood cells. This enhances the intensive aggregation of red blood cells, thereby promoting wound healing (Aguilar et al., 2019). In addition, the formed gel also can cover the wound to protect from bacterial invasion. Drugs for promoting skin tissue growth can also be added to the gel. Thus, chitosan hydrogels could potentially be used after surgery for would healing.

4.5.2.2 CH gel applications on osteomyelitis

Many studies have mentioned that chitosan can be developed into a new biomaterial for bone and dental tissues engineering (Aguilar et al., 2019, Yadav et al., 2021). In 1999, Aimin and their research group tried to add gentamicin into chitosan gel for the topical antibiotic treatment of osteomyelitis (Aimin et al., 1999; Dai et al., 2012). This was a bold attempt to block drug molecule (such as antibiotic) within the enclosed inflammatory areas

inside the bone. Thus, chitosan hydrogels may be a promising candidate material for the treatment of osteomyelitis.

To clarify, the infected bone marrow and dead bone are first surgically debrided (removal of bone marrow), including disinfectant of the infected area with hydrogen peroxide. And then, hypothetically, that the chitosan gel carrying antibiotic can fill up the empty bone void, playing the same role as the use of bone cement. This may increase the concentration of antibiotic within the infected area. At the same time the gel will (excepted) then degrade automatically precluding additional invasive procedures.

However, there are also many uncertainties to apply hydrogels in osteomyelitis in clinical. First, it has not been determined whether the chitosan hydrogel can be formed within a human's bone. For instance, the most prevalent superbug of post-traumatic osteomyelitis is called methicillin-resistant *Staphylococcus aureus* (MRSA), it always leads to the formation of acidic abscesses changing the pH value in the bone marine cavity to pH 5.5-6.5 (Zhang et al., 2024), which could inhibit gel formation. Second, it also has not been determined whether how long a gel might enables continuously release of antibiotic to the bone. This is important for the treatment because the bacteria/fungi may be antibiotic resistance if all the antibiotic was released at the beginning but without ongoing releasing. Third, the gel is expected to remain within the bone for a longer time, and then slowly degrade. If the degradation occurs too fast, the antibiotic will be entirely released and leave the site too soon. Also, if the entire gel degrades at the same time, the degraded gel liquid may accumulate in the cavity actually promoting bacteria growth. Overall, the gel should be expected to slowly degrade in a constant rate to make sure the degraded liquid can be absorbed on time. Overall, it requires more research to use chitosan hydrogels in the treatment of osteomyelitis.

4.5.2.3 Chitosan hydrogel applications in plant agriculture

Applications of hydrogels to plant agriculture may be easier to achieve. First of all, chitosan hydrogels may take advantage of chitosan's anti-infection properties to protect the roots and broken areas of plants from fungi or bacteria, such as *E. carotovora , A. tumefaciens, P. aeruginosa, P. oleovorans, A. niger* and *R. stolonifera* and so on (Román-Doval et al., 2023). Second, hydrogels can also be used to accurately deliver micronutrients or pesticides to specific areas, which could significantly reduce pesticide residues (Román-Doval et al., 2023; Michalik & Wandzik, 2020; Zhatkanbayev et al., 2023). Nutrients that promote plant growth can also be added to the gel which might decrease fertilizer cost. This may enable production of higher quality organic foods at lower prices. Third, the hydrogel structure can hold water molecules around the plants' root to provide moist growing environment for the plants (Zhatkanbayev et al., 2023). This can reduce required water supply for the production of agricultural products. This may enable crop agriculture in water-scarce territories or during extreme temperatures in the summer.

Reference

Vassilev, S. V., Baxter, D., Andersen, L. K., & Vassileva, C. G. (2010). An overview of the chemical composition of biomass. *Fuel*, *89*(5), 913-933.

Bar-On, Y. M., Phillips, R., & Milo, R. (2018). The biomass distribution on Earth. *Proceedings of the National Academy of Sciences*, *115*(25), 6506-6511.

McKendry, P. (2002). Energy production from biomass (part 1): overview of biomass. *Bioresource technology*, *83*(1), 37-46.

Ning, P., Yang, G., Hu, L., Sun, J., Shi, L., Zhou, Y., ... & Yang, J. (2021). Recent advances in the valorization of plant biomass. *Biotechnology for Biofuels*, *14*(1), 102.

Xu, Y., Liu, K., Yang, Y., Kim, M. S., Lee, C. H., Zhang, R., ... & Si, C. (2023). Hemicellulose-based hydrogels for advanced applications. *Frontiers in Bioengineering and Biotechnology*, *10*, 1110004.

Inyang, V., Laseinde, O. T., & Kanakana, G. M. (2022). Techniques and applications of lignocellulose biomass sources as transport fuels and other bioproducts. *International Journal of Low-Carbon Technologies*, *17*, 900-909.

Xu, H., Li, B., & Mu, X. (2016). Review of alkali-based pretreatment to enhance enzymatic saccharification for lignocellulosic biomass conversion. *Industrial & Engineering Chemistry Research*, *55*(32), 8691-8705.

Saidur, R., Abdelaziz, E. A., Demirbas, A., Hossain, M. S., & Mekhilef, S. (2011). A review on biomass as a fuel for boilers. *Renewable and sustainable energy reviews*, *15*(5), 2262-2289.

Chen, Y., Xie, Y., Ajuwon, K. M., Zhong, R., Li, T., Chen, L., ... & Everaert, N. (2021). Xylo-oligosaccharides, preparation and application to human and animal health: a review. *Frontiers in nutrition*, *8*, 731930.

Abolore, R. S., Jaiswal, S., & Jaiswal, A. K. (2023). Green and sustainable pretreatment methods for cellulose extraction from lignocellulosic biomass and its applications: a review. *Carbohydrate Polymer Technologies and Applications*, 100396.

Parikka, M. (2004). Global biomass fuel resources. *Biomass and bioenergy*, *27*(6), 613-620.

Zoghlami, A., & Paës, G. (2019). Lignocellulosic biomass: understanding recalcitrance and predicting hydrolysis. *Frontiers in chemistry*, *7*, 874.

MacDonald, H., Hope, E., de Boer, K., & McKenney, D. W. (2023). Sentiments toward use of forest biomass for heat and power in canadian headlines. *Heliyon*, *9*(2).

Natural Resources Canada. (2023). *How much forest does Canada have?* Retrieved from Natural Resources Canada website: https://natural-resources.canada.ca/our-natural-resources/forests/state-canadas-forests-report/how-much-forest-does-canada-have/17601#forest-area

Agriculture and Agri-Food Canada. (2023). *Overview of Canada's argriculture and argi-foo d sector.* Retrieved from Agriculture and Agri-Food Canada website: https://agriculture.canada.ca/en/sector/overview

Kumar, A., Cameron, J. B., & Flynn, P. C. (2003). Biomass power cost and optimum plant size in western Canada. *Biomass and Bioenergy*, *24*(6), 445-464.

Shahid, M. K., Batool, A., Kashif, A., Nawaz, M. H., Aslam, M., Iqbal, N., & Choi, Y. (2021). Biofuels and biorefineries: Development, application and future perspectives emphasizing the environmental and economic aspects. *Journal of environmental management*, *297*, 113268.

Moravvej, Z., Makarem, M. A., & Rahimpour, M. R. (2019). The fourth generation of biofuel. In *Second and third generation of feedstocks* (pp. 557-597). Elsevier.

Tursi, A. (2019). A review on biomass: importance, chemistry, classification, and conversion. *Biofuel Research Journal*, *6*(2), 962-979.

Novaes, E., Kirst, M., Chiang, V., Winter-Sederoff, H., & Sederoff, R. (2010). Lignin and biomass: a negative correlation for wood formation and lignin content in trees. *Plant physiology*, *154*(2), 555-561.

Mazlan, N. A., Samad, K. A., Yussof, H. W., Saufi, S. M., & Jahim, J. (2019). Xylooligosaccharides from potential agricultural waste: Characterization and screening on the enzymatic hydrolysis factors. *Industrial Crops and Products*, *129*, 575-584.

Tarasov, D., Leitch, M., & Fatehi, P. (2018). Lignin–carbohydrate complexes: properties, applications, analyses, and methods of extraction: a review. *Biotechnology for biofuels*, *11*, 1-28.

Chen, H., Liu, J., Chang, X., Chen, D., Xue, Y., Liu, P., ... & Han, S. (2017). A review on the pretreatment of lignocellulose for high-value chemicals. *Fuel Processing Technology*, *160*, 196-206.

Nishimura, H., Kamiya, A., Nagata, T., Katahira, M., & Watanabe, T. (2018). Direct evidence for α ether linkage between lignin and carbohydrates in wood cell walls. *Scientific reports*, *8*(1), 6538.

Ojo, A. O. (2023). An overview of lignocellulose and its biotechnological importance in high-value product production. *Fermentation*, *9*(11), 990.

Hasanov, I., Raud, M., & Kikas, T. (2020). The role of ionic liquids in the lignin separation from lignocellulosic biomass. *Energies*, *13*(18), 4864.

Brienza, F., Cannella, D., Montesdeoca, D., Cybulska, I., & Debecker, D. P. (2024). A guide to lignin valorization in biorefineries: traditional, recent, and forthcoming approaches to convert raw lignocellulose into valuable materials and chemicals. *RSC Sustainability*, *2*(1), 37-90.

Alberts, B., Johnson, A., Lewis, J., Raff, M., Roberts, K., & Walter, P. (2002). The plant cell wall. In *Molecular Biology of the Cell. 4th edition*. Garland Science.

McNamara, J. T., Morgan, J. L., & Zimmer, J. (2015). A molecular description of cellulose biosynthesis. *Annual review of biochemistry*, *84*(1), 895-921.

Morgan, J. L., McNamara, J. T., Fischer, M., Rich, J., Chen, H. M., Withers, S. G., & Zimmer, J. (2016). Observing cellulose biosynthesis and membrane translocation in crystallo. *Nature*, *531*(7594), 329-334.

Rongpipi, S., Ye, D., Gomez, E. D., & Gomez, E. W. (2019). Progress and opportunities in the characterization of cellulose–an important regulator of cell wall growth and mechanics. *Frontiers in Plant Science*, *9*, 1894.

MacCormick, B., Vuong, T. V., & Master, E. R. (2018). Chemo-enzymatic synthesis of clickable xylo-oligosaccharide monomers from hardwood 4-O-methylglucuronoxylan. *Biomacromolecules*, *19*(2), 521-530.

Qaseem, M. F., Shaheen, H., & Wu, A. M. (2021). Cell wall hemicellulose for sustainable industrial utilization. *Renewable and Sustainable Energy Reviews*, *144*, 110996.

Palaniappan, A., Antony, U., & Emmambux, M. N. (2021). Current status of xylooligosaccharides: Production, characterization, health benefits and food application. *Trends in Food Science & Technology*, *111*, 506-519.

Santibáñez, L., Henríquez, C., Corro-Tejeda, R., Bernal, S., Armijo, B., & Salazar, O. (2021). Xylooligosaccharides from lignocellulosic biomass: A comprehensive review. *Carbohydrate Polymers*, *251*, 117118.

Scheller, H. V., & Ulvskov, P. (2010). Hemicelluloses. *Annual review of plant biology*, *61*(1), 263-289.

Sharan, A. A., Bellemare, A., DiFalco, M., Tsang, A., Vuong, T. V., Edwards, E. A., & Master, E. R. (2024). Functional screening pipeline to uncover laccase-like multicopper oxidase enzymes that transform industrial lignins. *Bioresource Technology*, *393*, 130084.

Zheng, B., Yu, S., Chen, Z., & Huo, Y. X. (2022). A consolidated review of commercial-scale high-value products from lignocellulosic biomass. *Frontiers in Microbiology*, *13*, 933882.

Vanholme, R., Morreel, K., Darrah, C., Oyarce, P., Grabber, J. H., Ralph, J., & Boerjan, W. (2012). Metabolic engineering of novel lignin in biomass crops. *New Phytologist*, *196*(4), 978-1000.

Liu, Q., Luo, L., & Zheng, L. (2018). Lignins: biosynthesis and biological functions in plants. *International journal of molecular sciences*, *19*(2), 335.

Zhang, J., Choi, Y. S., Yoo, C. G., Kim, T. H., Brown, R. C., & Shanks, B. H. (2015). Cellulose–hemicellulose and cellulose–lignin interactions during fast pyrolysis. *ACS sustainable chemistry & engineering*, *3*(2), 293-301.

Rahmanian-Devin, P., Baradaran Rahimi, V., & Askari, V. R. (2021). Thermosensitive chitosan-β-glycerophosphate hydrogels as targeted drug delivery systems: an overview on preparation and their applications. *Advances in Pharmacological and Pharmaceutical Sciences*, *2021*(1), 6640893.

Taokaew, S., Kaewkong, W., & Kriangkrai, W. (2023). Recent development of functional chitosan-based hydrogels for pharmaceutical and biomedical applications. *Gels*, *9*(4), 277.

Aranaz, I., Alcántara, A. R., Civera, M. C., Arias, C., Elorza, B., Heras Caballero, A., & Acosta, N. (2021). Chitosan: An overview of its properties and applications. *Polymers*, *13*(19), 3256.

Elieh-Ali-Komi, D., & Hamblin, M. R. (2016). Chitin and chitosan: production and application of versatile biomedical nanomaterials. *International journal of advanced research*, *4*(3), 411-427.

Li, B., Elango, J., & Wu, W. (2020). Recent advancement of molecular structure and biomaterial function of chitosan from marine organisms for pharmaceutical and nutraceutical application. *Applied Sciences*, *10*(14), 4719.

Aguilar, A., Zein, N., Harmouch, E., Hafdi, B., Bornert, F., Offner, D., ... & Hua, G. (2019). Application of chitosan in bone and dental engineering. *Molecules*, *24*(16), 3009.

Islam, S., Bhuiyan, M. R., & Islam, M. N. (2017). Chitin and chitosan: structure, properties and applications in biomedical engineering. *Journal of Polymers and the Environment*, *25*, 854-866.

Inokuma, K., Hasunuma, T., & Kondo, A. (2016). Ethanol production from N-acetyl-D-glucosamine by Scheffersomyces stipitis strains. *Amb Express*, *6*, 1-7.

Li, A., Ma, B., Hua, S., Ping, R., Ding, L., Tian, B., & Zhang, X. (2024). Chitosan-based injectable hydrogel with multifunction for wound healing: A critical review. *Carbohydrate Polymers*, 121952.

Teixeira-Costa, B. E., & Andrade, C. T. (2021). Chitosan as a valuable biomolecule from seafood industry waste in the design of green food packaging. *Biomolecules*, *11*(11), 1599.

Feng, X., Hong, S., Zhao, H., Vuong, T. V., & Master, E. R. (2024). Biocatalytic cascade to polysaccharide amination. *Biotechnology for biofuels and bioproducts*, *17*(1), 34.

Vinsova, J., & Vavrikova, E. (2011). Chitosan derivatives with antimicrobial, antitumour and antioxidant activities-a review. *Current pharmaceutical design*, *17*(32), 3596-3607.

Xu, Y., Liu, K., Yang, Y., Kim, M. S., Lee, C. H., Zhang, R., ... & Si, C. (2023). Hemicellulose-based hydrogels for advanced applications. *Frontiers in Bioengineering and Biotechnology*, *10*, 1110004.

Hong, F., Qiu, P., Wang, Y., Ren, P., Liu, J., Zhao, J., & Gou, D. (2023). Chitosan-based hydrogels: From preparation to applications, a review. *Food Chemistry: X*, 101095.

Ahmadi, F., Oveisi, Z., Samani, S. M., & Amoozgar, Z. (2015). Chitosan based hydrogels: characteristics and pharmaceutical applications. *Research in pharmaceutical sciences*, *10*(1), 1-16.

Alavarse, A. C., Frachini, E. C. G., da Silva, R. L. C. G., Lima, V. H., Shavandi, A., & Petri, D. F. S. (2022). Crosslinkers for polysaccharides and proteins: Synthesis conditions, mechanisms, and crosslinking efficiency, a review. *International journal of biological macromolecules*, *202*, 558-596.

Resl, P., Bujold, A. R., Tagirdzhanova, G., Meidl, P., Freire Rallo, S., Kono, M., ... & Spribille, T. (2022). Large differences in carbohydrate degradation and transport potential among lichen fungal symbionts. *Nature communications*, *13*(1), 2634.

Clark, D. P., Pazdernik, N. J., & McGehee, M. R. (2019). Chapter 29—Molecular Evolution. *Molecular biology. 3rd ed. Amsterdam: Elsevier Inc*, 925-69.

Umbreit, W. W. (1962). II. THE COMPARATIVE PHYSIOLOGY OF AUTOTROPHIC BACTERIA. *Bacteriological Reviews*, *26*(2_pt_1-2), 145-150.

Sun, C. C., Zhao, W. J., Yue, W. Z., Cheng, H., Sun, F. L., Wang, Y. T., ... & Wang, Y. S. (2023). Polymeric carbohydrates utilization separates microbiomes into niches: insights into the diversity of microbial carbohydrate-active enzymes in the inner shelf of the Pearl River Estuary, China. *Frontiers in Microbiology*, *14*, 1180321.

Benoit, I., Culleton, H., Zhou, M., DiFalco, M., Aguilar-Osorio, G., Battaglia, E., ... & De Vries, R. P. (2015). Closely related fungi employ diverse enzymatic strategies to degrade plant biomass. *Biotechnology for biofuels*, *8*, 1-14.

Barrett, K., Jensen, K., Meyer, A. S., Frisvad, J. C., & Lange, L. (2020). Fungal secretome profile categorization of CAZymes by function and family corresponds to fungal phylogeny and taxonomy: Example Aspergillus and Penicillium. *Scientific Reports*, *10*(1), 5158–5158.

SMITH, D., MUSCATINE, L., & LEWIS, D. (1969). Carbohydrate movement from autotrophs to heterotrophs in parasitic and mutualistic symbiosis. *Biological Reviews*, *44*(1), 17-85.

Hess, J., Balasundaram, S. V., Bakkemo, R. I., Drula, E., Henrissat, B., Högberg, N., ... & Skrede, I. (2021). Niche differentiation and evolution of the wood decay machinery in the invasive fungus Serpula lacrymans. *The ISME Journal*, *15*(2), 592-604.

Lofgren, L. A., Nguyen, N. H., Vilgalys, R., Ruytinx, J., Liao, H. L., Branco, S., ... & Kennedy, P. G. (2021). Comparative genomics reveals dynamic genome evolution in host specialist ectomycorrhizal fungi. *New Phytologist*, *230*(2), 774-792.

Yin, D., Urresti, S., Lafond, M., Johnston, E. M., Derikvand, F., Ciano, L., ... & Brumer, H. (2015). Structure–function characterization reveals new catalytic diversity in the galactose oxidase and glyoxal oxidase family. *Nature communications*, *6*(1), 10197.

Wardman, J. F., Bains, R. K., Rahfeld, P., & Withers, S. G. (2022). Carbohydrate-active enzymes (CAZymes) in the gut microbiome. *Nature Reviews Microbiology*, *20*(9), 542-556.

Cantarel, B. L., Coutinho, P. M., Rancurel, C., Bernard, T., Lombard, V., & Henrissat, B. (2009). The Carbohydrate-Active EnZymes database (CAZy): an expert resource for glycogenomics. *Nucleic acids research*, *37*(suppl_1), D233-D238.

Ameri, R., García, J. L., Derenfed, A. B., Pradel, N., Neifar, S., Mhiri, S., ... & Bejar, S. (2022). Genome sequence and Carbohydrate Active Enzymes (CAZymes) repertoire of the thermophilic Caldicoprobacter algeriensis TH7C1T. *Microbial Cell Factories*, *21*(1), 91.

Morin, E., Kohler, A., Baker, A. R., Foulongne-Oriol, M., Lombard, V., Nagye, L. G., ... & Martin, F. (2012). Genome sequence of the button mushroom Agaricus bisporus reveals mechanisms governing adaptation to a humic-rich ecological niche. *Proceedings of the National Academy of Sciences*, *109*(43), 17501-17506.

Hage, H., & Rosso, M.-N. (2021). Evolution of Fungal Carbohydrate-Active Enzyme Portfolios and Adaptation to Plant Cell-Wall Polymers. *Journal of Fungi (Basel)*, *7*(3), 185-.

Levasseur, A., Drula, E., Lombard, V., Coutinho, P. M., & Henrissat, B. (2013). Expansion of the enzymatic repertoire of the CAZy database to integrate auxiliary redox enzymes. *Biotechnology for biofuels*, *6*, 1-14.

Sützl, L., Laurent, C. V., Abrera, A. T., Schütz, G., Ludwig, R., & Haltrich, D. (2018). Multiplicity of enzymatic functions in the CAZy AA3 family. *Applied microbiology and biotechnology*, *102*, 2477-2492.

Sützl, L., Foley, G., Gillam, E. M., Bodén, M., & Haltrich, D. (2019). The GMC superfamily of oxidoreductases revisited: analysis and evolution of fungal GMC oxidoreductases. *Biotechnology for Biofuels*, *12*, 1-18.

Alpdağtaş, S., Jankowski, N., Urlacher, V. B., & Koschorreck, K. (2024). Identification of redox activators for continuous reactivation of glyoxal oxidase from Trametes versicolor in a two-enzyme reaction cascade. *Scientific Reports*, *14*(1), 5932.

Whittaker, M. M., & Whittaker, J. W. (2003). Cu (I)-dependent biogenesis of the galactose oxidase redox cofactor. *Journal of Biological Chemistry*, *278*(24), 22090-22101.

Peterbauer, C. K. (2020). Pyranose dehydrogenases: Rare enzymes for electrochemistry and biocatalysis. *Bioelectrochemistry*, *132*, 107399.

Volc, J., Kubátová, E., Wood, D. A., & Daniel, G. (1997). Pyranose 2-dehydrogenase, a novel sugar oxidoreductase from the basidiomycete fungus Agaricus bisporus. *Archives of microbiology*, *167*, 119-125.

Staudigl, P., Krondorfer, I., Haltrich, D., & Peterbauer, C. K. (2013). Pyranose dehydrogenase from Agaricus campestris and Agaricus xanthoderma: characterization and applications in carbohydrate conversions. *Biomolecules*, *3*(3), 535-552.

Kittl, R., Sygmund, C., Halada, P., Volc, J., Divne, C., Haltrich, D., & Peterbauer, C. K. (2008). Molecular cloning of three pyranose dehydrogenase-encoding genes from Agaricus meleagris and analysis of their expression by real-time RT-PCR. *Current genetics*, *53*, 117-127.

Tan, T. C., Spadiut, O., Wongnate, T., Sucharitakul, J., Krondorfer, I., Sygmund, C., ... & Divne, C. (2013). The 1.6 Å crystal structure of pyranose dehydrogenase from Agaricus meleagris rationalizes substrate specificity and reveals a flavin intermediate. *PLoS One*, *8*(1), e53567.

Sygmund, C., Kittl, R., Volc, J., Halada, P., Kubátová, E., Haltrich, D., & Peterbauer, C. K. (2008). Characterization of pyranose dehydrogenase from Agaricus meleagris and its application in the C-2 specific conversion of D-galactose. *Journal of biotechnology*, *133*(3), 334-342.

Karppi, J., Zhao, H., Chong, S. L., Koistinen, A. E., Tenkanen, M., & Master, E. (2020). Quantitative comparison of pyranose dehydrogenase action on diverse xylooligosaccharides. *Frontiers in Chemistry*, *8*, 11.

Gonaus, C., Kittl, R., Sygmund, C., Haltrich, D., & Peterbauer, C. (2016). Transcription analysis of pyranose dehydrogenase from the basidiomycete Agaricus bisporus and characterization of the recombinantly expressed enzyme. *Protein Expression and Purification*, *119*, 36-44.

Volc, J., Sedmera, P., Halada, P., Přikrylová, V., & Haltrich, D. (2000). Double oxidation of d-xylose to d-glycero-pentos-2, 3-diulose (2, 3-diketo-d-xylose) by pyranose dehydrogenase from the mushroom Agaricusbisporus. *Carbohydrate Research*, *329*(1), 219-225.

Graf, M. M., Bren, U., Haltrich, D., & Oostenbrink, C. (2013). Molecular dynamics simulations give insight into D-glucose dioxidation at C2 and C3 by Agaricus meleagris pyranose dehydrogenase. *Journal of computer-aided molecular design*, *27*, 295-304.

Graf, M. M., Sucharitakul, J., Bren, U., Chu, D. B., Koellensperger, G., Hann, S., ... & Haltrich, D. (2015). Reaction of pyranose dehydrogenase from Agaricus meleagris with its carbohydrate substrates. *The FEBS Journal*, *282*(21), 4218-4241.

Yan, N., Luan, T., Yin, M., Niu, Y., Wu, L., Yang, S., ... & Bao, X. (2023). Co-Fermentation of Glucose–Xylose–Cellobiose–XOS Mixtures Using a Synthetic Consortium of Recombinant Saccharomyces cerevisiae Strains. *Fermentation*, *9*(8), 775.
Vuong, T. V., & Master, E. R. (2022). Enzymatic upgrading of heteroxylans for added-value chemicals and polymers. *Current Opinion in Biotechnology*, *73*, 51-60.

Freitas, C., Carmona, E., & Brienzo, M. (2019). Xylooligosaccharides production process from lignocellulosic biomass and bioactive effects. *Bioactive carbohydrates and dietary fibre*, *18*, 100184.

Yuan, Y., Teng, Q., Zhong, R., & Ye, Z. H. (2014). Identification and biochemical characterization of four wood-associated glucuronoxylan methyltransferases in Populus. *PLoS One*, *9*(2), e87370.

Shraddha, Shekher, R., Sehgal, S., Kamthania, M., & Kumar, A. (2011). Laccase: microbial sources, production, purification, and potential biotechnological applications. *Enzyme research*, *2011*(1), 217861.

Lv, R., Sun, S., Liu, J., Wang, K., Golubev, Y. A., Dong, F., ... & Tan, D. (2022). Bifunctional nanozyme of copper organophyllosilicate for the ultrasensitive detection of hydroquinone. *Analytical and Bioanalytical Chemistry*, 1-10.

Parikka, K., Master, E., & Tenkanen, M. (2015). Oxidation with galactose oxidase: multifunctional enzymatic catalysis. *Journal of Molecular Catalysis B: Enzymatic*, *120*, 47-59.

Cooper, J. A., Smith, W., Bacila, M., & Medina, H. (1959). Galactose oxidase from Polyporus circinatus, Fr.

Ito, N., Phillips, S. E., Yadav, K. D., & Knowles, P. F. (1994). Crystal structure of a free radical enzyme, galactose oxidase. *Journal of molecular biology*, *238*(5), 794-814.

Paukner, R., Staudigl, P., Choosri, W., Haltrich, D., & Leitner, C. (2015). Expression, purification, and characterization of galactose oxidase of Fusarium sambucinum in E. coli. *Protein expression and purification*, *108*, 73-79.

Cleveland, M. (2021). *Investigating catalytic diversity in copper radical oxidases for potential bioproduct applications* (Doctoral dissertation, University of British Columbia).

Mototsune, O. M., Hong, S. H., Naguib, H. E., & Master, E. R. (2024). Enzymatically Oxidized Carbohydrates As Dicarbonyl Biobased Cross-Linkers for Polyamines. *Biomacromolecules*, *25*(7), 4428-4439.

John, A., Shaikh, M. M., & Ghosh, P. (2008). Structural and functional mimic of galactose oxidase by a copper complex of a sterically demanding [N2O2] ligand. *Dalton Transactions : An International Journal of Inorganic Chemistry*, *21*, 2815–2824.

Figueiredo, C., De Lacey, A. L., & Pita, M. (2022). Electrochemical studies of galactose oxidase. *Electrochemical Science Advances*, *2*(5).

Chang, C. H., Hsiung, H. A., Hong, K. L., & Huang, C. T. (2018). Enhancing the efficiency of the Pichia pastoris AOX1 promoter via the synthetic positive feedback circuit of transcription factor Mxr1. *BMC biotechnology*, *18*, 1-10.

Reily, C., Stewart, T. J., Renfrow, M. B., & Novak, J. (2019). Glycosylation in health and disease. *Nature Reviews Nephrology*, *15*(6), 346-366.

Schotte, P., Dewerte, I., De Groeve, M., De Keyser, S., De Brabandere, V., & Stanssens, P. (2016). Pichia pastoris Mut S strains are prone to misincorporation of O-methyl-l-homoserine at methionine residues when methanol is used as the sole carbon source. *Microbial cell factories*, *15*, 1-9.

Mengwasser, K. E., Bryant, C. E., Gay, N. J., & Gangloff, M. (2011). LPS ligand and culture additives improve production of monomeric MD-1 and 2 in Pichia pastoris by decreasing

aggregation and intermolecular disulfide bonding. *Protein Expression and Purification*, *76*(2), 173-183.

Peterbauer, C. K., & Volc, J. (2010). Pyranose dehydrogenases: biochemical features and perspectives of technological applications. *Applied microbiology and biotechnology*, *85*, 837-848.

Fabbrizzi, L. (2020). The ferrocenium/ferrocene couple: a versatile redox switch. *ChemTexts*, *6*, 1-20.

Dolz, M., Monterrey, D. T., Beltrán-Nogal, A., Menés-Rubio, A., Keser, M., González-Pérez, D., ... & Alcalde, M. (2023). The colors of peroxygenase activity: Colorimetric high-throughput screening assays for directed evolution. *Methods in Enzymology*, *693*, 73-109.

Tressel, P., & Kosman, D. J. (1980). o, o-Dityrosine in native and horseradish peroxidase-activated galactose oxidase. *Biochemical and biophysical research communications*, *92*(3), 781-786.

Wu, Z., Shi, L., Yu, X., Zhang, S., & Chen, G. (2019). Co-immobilization of tri-enzymes for the conversion of hydroxymethylfurfural to 2, 5-diformylfuran. *Molecules*, *24*(20), 3648.

Stojkov, G., Niyazov, Z., Picchioni, F., & Bose, R. K. (2021). Relationship between structure and rheology of hydrogels for various applications. *Gels*, *7*(4), 255.

Whittaker, J. W. (1999). Oxygen reactions of the copper oxidases. *Essays in Biochemistry*, *34*, 155-172.

Gaweł, J., Milan, J., Żebrowski, J., Płoch, D., Stefaniuk, I., & Kus-Liśkiewicz, M. (2023). Biomaterial composed of chitosan, riboflavin, and hydroxyapatite for bone tissue regeneration. *Scientific Reports*, *13*(1), 17004.

Ou, Y., & Tian, M. (2021). Advances in multifunctional chitosan-based self-healing hydrogels for biomedical applications. *Journal of Materials Chemistry B*, *9*(38), 7955-7971.

Osma, J. F., Toca-Herrera, J. L., & Rodríguez-Couto, S. (2010). Uses of laccases in the food industry. *Enzyme research*, *2010*(1), 918761.

Guillén-Carvajal, K., Valdez-Salas, B., Beltrán-Partida, E., Salomón-Carlos, J., & Cheng, N. (2023). Chitosan, gelatin, and collagen hydrogels for bone regeneration. *Polymers*, *15*(13), 2762.

Li, A., Ma, B., Hua, S., Ping, R., Ding, L., Tian, B., & Zhang, X. (2024). Chitosan-based injectable hydrogel with multifunction for wound healing: A critical review. *Carbohydrate Polymers*, 121952.

Bektas, N., Şenel, B., Yenilmez, E., Özatik, O., & Arslan, R. (2020). Evaluation of wound healing effect of chitosan-based gel formulation containing vitexin. *Saudi Pharmaceutical Journal*, *28*(1), 87-94.

Che, X., Zhao, T., Hu, J., Yang, K., Ma, N., Li, A., Sun, Q., Ding, C., & Ding, Q. (2024). Application of Chitosan-Based Hydrogel in Promoting Wound Healing: A Review. *Polymers*, *16*(3), 344-.

Elangwe, C. N., Morozkina, S. N., Olekhnovich, R. O., Krasichkov, A., Polyakova, V. O., & Uspenskaya, M. V. (2022). A review on chitosan and cellulose hydrogels for wound dressings. *Polymers*, *14*(23), 5163.

Borhani, M., Dadpour, S., Haghighizadeh, A., Etemad, L., Soheili, V., Memar, B., ... & Rajabi, O. (2023). Crosslinked hydrogel loaded with chitosan-supported iron oxide and silver nanoparticles as burn wound dressing. *Pharmaceutical Development and Technology*, *28*(10), 962-977.

Dai, T., Tanaka, M., Huang, Y. Y., & Hamblin, M. R. (2011). Chitosan preparations for wounds and burns: antimicrobial and wound-healing effects. *Expert review of anti-infective therapy*, *9*(7), 857-879.

Zhang, W., Lu, H., Zhang, W., Hu, J., Zeng, Y., Hu, H., ... & Xu, F. (2024). Inflammatory Microenvironment-Responsive Hydrogels Enclosed with Quorum Sensing Inhibitor for Treating Post-Traumatic Osteomyelitis. *Advanced Science*, *11*(20), 2307969.

Yadav, L. R., Chandran, S. V., Lavanya, K., & Selvamurugan, N. (2021). Chitosan-based 3D-printed scaffolds for bone tissue engineering. *International Journal of Biological Macromolecules*, *183*, 1925–1938.

Román-Doval, R., Torres-Arellanes, S. P., Tenorio-Barajas, A. Y., Gómez-Sánchez, A., & Valencia-Lazcano, A. A. (2023). Chitosan: Properties and its application in agriculture in context of molecular weight. *Polymers*, *15*(13), 2867.

Aimin, C., Chunlin, H., Juliang, B., Tinyin, Z., & Zhichao, D. (1999). Antibiotic Loaded Chitosan Bar: An In Vitro, In Vivo Study of a Possible Treatment for Osteomyelitis. *Clinical Orthopaedics and Related Research (1976-2007)*, *366*, 239-247.

Michalik, R., & Wandzik, I. (2020). A mini-review on chitosan-based hydrogels with potential for sustainable agricultural applications. *Polymers*, *12*(10), 2425.

Zhatkanbayev, Y., Zhatkanbayeva, Z., Iskakova, Z., Kolpek, A., Serikov, A., Moldagulova, N., ... & Anuarbekova, S. (2023). Application of Chitosan-Based Hydrogel Obtained from Insects in Pine Planting. *International Journal of Biomaterials*, *2023*(1), 8175405.

Wu, Z., Peng, K., Zhang, Y., Wang, M., Yong, C., Chen, L., ... & Pan, M. (2022). Lignocellulose dissociation with biological pretreatment towards the biochemical platform: A review. *Materials Today Bio*, *16*, 100445.

WOO, S.-W., CHO, J.-S., HUR, B.-K., SHIN, D.-H., RYU, K.-G., & KIM, E.-K. (2003). Hydrogen peroxide, its measurement and effect during enzymatic decoloring of Congo red. *Journal of Microbiology and Biotechnology*, *13*(5), 773–777.

Ilyasov, I. R., Beloborodov, V. L., Selivanova, I. A., & Terekhov, R. P. (2020). ABTS/PP decolorization assay of antioxidant capacity reaction pathways. *International journal of molecular sciences*, *21*(3), 1131.

Lan, X., Fu, S., Song, J., Leu, S., Shen, J., Kong, Y., ... & Liu, H. (2024). Structural changes of hemicellulose during pulping process and its interaction with nanocellulose. *International Journal of Biological Macromolecules*, *255*, 127772.

Mittal, H., Al Alili, A., & Alhassan, S. M. (2023). Latest progress in utilizing gum hydrogels and their composites as high-efficiency adsorbents for removing pollutants from wastewater. *Journal of Molecular Liquids*, 123392.

Andberg, M., Mollerup, F., Parikka, K., Koutaniemi, S., Boer, H., Juvonen, M., ... & Kruus, K. (2017). A novel Colletotrichum graminicola raffinose oxidase in the AA5 family. *Applied and environmental microbiology*, *83*(20), e01383-17.

Dijkman, W. P., Binda, C., Fraaije, M. W., & Mattevi, A. (2015). Structure-based enzyme tailoring of 5-hydroxymethylfurfural oxidase. *ACs Catalysis*, *5*(3), 1833-1839.

Fong, J. K., Mathieu, Y., Vo, M. T., Bellemare, A., Tsang, A., & Brumer, H. (2024). Expansion of Auxiliary Activity Family 5 sequence space via biochemical characterization of six new copper radical oxidases. *Applied and Environmental Microbiology*, *90*(7), e01014-24.

Hernandez-Ruiz, J., Arnao, M. B., Hiner, A. N., GARCÍA-CÁNOVAS, F., & ACOSTA, M. (2001). Catalase-like activity of horseradish peroxidase: relationship to enzyme inactivation by H2O2. *Biochemical Journal*, *354*(1), 107-114.

Parikka, K., Leppanen, A. S., Pitkanen, L., Reunanen, M., Willfor, S., & Tenkanen, M. (2010). Oxidation of polysaccharides by galactose oxidase. *Journal of Agricultural and Food Chemistry*, *58*(1), 262-271.

Nguyen, Q. T., Romero, E., Dijkman, W. P., De Vasconcellos, S. P., Binda, C., Mattevi, A., & Fraaije, M. W. (2018). Structure-based engineering of Phanerochaete chrysosporium alcohol oxidase for enhanced oxidative power toward glycerol. *Biochemistry*, *57*(43), 6209-6218.

Cleveland, M., Lafond, M., Xia, F. R., Chung, R., Mulyk, P., Hein, J. E., & Brumer, H. (2021). Two Fusarium copper radical oxidases with high activity on aryl alcohols. *Biotechnology for Biofuels*, *14*(1), 138.

Appendix A Gel Pictures

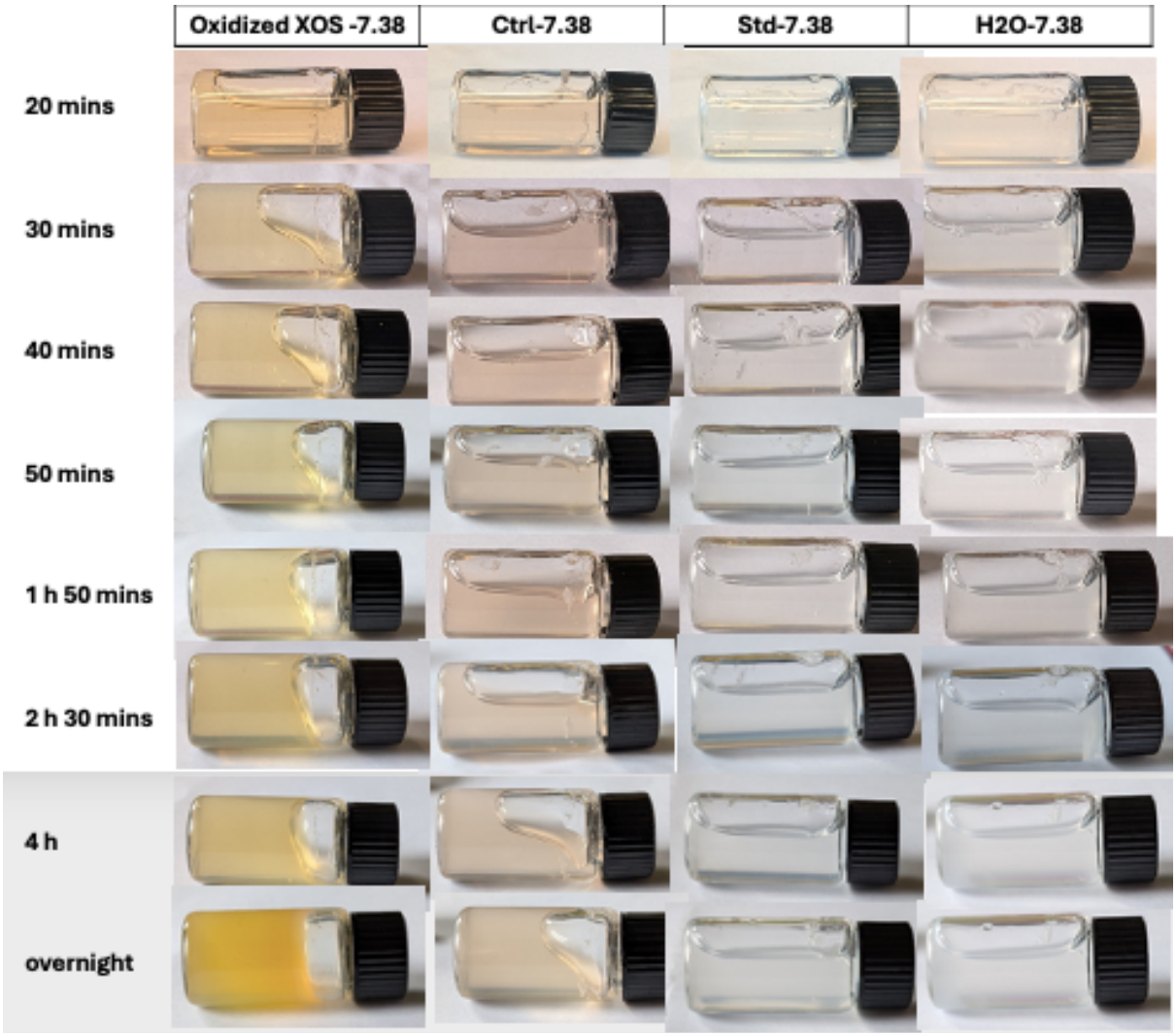

Figure A1: Gel pictures for 7.36 mg/ml chitosan gel formation with the Oxidated XOS as the crosslinker. (Pictures taken by Owen Monotsune)

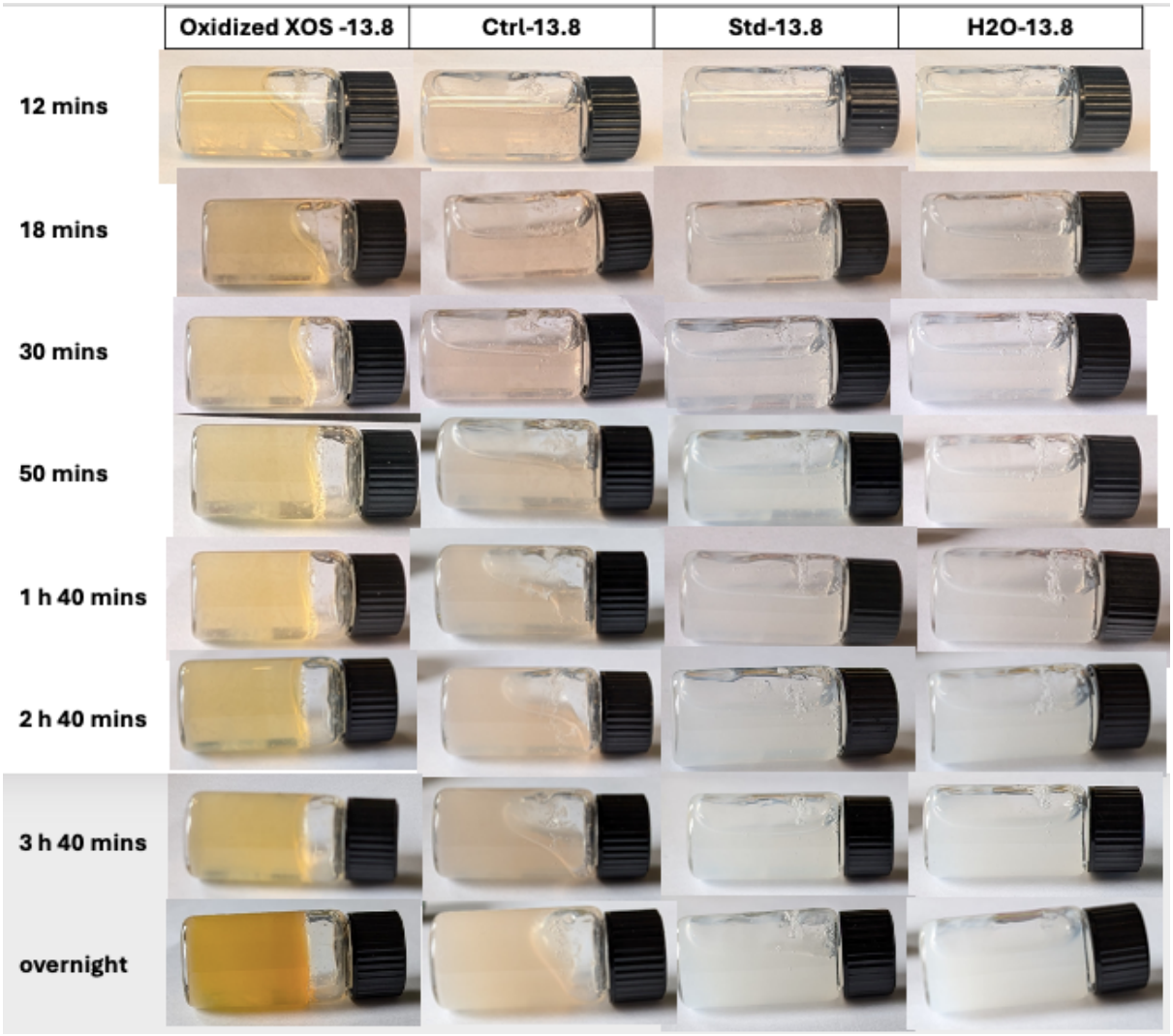

Figure A2: Gel pictures for 13.8 mg/ml chitosan gel formation with the Oxidated XOS as the crosslinker. (pictures taken by Owen Monotsune)

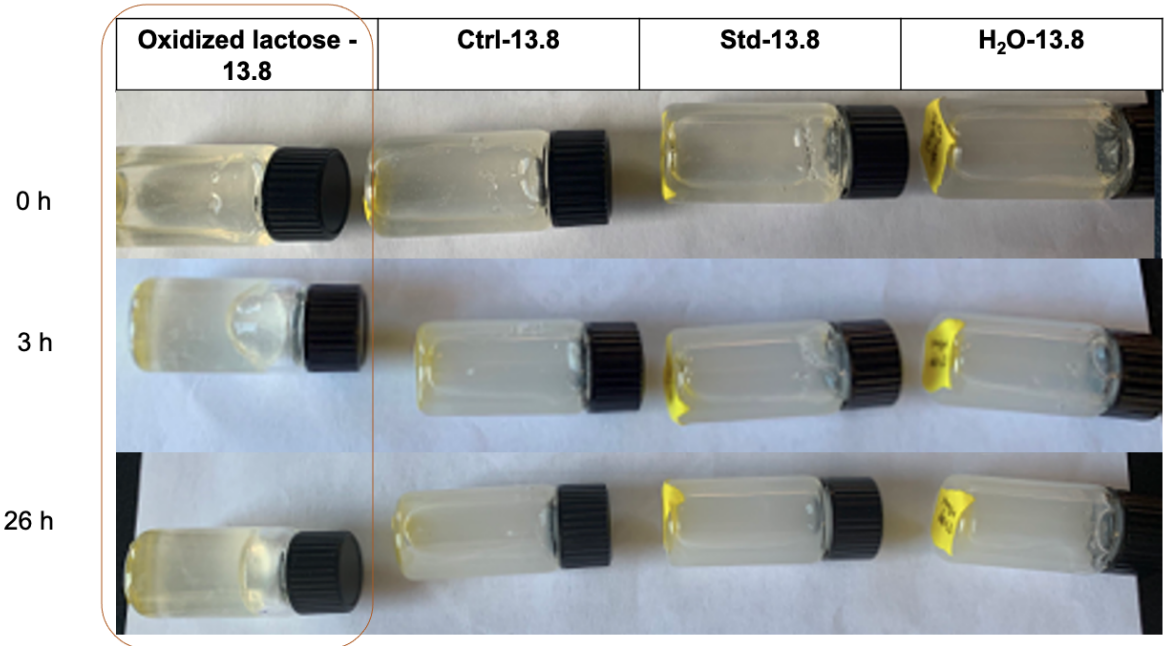

Figure A3: Gel pictures for 13.8 mg/ml chitosan gel formation with the oxidated-lactose as the crosslinker.